HYBRID ATOMIC-OPTOMECHANICAL SYSTEMS – OBSERVING QUANTUM EFFECTS IN MACROSCOPIC OSCILLATORS

by

Swati Singh

A Dissertation Submitted to the Faculty of the

DEPARTMENT OF PHYSICS

In Partial Fulfillment of the Requirements
For the Degree of

DOCTOR OF PHILOSOPHY

In the Graduate College

THE UNIVERSITY OF ARIZONA

2012

THE UNIVERSITY OF ARIZONA
GRADUATE COLLEGE

As members of the Dissertation Committee, we certify that we have read the dissertation prepared by Swati Singh
entitled Hybrid Atomic-Optomechanical Systems – Observing quantum effects in macroscopic oscillators
and recommend that it be accepted as fulfilling the dissertation requirement for the Degree of Doctor of Philosophy.

Date: 30 April 2012
Pierre Meystre

Date: 30 April 2012
Ewan M. Wright

Date: 30 April 2012
Alexander Cronin

Date: 30 April 2012
Koen Visscher

Date: 30 April 2012
Sumitendra Mazumdar

Final approval and acceptance of this dissertation is contingent upon the candidate's submission of the final copies of the dissertation to the Graduate College.
I hereby certify that I have read this dissertation prepared under my direction and recommend that it be accepted as fulfilling the dissertation requirement.

Date: 30 April 2012
Dissertation Director: Pierre Meystre

STATEMENT BY AUTHOR

This dissertation has been submitted in partial fulfillment of requirements for an advanced degree at the University of Arizona and is deposited in the University Library to be made available to borrowers under rules of the Library.

SIGNED: Swati Singh

ACKNOWLEDGEMENTS

I would like to take this opportunity to thank all the people who supported me during my time here in Arizona. However, since there is a one page limit, I can only list of some of them here – I hope the others are aware of my gratitude.

It is a privilege to be guided by Pierre Meystre- even though writing this thesis made me realize I still have a lot to learn. His instincts and encouragement are the biggest reasons why I am still in physics. Some of my favorite Pierre-isms include: "There are only 2 types of theorists– the harmonic oscillator ones, and the spin 1/2 ones.", "There are only 2 types of physicists– those who read papers, and those who write papers.", and "There aren't many problems in life that a stiff drink can't solve."I will forever proudly call myself a product of the Pierre Meystre school of quantum optics. Thanks as well to people in our group: Hermann Uys, Om Dutta, Wenzhou Chen, Mishkat Bhattacharya, HyoJun Seok, Rina Kanamoto, Dan Goldbaum, Lukas Buchmann, Aravind Chiruvelli, Hui Jing, Greg Phelps, Mehmet Tasgin, and Lin Zhang, for providing a stimulating environment to do physics, and particularly Steven Steinke for his support, and animated discussions.

I am indebted to Ewan Wright his guidance on several problems presented in my thesis and for patiently listening to me 'solve things a different way'. I am grateful to Alex Cronin, for his mentoring and asking probing questions that led me to a deeper understanding of the problems I was working on. Thanks to Koen Visscher for his interest in this work, and the graduate student issues I brought up. Thanks also to Sumit Mazumdar for agreeing to be on this committee.

This work was done in collaboration with several groups outside UA. I would like to take this opportunity to thank the Mukund Vengalattore and Markus Aspelmeyer groups for stimulating discussions and their hospitality during my stays in Ithaca and Vienna. A particular thank you to Keith Schwab for not only being an inspiration, but also for the pep talks 'reminding me of the only reason I am in Tucson'.

Thanks to the support staff in physics and optics, particularly Mike Eklund (for his concern and hugs), Phil Goisman, Lisa Shapouri, Patty Zeigler and Kina Barton.

Graduate School is rough at times, and I was fortunate to have made some great friends. Thank you to Mike and Sybil Kruse for being there– particularly Mike for his seemingly infinite patience, and for always listening to me. Thanks also to Matt and Sarah Leone for their encouragement. Thanks to Lance, Elizabeth, Chiara and particularly Aparna for making sure I stayed sane during my roughest times here.

Thank you to the Singh and Chaudhary families for their understanding during my years in Grad School. And lastly, thanks to my husband, Abhyudai– for his undying faith in *us* during our time apart.

DEDICATION

For those who encouraged me to question everything,
and let me search my own answers.
Thank you.

TABLE OF CONTENTS

TABLE OF CONTENTS – *Continued*

LIST OF FIGURES

LIST OF FIGURES – *Continued*

ABSTRACT

This thesis concentrates on generating and measuring non-classical states of mechanical oscillators by coupling them to atomic and molecular quantum systems.

We start with a discussion of what novel physics can be explored by mechanical systems operating in the quantum regime. We then discuss one technique making it a possibility- cavity optomechanics, particularly optomechanical cooling. We investigate the limits of optomechanical cooling and review how the coupling of mechanical oscillators to external heat baths limits the minimum attainable phonon occupation number. As a possible alternative for circumventing clamping losses, we consider an all-optical approach where the mechanical element (in this case, a Bragg mirror) is suspended via optical forces, and discuss some limitations of this approach.

We explore several schemes aimed at the generation of quantum states in mechanical oscillators. We consider specifically two examples: one in which the mechanical oscillator is coupled to polar molecules via dipole-dipole interaction, and another where it is magnetically coupled to a Bose condensate. The first example emphasizes that such an interaction can generate parametric squeezing and entanglement. The second scheme demonstrates that the backaction of BEC spin measurements can be used to generate quantum states of motion of a mechanical oscillator.

We then discuss possible methods for measuring the entire density matrix of a mechanical oscillator. The first method achieves the tomographic reconstruction of the mechanical Wigner function by coupling it simultaneously to a classical optical oscillator and a qubit. The second approach invloves a state transfer scheme between momentum excitations of a bose-condensate in a cavity and a moving mirror of the cavity that is entirely mediated by the light field. We conclude with a discussion of the broader implications of this work, and some future research directions.

CHAPTER 1

QUANTUM MECHANICS WITH MECHANICAL OSCILLATORS

This thesis explores the generation and measurement of quantum states of motion of macroscopic mechanical oscillators, e.g. superposition states, number states and squeezed states. Since mechanical oscillators are affected by any external force, irrespective of its nature, they are useful for a wide range of sensing applications. More specifically, mechanical systems operating in the quantum regime have implications in quantum metrology– making force or displacement sensors operating beyond the standard limits set by quantum mechanics. We can also use this feature of mechanical systems to functionalize them so that they can interact with disparate quantum systems simultaneously, making them ideal candidates for quantum transducers. In particular, future quantum communication protocols may rely on such elements, transferring quantum information between communication and memory or processor qubits. Furthermore, at a more fundamental level, there are several untested foundational aspects of quantum mechanics that can be explored with massive quantum systems– particularly those involving the quantum-classical transition.

We start this chapter by discussing these ideas in some detail, as a motivation for the work presented later in this thesis. We then outline a central aspects of the field that are making quantum mechanics with mechanical oscillators a realistic experimental possibility- cavity optomechanics. By utilizing the non-conservative nature of radiation pressure forces, we can effectively damp the motion of a mechanical oscillator to energies where quantum effects become dominant. We discuss key features of this coupled mechanical-optical system and introduce the minimal model of cavity optomechanics, since it is used repeatedly in this thesis. We then go over some physical implementations of systems where such effects are observed, and

conclude with an outline of this thesis, summarizing the ideas that will be discussed in the following chapters.

In order to cast the problem at hand in a modern context, it is useful to consider as a starting point another field with which we will draw strong analogies and inspiration, quantum optics. Quantum optics provides some well developed ideas for generating, controlling and measuring quantum states of bosonic fields. By confining laser light in a high-Q optical resonator, for example a Fabry-Pérot interferometer with highly reflective end-mirrors, we can isolate and amplify a single mode of the light field. In addition, its confinement in a small volume (relative to free space) greatly enhances what can be thought of as 'the electric field per photon'[1]. By then coupling these photons to nonlinear elements such as two-level systems (more fashionably, qubits), we can access the quantum ladder of photon states selectively. The ability to do so forms a basis for controlling individual quantum states of light. Such control techniques can then be used to generate or preserve arbitrary quantum states on demand (3; 4)[2].

From a foundational perspective, many counterintuitive effects of quantum physics have been explored exhaustively in the context of quantum optics over the last four decades, for example the demonstration of the violation of Bell's inequalities (10), or the decay of Schrödinger cat states of photons (11), giving results in agreement with the theory of decoherence as an environmental measurement induced collapse (12; 13; 14).

Advances in nanotechnology have recently led to sufficient isolation of a single mode of vibration (a phonon mode) in nano-mechanical resonators to investigate quantum features of these systems as well. We can now draw parallels with stan-

[1]For details about how to quantize light in a cavity, please refer to any standard book on quantum optics, e.g. (2).

[2]Quantum control has also been demonstrated in several other physical systems- including ions (5), atoms(6) and molecules (7), extending to solid-state systems like quantum dots (8), and trapped impurities in diamond (9).

dard quantum optics, where a single field mode is manipulated at the quantum level. A natural extension in this context is to investigate ways to generate a coupling to various nonlinear elements- particularly atomic systems where quantum control is so well established (6). The ability to do so lays the groundwork for the quantum control of mechanical resonators. Such quantum control can then be used for precision measurement or quantum information applications.

1.1 Motivation

Now that mechanical resonators are on the verge of being controlled at the single quantum level, it is justified to pause and ask *why?* What are the similarities and differences between quantum states of the electric field and quantum states of motion of a macroscopic object? As Dirac first pointed out (15), any dynamical system of non-interacting identical bosons is analogous to a set of independent quantum harmonic oscillators– one for each independent bosonic mode. In this sense, phonon states of a single mode mechanical oscillator are mathematically identical to photon states of a single mode of an electric field.

However, there are several key differences between quantum optical and mechanical systems- the most important being the fact that mechanical systems are massive, while photons are massless. For the application and fundamental studies that we have in mind, the fact that mechanical resonators range from being tens of nanometers and weighing pico-grams, as implemented in electro-mechanical setups (16), to tens of centimeters in size and weighing tons, in the case of gravitational wave detectors (17) is also of importance.

From a technological standpoint, mechanical oscillators make unprecedented force and displacement sensors. Major advances in nanotechnology, particularly spin microscopy (18) have made it possible to measure tiny forces below 10^{-18}N (19), and displacements in the 10^{-14}m regime (20) via state-of-the-art mechanical cantilevers

used in force microscopy[3]. These mechanical cantilevers permit to detect a single electron spin (22) or sense mass at atomic resolution (23). The current sensitivity is limited by thermal noise in the mechanics. However, as mechanical oscillators gets colder these sensitivities are fast approaching the limits set by quantum mechanics. For example, ref. (20) considers a 127 MHz cantilever with effective mass 100fg. Such an oscillator has a zero-point position uncertainty, $x_{zp} = \sqrt{\hbar/(2m\omega)}$ of 2.57×10^{-14}m, which is quite close to the measured displacement sensitivity of 3.9×10^{-14}m-Hz$^{-1/2}$. The question now is to determine whether it is possible to get around the standard limits set by quantum mechanics.

There has been great interest since the 70's in using quantum oscillators to measure classical forces, with early applications directed towards the interferometric detection of gravitational waves. This has led to a detailed understanding of the standard quantum limits to such interferometric force sensing schemes and methods to overcome them (24). One such idea stems from the fact that there is an important difference between an ideal classical and quantum measurement. While an ideal classical measurement does not add any extra noise to the system being monitored, the situation is quite different in the case of quantum mechanics. For example, the Heisenberg uncertainty principle dictates that a position measurement will give a random momentum kick to the oscillator whose position is being monitored. This, in turn will affect the position of the oscillator at a later time. This effect is called measurement backaction, and the reader is referred to ref. (25) for more details. However, using techniques like quantum non-demolition measurements (26), we can eliminate the backaction of a quantum measurement of a suitable quadrature (a combination of position and momentum) of such oscillators, sending the unwanted measurement noise in an orthogonal, non-measured quadrature (27). Current advances in nanotechnology is making it possible to test some of these ideas in table-top

[3]It should be noted that optical interferometric setups have demonstrated better displacement sensitivity at 10^{-19}m-Hz$^{-1/2}$ level(21)

laboratory experiments.

Another appealing aspect of mechanical systems is that they are influenced by any kind of force, electromagnetic or gravitational. By depositing a magnetic element or a charge on a mechanical element, we can make it interact strongly with atomic systems. Alternatively, integrating mechanical systems into a resonant optical structure such as an interferometer, one can increase the radiation pressure effects i.e. the optomechanical coupling between light and mechanical elements. This makes them ideal candidates for quantum transducers that shuttle quantum information from one quantum system like photons (ideal for long distance communication) to a mechanical or atomic system that is better suited for quantum memories. Such transducers will be essential to operation of any quantum network protocols.

This unprecedented range of parameter space in mass and size provided by mechanical systems can also be used to test theories of collapse of the quantum wavefunction in new regimes (28). The central question here is that if quantum mechanics applies to all physical systems, why do we never observe quantum superpositions of macroscopic objects? While several aspects of quantum behavior in macroscopic objects have been realized in the laboratory, such as superconductivity or superfluidity, and are known to exist in nature, for example in neutron stars, the demonstration of macroscopic superposition states in gapless systems remains a challenge. In particular, mechanical systems in the quantum regime may provide an unparalleled test bed for alternative theories of collapse of the quantum wavefunction due to external physical processes. These include a continuous spontaneous localization model, which predicts a localization whose strength is proportional to the mass of the object, or a collapse induced by the interaction of a massive object with Newtonian or quantum gravity. A recent article reviews these models, and compares their postulated decoherence rates scaling with mass to the more widely accepted environmental measurement induced collapse (29). Since mechanical systems vary

in mass over a large range, they are ideal candidates to test such theories.

Thinking of efficient ways to create and detect superposition states is an interesting theoretical and experimental challenge. On one extreme, we can think of space-based experiments, with an incomparable degree of isolation of a test mass, as discussed in ref. (30). A less exotic setup includes levitated objects, where a dielectric object is suspended using the optical dipole force provided by non-resonant lasers – this is the force used in optical tweezers. The isolation from environment provided by such systems makes them suitable candidates to explore the quantum-classical interface even in room temperature environments, as discussed in ref. (29). It should be noted that state of the art matter-wave experiments with large molecules, with superposition states consisting of around 10^4 atoms, are probably the most promising current systems for tests of wave function collapse theories (31). A more practical outcome of all such experiments with massive objects will be to better understand and quantify the role of the environment in the onset of decoherence, and ways to mitigate these effects.

There are other quantum phenomena that can be explored in mechanical systems operating deep in the quantum regime. For example, there was a recent proposal to accurately measure the position-momentum commutation relation using optomechanical systems in order to test for corrections due to quantum gravity (32). Another proposal considers the possibility of observing macroscopic tunneling of a mechanically compliant membrane in a double-well potential (33).

1.2 Optomechanical cooling

Having discussed some of the motivation for doing quantum mechanics with mechanical objects composed of billions of atoms, we now discuss how is it possible to isolate and cool mechanical harmonic oscillators to a point where quantum effects become dominant.

Let us begin with a comparison of energy scales involved in optical vs. me-

chanical oscillators. In the absence of external forces, an oscillator is in thermal equilibrium with its environment, having average energy $k_B T$, where k_B is the Boltzmann constant, and T is the temperature. For a quantum oscillator this average energy corresponds to $(\bar{n}_{\rm th} + 1/2)\hbar\omega$, where $\bar{n}_{\rm th}$ is the average number of quanta (phonons/photons) excited in the field mode at temperature T as determined by Planck's law,

$$\bar{n}_{\rm th} = \frac{1}{e^{\frac{\hbar\omega}{k_B T}} - 1}. \tag{1.1}$$

For a laser field with frequency $\omega \sim 2\pi \times 10^{15}$ rad/s, $\bar{n}_{\rm th} \approx 0$ even at room temperature. This implies that optical fields are not subject to thermal excitations, and as such they are well suited to the observation of quantum effects. However, things are quite different in case of mechanical oscillators. Considering a high frequency resonator of $\omega \sim 2\pi \times 10^9$ rad/s, $\bar{n}_{\rm th}$ is around 6000 at room temperature, and quantum effects are completely washed out by thermal excitations. We therefore have to cool mechanical systems such that $k_B T \lesssim \hbar\omega$ in order to observe quantum effects.

For high enough mechanical frequencies, the average number of thermal phonons can be reduced to practically zero by placing the system in a cryostat environment. The first demonstration of cooling a mechanical oscillator to its quantum mechanical ground state was achieved precisely in this way (34). In this experiment, a mechanical oscillator with COM frequency of 6GHz was placed in a dilution refrigerator with a bath temperature of around 25 mK, giving an average phonon occupation well below unity.

For lower frequency systems, however, this approach is no longer possible. Instead, recent work has used a laser cooling technique directly inspired by the laser cooling of trapped ions, for which the ground state cooling of mechanical motion was demonstrated in the 90's (35), following the pioneering laser cooling ideas developed for atoms (36) and ions (37). In a parallel development, the effect of radiation pressure forces was investigated in the context of gravitational wave interferometers.

Here, it was realized that similar to the case in atoms and ions, the non-conservative nature of radiation pressure force between optics and mechanics can be used to damp the motion of massive mechanical oscillators. One important difference is that the optomechanical cooling of massive objects does not rely on internal resonances, as is the case for ion or atom cooling. Rather, it combines a non-resonant radiation force acting on the mechanical system with the resonant enhancement provided by an artificially engineered structure, for instance a Fabry-Pérot interferometer.

In an interferometer with an oscillating end mirror, radiation pressure forces can lead to several non-intuitive effects. In the context of this thesis, the most important of these are the so-called "optical spring effect," which can result in a significant stiffening of the mirror motion and to optical bistability, and "cold damping", where the interaction itself provides the damping force needed to cool mechanical motion. A classical description these effects is reviewed in Appendix A. Here, we focus on a simple physical picture that explains the underlying coherent processes behind optomechanical cooling in terms of a Raman scattering analogy (38; 39).

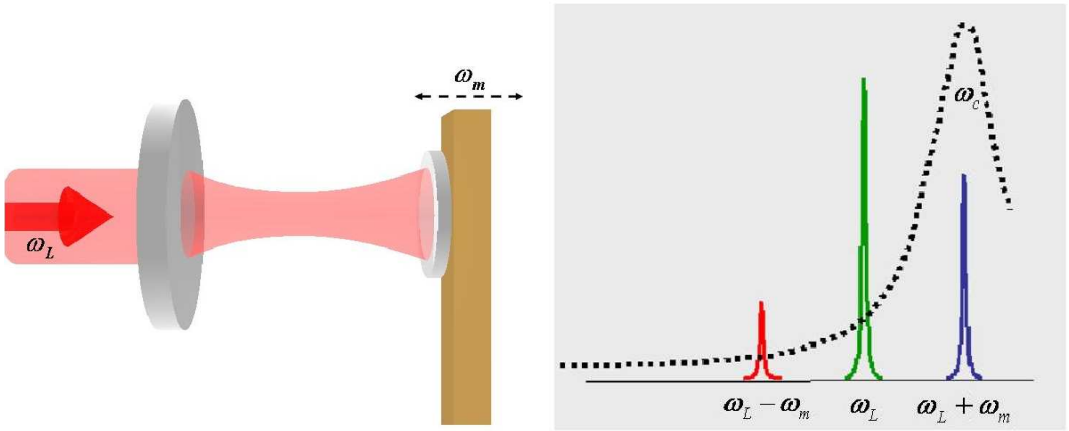

Figure 1.1: (a) Schematic of Fabry-Pérot interferometer with a moving mirror. (b) Quantum picture of optomechanical cooling, showing the two sidemodes due to mechanical oscillations, and the asymmetric cavity response that leads to cooling.

The non-resonant interaction between the laser and mechanical oscillator can be thought of as a Raman scattering process. The laser photons (of frequency ω_L) interact with the mechanical oscillator of frequency ω_m and are scattered off with frequencies ω_L, corresponding to elastic scattering, and also at frequency $(\omega_L - \omega_m)$ and $(\omega_L + \omega_m)$ due to interaction with the mechanical oscillator. The blue-shifted light at frequency $(\omega_L + \omega_m)$ results from the emission of a phonon of mechanical motion, and can be understood as an anti-Stokes process. On the other hand, the light at frequency $(\omega_L - \omega_m)$ is red-shifted due to absorption of a phonon, and corresponds to a Stokes process. If the damping of the anti-Stokes sidemode is somehow enhanced compared to that of the Stokes process, the oscillator will lose phonons overall, resulting in cooling of that mode of oscillation. This asymmetry in damping can be provided by the optical resonator, as depicted in Fig. 1.1(b): provided that the laser is detuned with respect to the cavity such that the Stokes process is suppressed by the cavity transmission, while the anti-Stokes process is enhanced. It is this asymmetric response to the two motional sidebands that leads to cooling of the mechanical motion. This process also puts stringent requirements for efficient cooling. Ideally, the cavity linewidth κ must be such that $\kappa \ll \omega_m$ in order to strongly distinguish the two modes in the cavity response, hence the name resolved sideband cooling. We shall discuss this cooling scheme and its limitations in more detail in Chapter 2.

1.3 Quantum optomechanical effects

Ground state cooling is not the only interesting physics that can be explored via optomechanical interaction. In order to discuss other quantum effects, we proceed by first deriving the simplest form of the optomechanical interaction Hamiltonian. We consider a single mode of a high-Q Fabry-Pérot cavity with one fixed and one harmonically oscillating end mirror, as depicted in Fig. 1a. The Hamiltonian for

this system is

$$H = \hbar\omega_c \hat{a}^\dagger \hat{a} + \hbar\omega_m \hat{b}^\dagger \hat{b}. \tag{1.2}$$

Here ω_c is the cavity frequency and ω_m is again the frequency of the center-of-mass motion of the oscillating mirror, and $\hat{a}$ and $\hat{b}$ are the bosonic field modes characterizing the two oscillators, light ($\hat{a}$) and mechanical oscillator($\hat{b}$). The optical mode frequency ω_c is modified by the mirror displacement, $\omega_c(x) \approx \omega_c + x\frac{\partial \omega_c}{\partial x} + \ldots$, so that keeping only the linear terms in mirror motion, and defining $g = \partial\omega_c/\partial x$, we get

$$H = \hbar(\omega_c + g\hat{x})\hat{a}^\dagger \hat{a} + \hbar\omega_m \hat{b}^\dagger \hat{b}. \tag{1.3}$$

For a Fabry-Pérot, $g = -\omega_c/L$, where L is the length of the cavity. Using the standard definition of $\hat{x} = x_{zp}(\hat{b} + \hat{b}^\dagger)$, where $x_{zp} = \sqrt{\hbar/2m\omega_m}$, the zero-point displacement, we arrive at

$$H = \hbar\omega_c \hat{a}^\dagger \hat{a} + \hbar\omega_m \hat{b}^\dagger \hat{b} + \hbar g_0 \hat{a}^\dagger \hat{a}(\hat{b}^\dagger + \hat{b}). \tag{1.4}$$

Here, $g_0 = g x_{zp}$ characterizes the coupling between a single photon and single phonon, and is called the optomechanical coupling strength in the literature.

The Hamiltonian in Eq. (1.4) allows us to briefly discuss several important phenomena that can be observed in such coupled systems. We start with simplifying the interaction by moving to a displacement picture. If the cavity field comprises of a macroscopic classical component $\langle a \rangle$, it is convenient to write the field operators as $\hat{a} \to \langle a \rangle + \delta\hat{a}$. Here, $\langle a \rangle$ is the classical field and δa is the bosonic field operator that describes its quantum features. The field photon number operator then becomes $\hat{a}^\dagger \hat{a} \approx \langle a^\dagger a \rangle + \langle a \rangle \delta\hat{a}^\dagger + \langle a^\dagger \rangle \delta\hat{a} + \ldots$, where we have ignored the second order term in the field operators. With this approximation, and assuming for simplicity that $\langle a \rangle$ is real, the optomechanical interaction simplifies to

$$V_I = \hbar g_0 \left[\langle a^\dagger a \rangle + \langle a \rangle (\delta\hat{a} + \delta\hat{a}^\dagger)\right](\hat{b} + \hat{b}^\dagger). \tag{1.5}$$

The first term leads to a Kerr-like nonlinearity whose main features can be understood in the context of the classical theory reviewed in Appendix A. It is also

responsible for an "optical spring effect", which can result in a very large increase in ω_m for appropriate laser-resonator detuning. From Eq. (1.1) it is obvious that although this is not a cooling process, increasing ω_m decreases the mean phonon number of the oscillator, and this is one method that can be used to reach the quantum regime.

Moving to a rotating frame where operators $\delta\hat{a}$ rotate at the laser frequency ω_L, the system Hamiltonian, including the interaction described by Eq. (1.5), becomes

$$H = \hbar\Delta_c \delta\hat{a}^\dagger \delta\hat{a} + \hbar\omega_m \hat{b}^\dagger \hat{b} + \hbar g_0 \langle a\rangle (\delta\hat{a} e^{i\Delta_c t} + \delta\hat{a}^\dagger e^{-i\Delta_c t})(\hat{b} + \hat{b}^\dagger), \tag{1.6}$$

where the detuning $\Delta_c = \omega_L - \omega_c$. If the detuning is such that $\Delta_c = -\omega_m$, after making the rotating-wave approximation, the interaction picture Hamiltonian becomes

$$H = \hbar G(\delta\hat{a}\hat{b}^\dagger + \delta\hat{a}^\dagger \hat{b}). \tag{1.7}$$

This Hamiltonian is known in quantum optics as the "beam-splitter" Hamiltonian (2). It leads to coherent state swapping between the photon and phonon modes. Thus, as long as $G \gg \kappa, \gamma_m$, we can have a perfect transfer of quantum states from optics to mechanics and vice-versa for $G\langle a\rangle t = \pi/2$. The use of this interaction for quantum state-transfer will be discussed in more detail in Chapter 4.

If the interaction between the two oscillators is very strong, it is characterized by normal mode splitting– when the mechanical and optical system are so strongly coupled that neither oscillator's energy eigenbasis is a good basis of the combined system. Instead, the system's eigenstates are superpositions of the two earlier eigenstates. Normal mode splitting is also observed in classical systems. However, its appearance in quantum systems implies coherent and reversible exchange of energy. Such sidemode splitting has been observed in several optomechanical systems, the first one being a movable mirror Fabry-Pérot cavity (1).

Finally, if $\Delta_c = \omega_m$, the interaction hamiltonian becomes

$$H = \hbar G(\delta\hat{a}\hat{b} + \delta\hat{a}^\dagger \hat{b}^\dagger). \tag{1.8}$$

This Hamiltonian is known as the "two-mode squeezing" Hamiltonian in quantum optics (2). In addition to two-mode squeezing, it can also lead to quantum entanglement between optics and mechanics. We discuss this interaction in more detail in Chapter 3. That form of the optomechanical interaction also gives rise to a range of interesting nonlinear effects that include self-induced mechanical motion, sometimes called phonon lasing, dynamical instabilities, and a number of other effects. We do not discuss any of these features in this thesis, and refer the reader to ref. (40) for more details.

Having discussed two harmonic oscillators, it is only logical to briefly mention quantum effects in three harmonic oscillators coupled to each other. If two oscillators $(\hat{b}_1, \hat{b}_2)$ are coupled to a third one $(\hat{a})$ in a regime where the rotating wave approximation is valid, the linearized (interaction picture) system Hamiltonian has the form

$$H = \hbar G \hat{a}^\dagger (\hat{b}_1 + \hat{b}_2) + c.c., \tag{1.9}$$

where for simplicity we have assumed equal coupling strengths G. This Hamiltonian can be diagonalized exactly, and rewritten as $H = \hbar G \sum_{i=+,-,\mathrm{dk}} \hat{c}_i^\dagger \hat{c}_i$, with

$$\begin{aligned} \hat{c}_\pm &= (\hat{c}_{\mathrm{br}} \pm \hat{a})/\sqrt{2} \\ \hat{c}_{\mathrm{dk}} &= (\hat{b}_1 - \hat{b}_2)/\sqrt{2}, \end{aligned}$$

where $\hat{c}_{\mathrm{br}} = (\hat{b}_1 + \hat{b}_2)/\sqrt{2}$

The existence of a mode c_{dk} that is only a linear combination of oscillators b_1 and b_2 implies that under certain conditions, the quantum probability amplitudes for the energy transition from system b_1 to a and transition from b_2 to a can interfere destructively leading to zero transition probability to mode a from either of the two modes. This phenomenon is called electromagnetically induced transparency and it has been previously studied in atomic systems (41). An extension of this scheme to mechanical systems was observed in radiation pressure coupled optical oscillators (42; 43). In an optomechanical system, this technique can lead to tunable and

efficient delay of light pulses.

Finally, we briefly comment on an optomechanical resonator geometry called the "membrane-in-the-middle" configuration. In geometries where the oscillating mechanical element is placed inside the resonator, instead of playing the role of an end mirror, it is possible to achieve conditions where the optomechanical coupling is no longer linear in $\hat{x}$, but rather quadratic. A quadratic coupling can then enable quantum non-demolition measurement of the membrane motion (26). A simple treatment of static effects in such 3-mirror systems was studied theoretically by Meystre *et. al* as early as 1985 (44). More recently Harris and co-workers physically implemented a membrane-in-the-middle system (45), and observed this dispersive and later the strong coupling (46) in these systems. One important feature of this geometry is the ability of tune the optomechanical coupling from linear to quadratic dynamically. Along with the ability to do non-destructive quantum measurements, such couplings can also lead to squeezed and entangled state generation.

1.4 Experimental implementations

Optical interferometers with suspended end-mirrors were first considered by the gravitational wave detection community, which developed a detailed understanding of their noise properties, understood first the role of shot noise and radiation pressure noise in their operation, and demonstrated a number of their fundamental classical properties, for example the modification of spring constant and cooling (47). The first demonstation of bistability due to radiation pressure effects was also achieved in such a setup (48). An extreme of this scheme is depositing highly reflective coatings on a micro-mechanical cantilever and using it as the moving mirror of a Fabry-Pérot. Such configurations have been used to demonstrate active feedback cooling schemes involving radiation pressure (49) and observe strong coupling effects in optomechanics (1).

With rapid advances in nano fabrication there is now a growing number of other

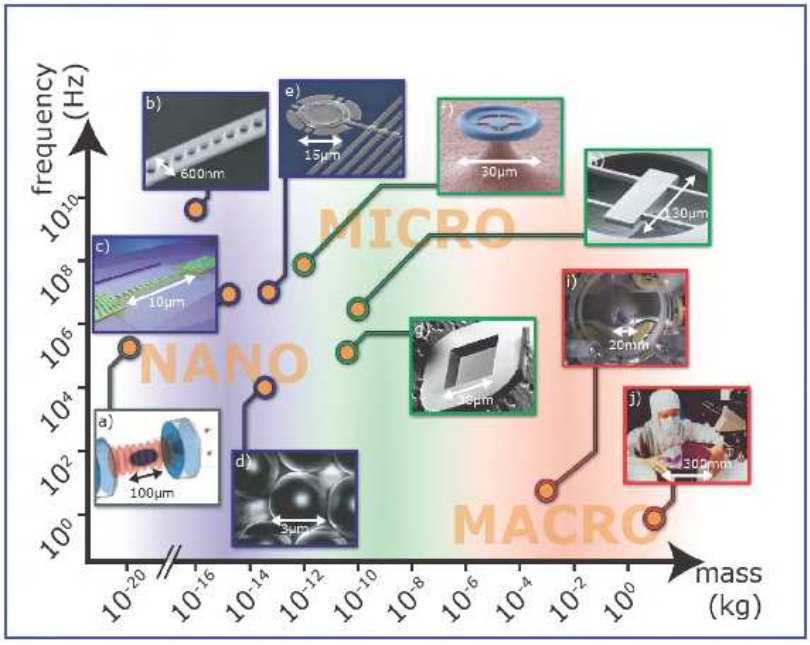

Figure 1.2: Current experimental implementations of optomechanical systems, ranging over many orders of magnitude in resonant frequency and mass of the mechanical element. (a)Ultra-cold atoms in a cavity, (b) Nano-beams in photonic crystals, (c)Integrated silicon photonic circuit, (d) levitated microspheres, (e) capacitors in superconducting microwave circuits, (f) Microtoroid optical resonators, (g)Membranes inside optical cavities, (h)micro-cantilevers with mirror coatings, (i,j) suspended mirrors in gravitational wave detectors. Figure courtesy of P. Meystre, M. Aspelmeyer and K. C. Schwab.

coupled optical-mechanical systems in which dynamical effects due to radiation pressure have been observed, as depicted in Fig. 1.2.

One class of systems involves optical micro-resonators instead of Fabry-Pérot interferometers, where the whispering gallery mode of a circular resonator is used as the optical resonator. A mechanical breathing mode of the structure changes the effective optical path length, leading to optomechanical effects. Such systems have high optical and mechanical quality factors and have been used to demonstrate

several dynamical backaction effects (50), including resolved-sideband cooling of mechanical motion (51) and optomechanically induced transparency (42).

Nano-beams made out of photonic-crystal cavities provide strong optomechanical couplings and have been used to demonstrate ground-state cooling (52), optomechanically induced transparency (43) and are currently the most promising candidates for observation of nonlinear photon-phonon interaction in solid-state mechanical systems, along with the ability to be integrated with several silicon based optical or mechanical devices.

In the microwave regime, an LC circuit forms the 'optical' resonator. If the capacitor is designed such that one of the plates is suspended and can undergo harmonic motion, we have the equivalent of an optomechanical setup. Such setups have been used to demonstrate ground state cooling(16) and strong coupling between mechanical and optical systems (53). One additional advantage of these schemes is the ability to couple to solid-state 2-level systems such as Cooper-pair boxes (54) or Josephson junction qubits (34).

In order to suppress clamping losses, several groups are investigating a levitated dielectric object using optical gradient forces (55), as routinely done with optical tweezers in atomic or biophysics (56). The center-of-mass motion of this trapped isolated system forms a mechanical oscillator to be cooled. In chapter 2, we discuss one such implementation of levitated dielectrics as optomechanical systems.

Lastly, ultracold atoms in optical cavities can be used to realize optomechanical interaction, and have been used to demonstrate effects like bistability (57; 58). Since they are already cooled to their motional ground state, they form ideal canonical systems to study nonlinear optomechanical effects. One such system, momentum excitations of a Bose-Einstein condensate (BEC), is discussed in more detail in Chapter 4.

This is not an exhaustive list of experimental systems being used to study mechanical systems in the quantum regime, and the list is rapidly growing. However,

it introduces most of the experimental systems considered in this thesis. For a more detailed discussion of experimental realizations and their advantages and disadvantages, the reader is referred to several recent review articles on cavity optomechanics (40).

1.5 Outline of this thesis

As mentioned earlier, this thesis primarily concentrates on generating and measuring non-classical states of mechanical oscillators by coupling them to atomic and molecular quantum systems (and sometimes vice-verse). Here we summarize the contents of the following chapters.

Chapter 2 provides an example of cooling a mechanical element to its ground state via optomechanical effects. We start with a discussion of the limits of optomechanical cooling and how the coupling of mechanical system to an external heat bath via structural supports limits the minimum attainable phonon occupation number. We then discuss an all-optical approach towards ground state cooling where the mechanical element (in this case, a Bragg mirror) is suspended via optical forces. Finally, we conclude with the discussion of the limitations of such an all-optical approach towards cooling mechanical motion to its quantum ground state.

The generation of quantum states of a harmonic oscillator by coupling it to another oscillator or spin systems forms the bulk of Chapter 3. We discuss two nonlinear interactions: one in which an oscillator is coupled quadratically to another oscillator, and another case where an oscillator is coupled to a spin. The first is concerned with generating squeezed and entangled states of motion of polar molecules by coupling their motion to mechanical motion. Here, we show that the nonlinearity produced by dipole-dipole interaction can generate parametric squeezing and entanglement. The second project deals with a BEC that is magnetically coupled to a membrane mechanical oscillator. This coupling between spin and position is then used to demonstrate the generation of measurement backaction induced quantum

states of motion. We comment on the conditional nature of these states, and the effect of thermal dissipation of the mechanical element on quantum features of the non-classical states generated.

Chapter 4 explores ways to measure non-classical states. We discuss two projects that deal with measuring the entire density matrix of a state. The first one is about tomographic reconstruction of mechanical density matrix (or equivalently the Wigner function) by coupling it simultaneously to a classical optical oscillator and a qubit. The second project concerns a state transfer scheme between momentum excitations of a bose-condensate in a cavity and a moving mirror of the cavity that is entirely mediated by the light field.

Finally, Chapter 5 discusses the broader implications of this work, and some future research directions.

CHAPTER 2

TOWARDS THE GROUND STATE

As discussed in chapter 1, operating macroscopic objects in the quantum regime is a challenge whose successful completion will have profound implications, ranging from an improved fundamental understanding of the quantum-classical interface and of the quantum measurement process to the development of quantum detectors of unsurpassed sensitivity. Cooling a nanomechanical system to its ground state of center-of-mass motion is an important step toward that goal, and spectacular progress has recently occurred via an interdisciplinary approach combining tools from nanoscience, quantum optics, and condensed matter physics.

One of the simplest systems being considered in this quest consists of a small vibrating element that forms one of the end-mirrors of a Fabry-Pérot cavity, and we discussed optomechanical interactions in such a setup in the previous chapter and in Appendix A. We start this chapter by a discussion of the limits to dynamical optomechanical cooling. Here we introduce the coupling of an oscillator to a thermal bath, and how it sets the limit to its minimum thermal excitation. So far the biggest hurdle in achieving ground-state cooling of such a mirror has been its coupling to a thermal reservoir by way of a mechanical support, which acts as the dominant source of dissipation and decoherence. We then theoretically discuss an alternative configuration where the mechanical clamping of the system is replaced by an optical spring realized by an optical tweezer. We conclude with a discussion of additional sources of dissipation and decoherence, and the limits to this optomechanical scheme in reaching the quantum regime.

2.1 Limits of optomechanical cooling scheme

The rate equation that governs the change in the mean energy $\langle E \rangle$ of a system coupled to a thermal bath at temperature T_{bath} is given by

$$\frac{d\langle E \rangle}{dt} = -\gamma_m \langle E \rangle + \gamma_m k_B T_{\text{bath}}. \tag{2.1}$$

Here, γ_m determines the coupling rate of the system – here a mode of vibration of the mechanical resonator – to the bath. As energy is dissipated into the environment at a rate γ_m, heat creeps into the system for the heat bath as well, ensuring that the steady state reaches thermal equilibrium with its surrounding. Ideally, we need a strong coupling to a very cold bath to cool any system fast. As discussed in section 1.2, the idea of cold damping in cavity optomechanics is to couple the oscillator to a second thermal bath that is effectively at zero temperature. This is achieved via the coupling of the mechanical oscillator to an intracavity optical field subject to a damping rate $\Gamma_{\text{opto}} > 0$. Due to the high frequency of optical fields, they are coupled to a thermal reservoir that is effectively at zero temperature, so that Eq. (2.1) becomes

$$\frac{d\langle E \rangle}{dt} = -(\gamma_m + \Gamma_{\text{opto}}) \langle E \rangle + \gamma_m k_B T_{\text{bath}}. \tag{2.2}$$

From the equipartition theorem applied to a single oscillator we have that in steady state $\langle E \rangle = k_B T_{\text{eff}}$, such that

$$T_{\text{eff}} = \frac{\gamma_m}{\gamma_m + \Gamma_{\text{opto}}} T_{\text{bath}}. \tag{2.3}$$

Alternatively, with $\langle n \rangle \approx k_B T / \hbar \omega_m$ we have for the average phonon excitation of the mechanical oscillator

$$\langle n \rangle_{\text{min,R}} = \frac{\gamma_m}{\gamma_m + \Gamma_{\text{opto}}} \bar{n}_{\text{th}}. \tag{2.4}$$

Along with the limit to minimum phonon number set by the reservoir, there is the limit set by the cooling scheme itself. The cooling scheme is implemented in

optomechanics relies on dynamical backaction, and classically the cooling rate is given by Eq. (A.18). Here, we shall state its quantum mechanical equivalent. The detailed derivation is given elsewhere, for example in ref. (59), and we refer the reader to this review article for more information.

We start with Eq.(A.18) describing the cooling rate for the mechanical oscillator. We can re-write Eq.(A.18) in a more intuitive manner as

$$\begin{aligned}\Gamma_{\text{opto}} &= g_0^2 \frac{P_{\text{in}}}{\hbar\omega_c} \frac{\kappa}{\Delta_c^2 + (\kappa/2)^2} \left[\frac{\kappa/2}{(\Delta_c + \omega_m)^2 + (\kappa/2)^2} - \frac{\kappa/2}{(\Delta_c - \omega_m)^2 + (\kappa/2)^2} \right]. \\ &= A^- - A^+. \end{aligned} \tag{2.5}$$

Here, $g_0 = g x_{zp} = (\omega_c/L)\sqrt{\hbar/2m\omega_m}$ characterizes the coupling between a single photon and single phonon, ω_c is the cavity frequency, Δ_c is the detuning of the laser with respect to the cavity, ω_m is the mechanical resonance frequency and L is the length of the cavity. As mentioned in section 1.2, the overall cooling rate is simply the difference of two processes: A^+ is the rate of the Stokes process that leads to phonon gain and A^- is the rate of the anti-Stokes process that leads to phonon loss.

This classical result needs to be corrected to account for the fact that the annihilation and creation of phonons go with prefactors $(n+1)$ and n respectively, due to their bosonic character. Thus, the transition rate between adjacent phonon excitation states becomes

$$\begin{aligned}\Gamma_{n\to(n+1)} &= (n+1)A^+, \\ \Gamma_{n\to(n-1)} &= nA^-. \end{aligned}$$

We combine this rate with the heating due to the environment, characterized by

$$\begin{aligned}\Gamma_{n\to(n+1)} &= (n+1)A^+_{\text{th}}, \\ \Gamma_{n\to(n-1)} &= nA^-_{\text{th}}, \end{aligned}$$

where $A^+_{\text{th}} = \bar{n}_{\text{th}}\gamma_m$ and $A^-_{\text{th}} = (\bar{n}_{\text{th}} + 1)\gamma_m$. Furthermore, using the fact that the average phonon occupation $\bar{n} = \sum_0^\infty nP_n$, where P_n is the probability to be state n,

the rate of change of $\bar{n}$ due to cooling and coupling to thermal bath becomes

$$\dot{\bar{n}} = (\bar{n}+1)(A^{+}+A^{+}_{\mathrm{th}}) - \bar{n}(A^{-}+A^{-}_{\mathrm{th}}). \tag{2.6}$$

Solving for the steady state gives us the final occupation number

$$\langle n \rangle_{\mathrm{min}} = \frac{A^{+}+\bar{n}_{\mathrm{th}}\gamma_m}{\Gamma_{\mathrm{opto}}+\gamma_m}. \tag{2.7}$$

For completeness, the minimum occupation number in the absence of the reservoir is simply

$$\langle n \rangle_{\mathrm{min,C}} = \frac{A^{+}}{\Gamma_{\mathrm{opto}}}. \tag{2.8}$$

Eq. (2.7) gives us a few physical insights into efficient optomechanical cooling. In order to achieve ground state cooling, i.e. $\langle n \rangle_{\mathrm{min}} < 1$, we can see that it is advantageous to start with a cold reservoir (hence smaller $\bar{n}_{\mathrm{th}}$). In addition, for optomechanical cooling to work efficiently, we also need to have $\omega_m >> \kappa$, i.e. to be in the resolved sideband regime. This condition ensures that the Stokes heating of the mechanics is highly suppressed by the cavity. However, most current experimental realizations of optomechanical cooling are only marginally in the resolved sideband regime. Thus, the coupling of mechanical element to the reservoir sets the limit to the lowest average phonon occupation number. In the following, we show ground state cooling can be demonstrated even in the marginally resolved sideband regime even for a room temperature bath if the mechanical resonator is suspended in vacuum via optical tweezers. The work presented in the following sections is published in ref. (60).

2.2 All-optical optomechanics

There is a large volume of work on the trapping of dielectric particles – from atoms to bacteria, in the focus of laser beams far-detuned from any electronic resonance (56). Over the last two decades optical tweezers have matured into a well established tool, providing elegant and relatively simple ways to control the motion and

to measure the weak forces acting on particles suspended in a fluid or in vacuum. Exploiting this idea, several recent theoretical proposals have considered levitating macroscopic objects (spheres or even living organisms) in a cavity and cooling them to their ground state of center-of-mass motion (61; 62; 63). A key observation in the present context is that macroscopic objects optically levitated in vacuum are remarkably isolated from most environmental noise sources (64). This leads us to introduce the paradigm of an optical spring mirror, in which an optomechanical cavity mirror is suspended by light rather than by mechanical clamps. This approach provides an elegant route toward the elimination of the mirror clamping losses already mentioned, and has the potential to relatively easily reach the quantum regime. We also remark that trapping and cooling a dielectric end mirror of a resonator, rather than an object inside a resonator, results in scattering losses significantly reduced compared to the case of spheres. The optical spring mirror that we propose is a dual-disk structure comprised of a silica disc that is connected via a silica pillar or pedestal to a disk mirror, the geometry of which is illustrated in the inset in Fig. 2.1. The idea is that the structure is held in vacuum by the optical gradient force due to two linearly polarized elliptical gaussian beams of equal wavelength λ that are applied solely to the silica disk to avoid laser heating of the disk mirror. The disk mirror is a Bragg mirror composed of alternating layers of two dielectrics that acts as an end mirror for the cavity. The silica disk axis is along the z-axis of the Fabry-Pérot interferometer, and perpendicular to the trap beams, see Fig. 2.1. The tweezer beam traveling in the x-direction is polarized along the y-direction, and the beam traveling in the y-direction is polarized in the x-direction; the orthogonal polarizations being chosen to avoid the onset of interferences in the overlap region of the beams. Both beams have an elliptical transverse profile with the smallest beam waist along z, so as to provide a tight confinement along that axis and to avoid overlap with the disk mirror. The total intensity of the trapping beams has

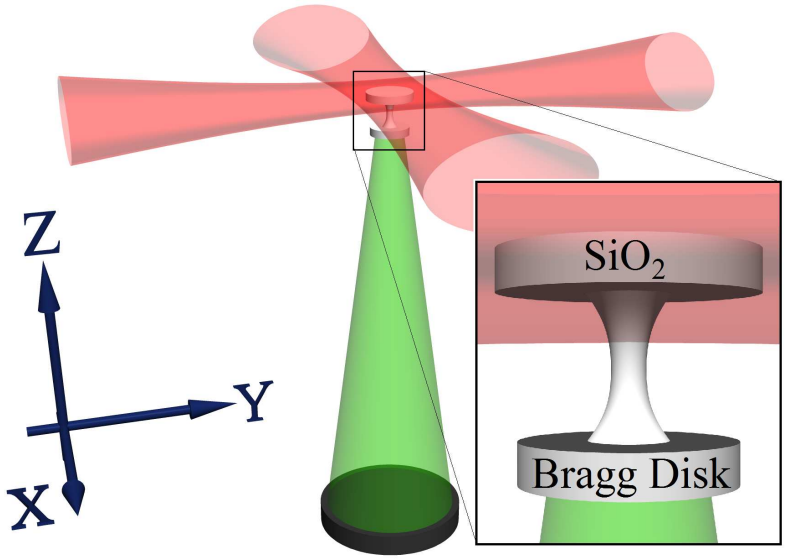

Figure 2.1: Arrangement for an optomechanical cavity without clamping losses. The disk mirror is trapped in the optical tweezer by the crossed elliptical Gaussian beams shown in red, and provides the moving mirror for the Fabry-Pérot aligned along the z-axis shown in green.

the form

$$I(\mathbf{r}) = I_{0x}\frac{\exp\left[\frac{-2y^2}{w_{0y}^2(1+x^2/y_r^2)}+\frac{-2z^2}{w_{0z}^2(1+x^2/z_r^2)}\right]}{\sqrt{(1+x^2/y_r^2)\,(1+x^2/z_r^2)}} + I_{0y}\frac{\exp\left[\frac{-2x^2}{w_{0x}^2(1+y^2/x_r^2)}+\frac{-2z^2}{w_{0z}^2(1+y^2/z_r^2)}\right]}{\sqrt{(1+y^2/x_r^2)\,(1+y^2/z_r^2)}}, \tag{2.9}$$

where I_{0x} and I_{0y} are the on-axis intensities of the laser beams traveling in the x and y directions, $w_{0\mu}$ is the focused beam waists with $\mu = x, y, z$, and $\mu_r = \pi w_{0\mu}^2/\lambda$ the Rayleigh ranges along the respective directions.

For concreteness we consider the case of a Nd:YAG trapping laser (λ=1.064 μm) that is far detuned from any material resonance in the silica disk. In this far-detuned limit we may assume that the field induces a dipole moment $\mathbf{p} = \alpha\mathbf{E}$ in the material, where α is the polarizability tensor and $\mathbf{E}$ the electric field envelope. Further assuming that the field envelope varies little over the dimensions of the disk, the components of the polarizability tensor can be approximated by those

induced by a uniform electric field, and the trapping potential can be approximated by that of a static field, with a factor of 2 reduction due to time averaging. The static polarizability of a dielectric cylinder in a uniform static field has previously been calculated numerically (65). Instead, we use the analytical expression for the polarizability of a spheroid (66), which is close to that of a cylinder of the same permittivity ϵ and aspect ratio. For our parameters, that approximation results in an error of about 3% in the value of the components of the polarizability tensor. The transverse and longitudinal polarizabilities of a spheroid of diameter d, height h, length l, eccentricity $e = \sqrt{(d/h)^2 - 1}$ and volume V are then given by

$$\alpha_{\perp,z} = \epsilon_0 V \left[\frac{\epsilon_r - 1}{1 + N_{\perp,z}(\epsilon_r - 1)} \right], \tag{2.10}$$

where $\epsilon_r = \epsilon/\epsilon_0$ is its relative permittivity, $N_z = (1 + e^2)\,(e - \arctan e)\,/e^3$, and $N_\perp = 0.5(1 - N_z)$.

We next estimate the optical trap frequencies for our optical spring mirror. For a silica disk of dimensions $d = 60$ μm, $h = 2.5$ μm, and a net mass $m = 3.87 \times 10^{-11}$ kg for the dual -disk structure (the mirror diameter and height being 50μm and 3.04μm respectively), this gives $\alpha_\perp = 1.66 \times 10^{-25}$ C$\cdot$m^{2}V^{-1} and $\alpha_z = 4.88 \times 10^{-26}$ C$\cdot$m^{2}V^{-1}. The optical potential due to the gradient force is then

$$V(\mathbf{r}) = -\alpha_\perp I(\mathbf{r})/(2\epsilon_0 c), \tag{2.11}$$

$\mathbf{r}$ being small displacements about the origin. For small deviations along the z-axis this yields a harmonic potential of frequency

$$\omega_z = \left[\frac{2\alpha_\perp}{mc\epsilon_0 w_{0z}^2} (I_{0x} + I_{0y}) \right]^{1/2}, \tag{2.12}$$

For Nd:YAG laser beams of intensity .1 W/μm^2 and beam waists $w_{0x} = w_{0y} = 100$ μm and $w_{0z} = 4$ μm, we then find $\omega_z = 2.01 \times 10^5$ rad/s, and in a similar manner we find $\omega_{x,y} = 8.29 \times 10^3$ rad/s for the transverse trapping frequencies.

Next we assess the angular motion of the disk with respect to the x and y axes, see Fig. 2.1. In particular, we calculate the wobble frequency $\omega_{\rm wob}$ of the disk when it is misaligned by an angle θ with respect to the x-axis. Such motion of asymmetric isotropic objects in linearly polarized optical traps has previously been studied in detail, for example in Ref. (67). We estimate $\omega_{\rm wob}$ by considering a light beam propagating in the y-direction and polarized along x. For a disk misaligned by an angle θ with respect to the x-axis the induced dipole moment is

$$\mathbf{p} = [\alpha_\perp E_0 \cos\theta \hat{\mathbf{x}} + \alpha_z E_0 \sin\theta \hat{\mathbf{z}}]. \tag{2.13}$$

An analysis of small angle harmonic rotational motion along y shows that it has the frequency

$$\omega_{\rm wob} = \left[\frac{12 I_{0y}(\alpha_\perp - \alpha_z)}{\epsilon_0 c \mathcal{I}_x}\right]^{1/2}, \tag{2.14}$$

where $\mathcal{I}_x = m(3d^2/4 + h^2)$ is the moment of inertia of the disk along x. For our parameters we find $\omega_{\rm wob} = 2.3 \times 10^4$ rad/s. We note that $\omega_z >> \omega_{\rm wob}$ thereby ruling out any parametric coupling between the wobble mode and the longitudinal mirror motion. This means that the wobble mode should not be detrimental to cooling the longitudinal mirror motion.

Although the silica disk is nominally transparent to the trapping lasers, it will absorb some light, and with no heat sinking the only way to dissipate this energy is through blackbody radiation (61). Taking the absorption coefficient $\alpha = 10^{-5}$/m due to UV absorption, we find that the temperature of the mirror increases by a modest 0.4 K, thereby causing no material damage. [1]

Having established the mechanical properties of the trapped Bragg disk, we now turn to a discussion of the Fabry-Pérot in which the Bragg disk serves as a vibrating

[1] The high laser power requirement (around 50 W) is a consequence of our simplified calculation of the slab polarizability tensor. This requirement can be easily reduced by using tightly focused beams, but they require a more careful description of $\alpha_{\perp,z}$, an unnecessary complication for our proof of principle analysis.

end-mirror . The fixed mirror of the Fabry-Pérot interferometer, assumed to have a reflectivity R_f=0.999998, is placed at a distance L= 3.999 cm from the movable mirror of lower reflectivity R_m= 0.9998. We note that small mirrors of comparable or smaller sizes with reflectivity exceeding 0.9998 are already being used in experiments (68; 1). For $\lambda = 852$ nm, the cavity damping rate is $\kappa = \pi c/\mathcal{F}L \approx 7.5\times10^5$ rad/s ($\mathcal{F}$ is the finesse), a value comparable to the optical trap frequency, so that the system is only marginally approaching the resolved side-band limit of radiation pressure cooling. Ignoring all sources of noise, these parameters result in a minimum thermal phonon occupation number of

$$\langle n\rangle_{\rm min,C} = -\frac{4(\Delta+\omega_z)^2+\kappa^2}{16\omega_z\Delta}. \tag{2.15}$$

For our parameters and a detuning $\Delta = (\omega_{\rm laser} - \omega_c) = -4.25\times10^5$ rad/s from the cavity resonance (ω_c), we get $\langle n\rangle_{\rm min,C} \simeq 0.56$, well into the quantum regime. We remark that we may reduce this value by using tighter trapping, though this would violate our approximation that the field varies little over the dimensions of the disk. The quoted value is thus an upper-bound consistent with our approximations, but by no means a fundamental limit.

2.3 Limitations of the scheme

In calculating $\langle n\rangle_{\rm min}$ we have ignored all effects of noise. The major sources of noise are the fluctuations of the trapping and the Fabry-Pérot cavity lasers, and background gas collisions. We next evaluate their impact on $\langle n\rangle_{\rm min}$, as mentioned in Eq. (2.7).

2.3.1 Trapping laser fluctuations

There are three noise sources due to the optical tweezer laser beams: intensity fluctuations, beam-pointing fluctuations, and photon scattering losses. The first two noise sources have been studied extensively in the context of trapping alkali atoms

in optical traps (69). The intensity fluctuations lead to a change in trap frequency, see Eq. (2.12), resulting in transitions $n \rightarrow n \pm 2$ between states of vibration of the trapped mirror. This produces a rate of parametric heating due to intensity fluctuations given by

$$\gamma_I = \frac{1}{4}\omega_z^2 S_I(2\omega_z), \tag{2.16}$$

where $S_I(2\omega_z)$ is the noise power spectrum of the laser. For example, using $S_I = 10^{-10}$ Hz^{-1} results in an exponential energy growth rate of 1.01 rad /s. We note that Nd:YAG lasers with a lower noise spectrum are available and would further reduce this source of heating.

Beam-pointing fluctuations cause fluctuations of the trap center and lead to a constant heating rate given by

$$\gamma_x = \frac{1}{4}\omega_z^4 m S_x(\omega_z). \tag{2.17}$$

For a spectrum of position fluctuations $S_x(\omega_z)$ of 10^{-10} μm^2 Hz^{-1} this yields a negligible constant heating rate of the order of 10^{-12} J/s.

We next turn to scattering losses. An object with a diameter much bigger than the wavelength of light, such as our "floating" mirror, can be thought of as being comprised of a collection of optically driven induced dipoles. Scattering from these dipoles is the mechanism behind Rayleigh scattering (70). The momentum kicks due to the scattering average to zero, but their fluctuations in the z direction result in heating. Details of this scattering loss can be found e.g. in Ref. (70). Here we summarize the main results.

For a light intensity I_0 incident on a scatterer of volume V, the scattered power per solid angle is given by

$$\frac{dP}{d\Omega} = I_0 V R, \tag{2.18}$$

where the scattering coefficient can be obtained by thermodynamic arguments and is given by

$$R = \frac{\omega^4}{16\pi^2 c^4}\gamma_e C_T k_B T \sin^2\phi. \tag{2.19}$$

Here, ω is the frequency of the (trapping) laser, $\gamma_e = (n^2-1)(n^2+2)/3$ where n is the index of refraction, C_T is the isothermal compressibility, T_e is the effective temperature of the density fluctuations and ϕ the angle from the direction of propagation (say the x-axis). All other constants have their usual meaning. The power is the rate of optical energy scattered, E_{scatt}, and $\langle E_{\text{scatt}}\rangle = \langle N_{\text{scatt}}\rangle \hbar\omega$, where N_{scatt} is the number of photons scattered.

The component of the trapping photon momentum along z is $p_z = \hbar k \cos\phi$, resulting in an increase $\langle E_{\text{kin}}\rangle$ in kinetic energy of the trapped mirror. The fraction of scattered optical energy per photon that contributes to that increase is $\eta = \frac{1}{\hbar\omega}\frac{(\hbar k\cos\phi)^2}{2m}$. Integrating over the solid angle $d\Omega$, we find the scattered power to be

$$\frac{d}{dt}\langle E_{\text{kin}}\rangle = \frac{8\hbar\pi^4 I_0 V \gamma_e C_T k_B T_e}{15mc\lambda^5}. \tag{2.20}$$

For our parameter we find $\eta = 2.68\times10^{-26}\cos^2\phi$ — which confirms the intuitive argument that most of the scattered light does not contribute to the heating of the center-of-mass mode — which leads to a negligible constant heating rate of 1.93×10^{-32} J/s. This is in contrast to the situation with nanospheres, where dipole scattering is the dominant source of noise (61; 62).

2.3.2 Fabry-Pérot laser fluctuations

Another source of noise that places a fundamental limit on the occupation number of the center-of-mass motion of the moving mirror is the linewidth of the Fabry-Pérot laser [2](72). Here we model the laser linewidth in terms of a phase diffusion process that drives the laser field $E_{in}e^{i\phi(t)}$. The phase $\phi(t)$ is given by $\phi(t) = \sqrt{2\Gamma_L}\int_0^t \eta(s)ds$, where Γ_L is the laser linewidth and $\eta(s)$ is a gaussian white noise process with mean $\langle\eta(s)\rangle = 0$ and correlation $\langle\eta(s)\eta(v)\rangle = \delta(s-v)$. For $|(\omega_c z)/(\omega_z L)| \ll 1$ this results

[2]The calculations presented in this subsection were done by G. A. Phelps and are mentioned for completeness. More details about the effect of phase noise can also be found in Ref.(71)

in the linewidth-modified cooling rate

$$\Gamma_{\rm opto} = -\left(\frac{\omega_c \kappa}{m\omega_z L^2}\right) \frac{8P_{in}\left[A_- - A_+\right]}{\left[(2\Gamma_L + \kappa)^2 + 4\Delta^2\right](\kappa^2 + \omega_z^2)} \tag{2.21}$$

where P_{in} is the input power and $A_\pm$ is given by

$$A_\pm = \frac{(\Gamma_L + \kappa)(2\Gamma_L + \kappa)^2 + 2\Gamma_L((\Delta \pm \omega_z)^2 + \Delta^2) + \kappa\omega_z^2}{(2\Gamma_L + \kappa)^2 + 4(\Delta \pm \omega_z)^2}. \tag{2.22}$$

The laser linewidth generally results in less efficient backaction cooling, but there is a range of detunings Δ for which the cooling rate is essentially unchanged from the ideal case, a result of the excitation of the anti-Stokes sideband from higher frequencies in the laser spectrum. For our parameters, a 1 μW laser of linewidth 10×10^3 rad/s, detuned -4.25 $\times$ 10^5 rad/s from the cavity resonance results in a cooling rate $\Gamma_{\rm opto}$ of 5.2×10^4 rad/s.

2.3.3 Background gas collisions

The fluctuations in mirror motion due to background gas collisions can be described by the Langevin equation

$$\ddot{z} + \gamma_{\rm bg}\dot{z} = \xi(t) \tag{2.23}$$

where the fluctuating force $\xi(t)$ obeys the Markovian correlation relations

$$\begin{aligned} \langle \xi(t) \rangle &= 0, \\ \langle \xi(t)\xi(t') \rangle &= q\delta(t - t') \end{aligned} \tag{2.24}$$

with q given by the fluctuation-dissipation theorem as $q = 2k_B T\gamma_{bg}/m$. To derive an expression for γ_{bg} we consider motion along the z-axis only. A gas molecule of mass m_g and velocity v_g undergoing an elastic collision with the disk imparts a momentum change $\delta p = 2m_g v_g$. In the moving frame of the disk, this gives $\Delta p_{\rm disk} = 2m_g(v_g - v_{disk}) - 2m_g(v_g + v_{disk})$, the two contributions corresponding to forward and backward collisions. The rate of momentum transfer is then obtained

by multiplying this expression by the number of collisions per unit time ($nAv_g/2$), where n is the number density of gas molecules, A is the cross-section area of the disk, and v_g is the mean speed of the molecules, taken to be to be the average thermal velocity for an ideal gas of pressure P. This gives

$$\gamma_{bg} = \frac{4PA}{mv_g}. \tag{2.25}$$

For a pressure of 10^{-8} torr, $\gamma_{bg} = 2.55 \times 10^{-6}$rad/s. We note also that background gas collisions do not introduce any significant wobble.

Both intensity fluctuations and background collisions are mechanisms of damping for the disk mirror and provide the equivalent of a mechanical Q-factor. For very small mechanical dissipation, the minimum attainable mean phonon number can be approximated as

$$\langle n \rangle_{\min} \approx \langle n \rangle_{\min,\mathrm{C}} + \frac{\gamma_{bg}\bar{n}_{\mathrm{th}}}{(\gamma_{rp} - \gamma_I)}, \tag{2.26}$$

n_R being the average occupation number of the relevant mode before cooling, $n_R \simeq k_B T/\hbar\omega_z$. For our parameters, at room temperature, the contribution of this mechanical damping is very small, $\simeq 0.01$, and can be reduced further via better stabilized lasers and an improved vacuum.

2.4 Conclusion

In conclusion, we have shown that the coupling to the thermal reservoir in standard optomechanical setups can be completely eliminated by optical levitation of the Fabry-Pérot mirror, resulting in mean phonon occupation numbers significantly below unity. Following the argument of Ref. (62) it can also be shown that for the parameters considered here a levitated mirror cooled to its quantum mechanical ground state would undergo of the order of 10^4 oscillations before undergoing a shot-noise induced quantum jump.

As noted earlier the quoted value of $\langle n \rangle_{\min}$ can be reduced by stiffening the optical spring. The optical spring effect has been studied extensively in the gravitational

wave detection community (73), where the moving mirror's mechanical resonance frequency has been greatly enhanced using a two-color laser configuration. A similar approach could also increase ω_z in our case without increase in the intensity of the trapping lasers.

Since this work was published (60), more rigorous numerical calculations of the forces involved in trapping a disk structure have been performed. We found that stable trapping is possible in our parameter range with similar trap frequencies. Furthermore, we investigated other ways to generate a stiffer trap for less laser power. These include, injecting a guided mode into the disk structure, or using higher order gaussian modes in order to have larger gradient.

Future work will include the extension of this proposal to a three-mirror geometry, as well as the coupling of the levitated mirror to ultracold atomic and molecular systems, either for the quantum control of the state of the mirror, or conversely for the manipulation of the atoms. In particular, the generation, detection and control of non-classical motional states of the mirror will be considered.

CHAPTER 3

GENERATION OF NON-CLASSICAL STATES

One immediate motivation to consider mechanical systems operating in the quantum regime is their ability to make precise and accurate measurements of feeble forces and fields. In this context, *hybrid systems* consisting of coupled atomic (or molecular) and nanomechanical systems may prove particularly useful. The robust and scalable infrastructure provided by NEMS/MEMS devices coupled with the high precision measurement capability of quantum gases (74; 75; 76) makes them an attractive combination for sensitive force measurements, as well as for a quantitative study of dissipation and decoherence processes at the quantum-classical interface. There are ongoing experimental (77; 78) and theoretical (79; 80; 81; 82; 83) efforts toward coupling mechanical systems to atomic ensembles.

Along with precision measurement applications, by coupling mechanical systems to well-controlled quantum systems like atoms and molecules we can explore a wide range of quantum effects in mechanics, for example the generation and measurement of non-classical states of mechanical motion. In this chapter we study two such examples. First, we discuss how a mechanical oscillator coupled to a polar molecule via the electric dipole-dipole interaction can result in the parametric squeezing of molecular motion, and then expand these considerations to demonstrate how an array of molecules can generate entangled states of different phonon modes of the chain. This work is published is ref. (84).

In a second example we consider a mechanical system magnetically coupled to a spinor Bose-Einstein condensate, and show that the back-action of measurements of the spin state of the atoms can create conditional non-classical states of the membrane. A portion of this work is published in ref. (85).

3.1 Squeezed state generation via coupling to polar molecules

Due to the anisotropic, long-range interaction between these molecules, ensembles of ultra-cold polar molecules are believed to have a rich phase diagram and are the subject of intense theoretical and experimental interest (86).This section investigates the coupling of a laser-cooled nanomechanical cantilever to an ultracold lattice of polar molecules. The cantilever-molecule coupling is assumed to be enabled by a ferroelectric domain mounted on the former, leading to a strong dipole-dipole interaction. A strong polarizing DC field (of upto 100 kV/cm) freezes out the rotational degrees of freedom of the dipoles (87).

To set the stage for the discussion we consider first the simple case of a single molecule, see setup A of Fig. 3.1, and demonstrate that its coupling to the cantilever leads to the parametric squeezing of its center-of-mass motion. These considerations are then generalized to the situation of a linear chain of electric dipoles (setup B). Such a self-arranged crystal has recently been proposed as memory for quantum information processing (88). We find that for an appropriate choice of cantilever frequency, the phonons in the crystal can be two-mode squeezed, i.e. entangled (89; 90), hinting at the possibility of exploiting such a set-up for the coherent control of the quantum state of the dipolar lattice.

3.1.1 Cantilever coupled to a single molecule

The Hamiltonian describing the coupling of the cantilever to a single molecule is $H = H_c + H_m + V_I$, where

$$H_c = \hbar\omega_c \left(a^\dagger a + \frac{1}{2} \right), \tag{3.1}$$

describes the quantized (single mode of) vibration of the cantilever of effective mass m_c at frequency ω_c, a and $a^\dagger$ being bosonic annihilation and creation operators obeying the commutation rules $\left[a, a^\dagger\right] = 1$. In terms of the displacement y_c of the

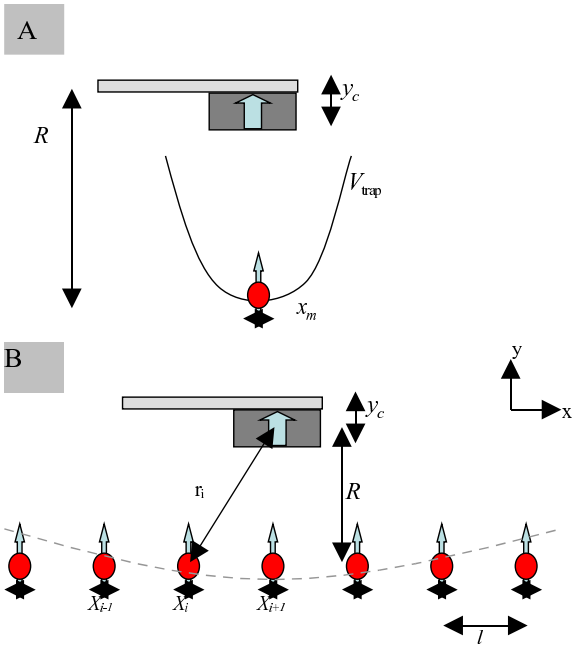

Figure 3.1: Arrangement considered for the coupling a nanomechanical oscillator to a dipolar "crystal". In setup A, a single molecule is coupled to the oscillator. In setup B, the oscillator is again at a distance R from the linear chain of molecules. A weakly confining harmonic trap for the dipoles is shown along the x axis.

cantilever along the y-axis, we have

$$y_c = \sqrt{\frac{\hbar}{2\omega_c m_c}}(a + a^\dagger). \tag{3.2}$$

The Hamiltonian

$$H_m = \hbar\omega_t \left(b^\dagger b + \frac{1}{2} \right) \tag{3.3}$$

describes the center-of-mass motion of the trapped dipole of mass m, where ω_t is the trap frequency and $b, b^\dagger$ are bosonic creation and annihilation operators with

$$x_m = \sqrt{\frac{\hbar}{2\omega_t m}}(b + b^\dagger), \tag{3.4}$$

x_m being the displacement of the molecule along the x-axis. Finally, the interaction between the molecule and the oscillator is given by the electric dipole-dipole

interaction

$$V_{dd} = G_{dd}\frac{d_m.d_c - 3(\hat{r}.d_m)(\hat{r}.d_c)}{r^3}, \tag{3.5}$$

where G_{dd} is $1/4\pi\epsilon_0$. The molecule has an electric dipole moment of d_m, and d_c is the dipole moment of the ferroelectric domain attached to the tip of the nanomechanical cantilever. Let the equilibrium distance between the cantilever and particle be R. In the presence of dipole-dipole interaction, there is small displacement around this equilibrium position. In the case described in Fig.(3.1), y_c is parallel to R. The total distance r is given by $r^2 = (R+y_c)^2 + x_m^2$, so that the dipole-dipole interaction for this geometry becomes

$$V_I = \frac{d_m d_c}{4\pi\epsilon_0 r^3}\left[1 - \frac{3(R+y_c)^2}{r^2}\right]. \tag{3.6}$$

For $R \gg x_m, y_c$ the dipolar interaction can be approximated as

$$V_I \approx \frac{1}{2\pi\epsilon_0}\frac{d_c d_m}{R^3}\left[-1 + 3\frac{y_c}{R} + 3\frac{x_m^2}{R^2} - 6\frac{y_c^2}{R^2} - 15\frac{x_m^2 y_c}{R^3} + 10\frac{y_c^3}{R^3} + \cdots\right]. \tag{3.7}$$

The first term in eq. 3.7 is a constant, and can be set to zero. The second term leads to a new equilibrium position for the molecule. The third term gives us a tighter trap for the molecule and the fourth term reduces the trap depth for the cantilever, but we shall ignore this term since the cantilever mass is much higher than that of the molecule. Finally, the fifth term is reponsible for parametric squeezing. The remaining terms have comparatively insignificant contributions, and are ignored for this work because they just lead to higher order anharmonicities.

The presence of the cantilever has two major effects on the molecule dynamics. First, it leads to a tightening of the trap for small distances R, resulting in a shifted trapping frequency

$$\omega_t' = \left[\omega_t^2 + \frac{3d_m d_c}{\pi\epsilon_0 m R^5}\right]^{1/2}. \tag{3.8}$$

The second, more interesting effect is parametric squeezing. In an interaction picture with respect to the free Hamiltonian $H_c + H_m$, taking $\omega_c = 2\omega_t'$, performing the

rotating-wave approximation, and further assuming that the cantilever motion can be treated classically (operator $a \rightarrow$ complex number $\alpha = \langle a \rangle$), the interaction potential V_I reduces to

$$V_I = -\hbar C \left(b^2 + b^{\dagger 2} \right) \tag{3.9}$$

where

$$C = L_c \frac{15 d_m d_c}{4\pi\epsilon_o m \omega_t' R^6}. \tag{3.10}$$

Here, L_c is the amplitude of oscillation of the classical cantilever. For a temperature T_c and a mean number of excitations $\bar{N} = k_B T_c / \hbar\omega_c$, we have

$$L_c = \sqrt{\bar{N}} \left(\frac{\hbar}{2 m_c \omega_c} \right)^{1/2}. \tag{3.11}$$

Eq. (3.9) is the standard squeezing Hamiltonian familiar from studies of the degenerate parametric amplifier in quantum optics, see e.g. Ref. (91).

While the typical trap level spacing is much larger than the thermal energy of the ultracold molecule, which justifies its zero-temperature description, thermal effects in the cantilever must be taken into account. We introduce thermal noise in the form of phase fluctuations in the cantilever field. These fluctuations are related to the cantilever damping rate, D by the fluctuation-dissipation theorem. For times t such that $D < t^{-1} < 2C$, the variance in the dimensionless position quadrature for the molecule, $x_1 = \frac{1}{2}(b + b^\dagger)$, is then given by (91)

$$(\Delta x_1)_t^2 = \frac{1}{4} e^{-2u} + \frac{1}{8} e^{2u} D t \tag{3.12}$$

where $u = 2Ct$ is the squeezing parameter.

Consider for example a nanomechanical cantilever with frequency $\omega_c = 4$MHz, effective mass $m_c = 10^{-16}$kg, and linewidth $D = 1$Hz. A ferroelectric domain with dipole moment $d_c = 2.1 \times 10^{-23}$C-m is attached to the cantilever and is placed at $R = 2\mu$m from a SrO molecule. These parameters give an oscillator frequency $\omega_t' = 2$MHz. We assume $\bar{N} = 100$, yielding $C = 20.4$ Hz. Fig. 3.2 shows the variance

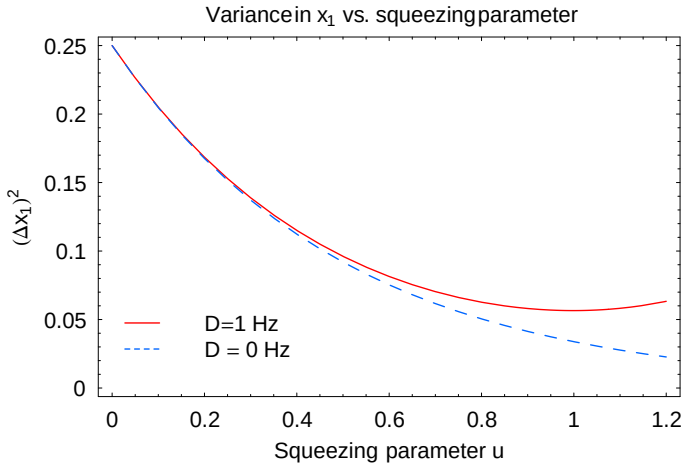

Figure 3.2: Variance in the quadrature component x_1 (Eq. 12), vs. squeezing parameter u, for a SrO molecule interacting with a cantilever. The two curves are for the cantilever damping rates linewidth D = 1 Hz (solid curve) and 0 Hz (dashed curve). Squeezing occurs when the variance in x_1 is below 1/4, and is eventually destroyed due to phase noise in the cantilever.

in x_1 as a function of the squeezing parameter for that example. We remark that the squeezing in single trapped ions (5) and atoms (92) has been experimentally demonstrated, and similar measurement techniques can possibly be implemented to detect squeezing in the present case.

3.1.2 Cantilever coupled to a 1D lattice of polar molecules

We now extend these considerations to the case of a lattice of N heteronuclear molecules contained in a harmonic trap V_t, as shown in Fig. 1.B. The trap is arranged so as to confine the sample weakly along x, tightly along y and tightly or weakly along the z direction depending on whether a one- or two-dimensional lattice crystal is desired. (We restrict our considerations to the case of a one-dimensional chain in the following.) A polarizing DC electric field is provided along y so that all the dipoles align along that direction. The system can be described by the

Hamiltonian

$$H_p = \sum_i^N \frac{p_i^2}{2m} + \frac{d_m^2}{4\pi\epsilon_o} \sum_{i<j}^N \frac{1}{|x_i - x_j|^3} + V_t, \tag{3.13}$$

where x_i, p_i are the position and momentum of the ith molecule and V_t is the external trapping potential. The first term in Eq. (3.13) corresponds to the kinetic energy of the dipoles, the second to their dipole-dipole interaction and the last term denotes the trap energy.

Due to their mutual repulsion along the x direction the molecules self-organize into a linear lattice (88). We assume that these dipoles do undergo small displacements x_i around their equilibrium position, which is much smaller than the lattice spacing l between two dipoles. Simplifying further by considering only the nearest neighbor interaction, the above expression for dipole-dipole interaction boils down to:

$$V_{dd} = \frac{G_{dd}\ d_m^2}{2l^3} \sum_i (1 + \frac{x_i - x_{i+1}}{l})^{-3} \tag{3.14}$$

Expanding around the equilibrium position, the smallest non-zero term is quadratic in particle displacement. This simplifies the dipole-dipole interaction to

$$V_{dd} = \frac{3G_{dd}\ d_m^2}{l^5} \sum_i (x_i - x_{i+1})^2 \tag{3.15}$$

This last approximation is called the harmonic approximation for obvious reasons, and is responsible for the generation of phonons- the quanta of lattice vibrations. The frequency associated with this oscillator is given by

$$\omega_o = \left(\frac{3d_m^2}{2\pi\epsilon_0 m l^5} \right)^{1/2}, \tag{3.16}$$

where m is the mass of the molecule. The mathematical procedure to go from here to the phonon dispersion relation is pretty standard and is derived in many condensed matter textbooks, for example (93). The dispersion relation is given by

$$\omega(k) = 2\omega_0 |\sin(kl/2)| \tag{3.17}$$

At low temperature, we are in the Debye limit (93), where $\omega = vk$, v being the speed of sound in the medium. Eq. (3.13) can therefore be expressed in terms of acoustic phonon modes of momentum k and energy $\hbar\omega_k$,

$$H_p = \sum_k \hbar\omega_k \left(b_k^\dagger b_k + \frac{1}{2} \right), \tag{3.18}$$

where $b_k, b_k^\dagger$ are the phonon annihilation and creation operators obeying the bosonic commutation rules $\left[b_k, b_{k'}^\dagger \right] = \delta_{kk'}$.

We note that the higher order terms in the expansion of dipole-dipole interaction give us the lifetime of the crystal. In case of a simple monoatomic chain, the effect of these terms is well understood analytically (94). The cubic term primarily leads to a temperature dependent linewidth to the normal modes and is responsible for dissipation of energy. At zone boundary, this linewidth is given by:

$$\Gamma = \frac{3}{32}(\frac{\delta^2}{\gamma^3})(\omega_0 k_B T) \tag{3.19}$$

In our case, $\gamma = 6G_{dd}d_m^2/l^5$ and $\delta = 10G_{dd}d_m^2/l^6$.

We consider ultracold molecules at a temperature T such that $k_B T \ll \hbar\omega_o$, so that a $T = 0$ description is appropriate as before. The energy of the nanomechanical cantilever is again given by Eq. (3.1), so that the interaction between the chain of molecules and the oscillator is

$$V_I = \sum_i \frac{d_m d_c}{4\pi\epsilon_o r_i^3} \left[1 - \frac{3(R + y_c)^2}{r_i^2} \right], \tag{3.20}$$

where d_c is the dipole moment of the ferroelectric domain attached to the tip of the cantilever. Here y_c is the displacement of the cantilever along the y axis, R is its distance from the center of the dipolar crystal and its distance from the ith molecule is given by $r_i = [(R + y_c)^2 + (il + x_i)^2]^{1/2}$. Exploiting the hierarchy of length-scales, $x_i \ll l, Nl \ll R$, we expand Eq. (3.20) to find that the oscillator produces a slight shift in the phonon frequency,

$$\omega_k' = \left[\omega_k^2 + \frac{3d_m d_c}{\pi\epsilon_o m R^5} \right]^{1/2}. \tag{3.21}$$

and the coupling of the cantilever to the phonons is given by

$$V_I = -\sum_k \hbar C'_k \left(a + a^\dagger\right) \left(b_k b_{-k} + b_k^\dagger b_{-k}^\dagger + b_k^\dagger b_k + b_{-k} b_{-k}^\dagger\right), \tag{3.22}$$

$$C'_k = -\frac{17 d_m d_c}{16\pi\epsilon_o m \omega'_k R^6} \left(\frac{\hbar}{2 m_c \omega_c}\right)^{1/2}. \tag{3.23}$$

We remark that for sufficiently small R and/or sufficiently large d_c the cantilever will couple to the individual dipoles rather than collectively to the acoustic phonons.

Following an approach that parallels the single-molecule description we work in an interaction picture with respect to the free Hamiltonian of the cantilever and the (frequency shifted) phonon mode. We further choose the cantilever frequency such that $\omega_c = 2\omega'_k$, with $k = \pi/l$, implying that the cantilever couples primarily to excitations near the edge of the first Brillouin zone, where the density of phonon states is largest. We assume for simplicity that the motion of the nanomechanical cantilever can be described classically just as in the single molecule case, (again, operator $a \rightarrow$ complex number α), a reasonable approximation since it is still challenging to cool these systems to their quantum regime. Performing the rotating wave approximation we then obtain the approximate interaction picture interaction Hamiltonian

$$V_I = -\hbar C_k \left(b_k b_{-k} + b_{-k}^\dagger b_k^\dagger\right), \tag{3.24}$$

where $C_k = \sqrt{\bar{N}} C'_k$ and $\bar{N}$ is the average occupation number of the cantilever. This Hamiltonian is known from quantum optics to lead to the generation of two-mode squeezing between acoustic phonon modes of momenta $\pm k$ (within the bandwidth of the nanomechanical resonance), and hence their quantum entanglement.

In order to characterize that two-mode squeezing we introduce the two dimensionless quadratures

$$s_1 = \frac{1}{\sqrt{2}}(b_k + b_{-k} + b_k^\dagger + b_{-k}^\dagger), \tag{3.25}$$

$$s_2 = \frac{1}{\sqrt{2}i}(b_k - b_k^\dagger - b_{-k} + b_{-k}^\dagger). \tag{3.26}$$

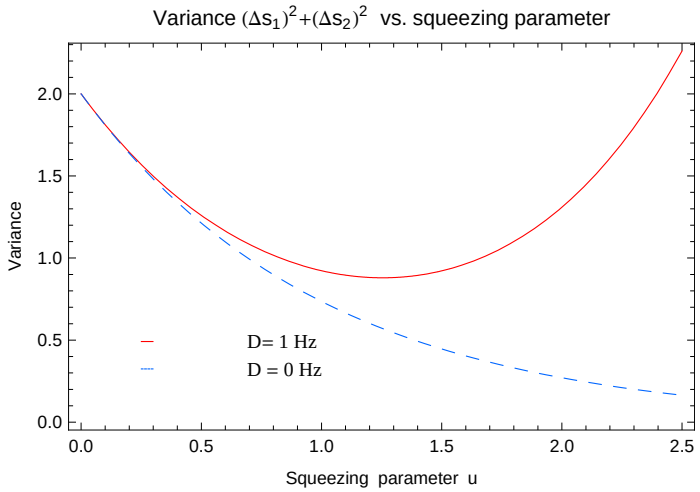

Figure 3.3: Sum of variances of s_1 and s_2, vs. squeezing parameter u, for a SrO dipolar crystal interacting with a cantilever. The two curves are for cantilever damping rates of D = 1 Hz (solid curve) and 0 Hz (dashed curve). Phase fluctuations of the cantilever eventually increase the sum of variances to a value larger than 2, indicative of the loss of entanglement between the two phonon modes.

Taking into account the phase fluctuations in the cantilever motion resulting from thermal noise, the sum of variances in the two quadratures is then (95):

$$\begin{aligned}(\Delta s_1)^2 + (\Delta s_2)^2 &= \frac{e^{-\frac{Dt}{2}}}{C_{k0}}\{D\sinh(C_{k0}t) + 2C_{k0}\cosh(C_{k0}t)\} \\ &\quad - \sum_{i,j,k,i\neq j,j\neq k} e^{\lambda_i t}\frac{2C_{k0}(\lambda_i + 4D)}{(\lambda_i - \lambda_j)(\lambda_i - \lambda_k)},\end{aligned} \tag{3.27}$$

where u is the squeezing parameter and is equal to $2C_{k0}t$, with $C_{k0} = \frac{1}{2}\sqrt{4C_k^2 - D^2}$ and the λ_i's are the roots of the cubic equation:

$$\lambda^3 + 5D\lambda^2 + (4D^2 - C_{k0}^2)\lambda - 2C_{k0}^2 D = 0. \tag{3.28}$$

For example, let us consider a nanomechanical cantilever with frequency ω_c = 2MHz, effective mass $m_c = 10^{-16}$kg, and linewidth D = 1Hz. We assume an average occupation number of 100. A ferroelectric domain with dipole moment

$d_c = 2.1 \times 10^{-23}$C-m is attached to the cantilever and is placed at $R = 2\mu$m from a one dimensional SrO crystal. The crystalline phase of these dipolar molecules is formed with inter-molecular distances $l \approx 200$nm. These parameters give a phonon frequency $\omega_o = 4$MHz, and thus an interaction $C_k = 4.4$. The squeezing parameter u is given by $2C_k t$. Fig. 3.3 gives the sum of variances of s_1 and s_2 as a function of the squeezing parameter for this system.

The sum of the variances in Eq. (3.27) is actually a measure of the entanglement of the system (96). In our case, this inseparability criterion implies that the system is entangled if the sum of the variances is less than 2. We observe from Fig. 3 that as expected intuitively the introduction of phase fluctuations destroys the entanglement over time. As far as the experimental verification of this prediction is concerned we remark that squeezed states of phonons have been previously detected experimentally in solid-state systems (89), and similar techniques can possibly be used to detect squeezed phonon modes in the present system.

As indicated earlier, our results assume that the motion of the cantilever is classical and dominated by thermal rather than quantum fluctuations. In addition to being a realistic description of the current experimental situation, this approximation enabled us to present the physics of the coupling between the cantilever and the dipolar molecules using simple analytical models. However, our results are expected to still hold at least qualitatively when treating the cantilever quantum-mechanically. Exact numerical solutions for one-mode and two-mode squeezing using a coherent pump with low $\bar{N}$ are available in the literature (97; 98). These results are consistent with our simple analytical treatment and point to the existence of squeezing for this system.

In conclusion, we studied the coupling of nanomechanical cantilevers to dipolar molecules. We found that for a single trapped molecule, the presence of the cantilever leads to tighter confinement and parametric squeezing. We also demonstrated squeezing and entanglement of the phonon modes of a linear chain of dipolar

molecules. These results open up the way to extremely promising novel methods for the quantum manipulation and control of the state of ultracold dipolar systems, and are indicative of the general use of nanoscale cantilevers in the detection and control of atomic and molecular systems.

Since the publication of these results, we have investigated another scheme for squeezing mechanical motion that relies on nonlinearity of dipole-dipole interaction. It relies on the dipole-dipole coupling between a magnetic dipole mounted on the tip of a cantilever to equally oriented dipoles located on a mesoscopic tuning fork. (99).

3.2 Backaction induced states in coupled BEC- mechanical systems

We now turn to a second approach to the generation of non-classical states, measurement induced backaction. Specifically, we study theoretically the dynamics of a a hybrid optomechanical system consisting of a macroscopic mechanical membrane magnetically coupled to a spinor Bose-Einstein condensate via a nanomagnet attached at the membrane center. We demonstrate that this coupling permits to indirectly monitor the center-of-mass position of the membrane via a non-destructive measurement of the Larmor precession frequency of the condensed atoms. This measurement induces a significant back-action on the membrane motion, which we quantify for the cases of thermal and coherent initial states of the membrane. We discuss the possibility of measuring that quantum back-action via repeated measurements, and show that it can be done for observable experimental parameters. We also investigate the potential to generate non-classical states of the membrane, in particular Schrödinger cat states, via such repeated measurements, and the effect of thermal dissipation on such mechanical states.

The system that we consider consists of a mechanical membrane magnetically coupled to a spinor Bose-Einstein condensate as shown in Fig. 3.4, an arrangement somewhat similar to a system previously considered in Refs. (79; 82). The magnetic

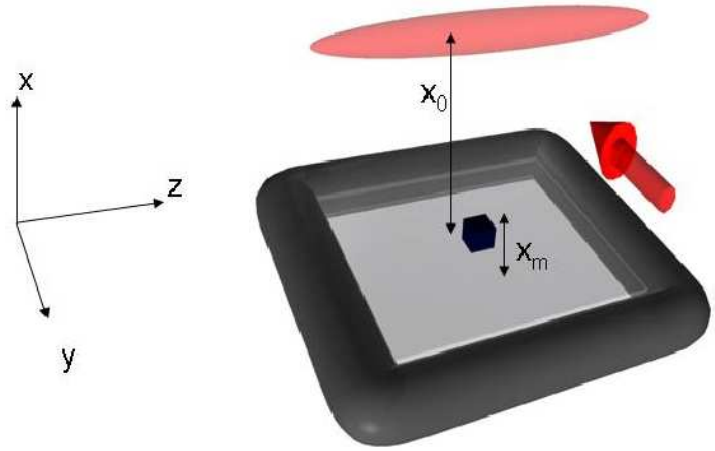

Figure 3.4: Proposed experimental setup for back-action detection, involving a magnetic particle located at the center of a vibrating membrane and polarized along the z-axis. This setup produces a spatially inhomogeneous magnetic field that is detected by the BEC. The BEC's long axis is along the z-direction, the probe light (red arrow) is along y, and the membrane oscillations are along the x-axis.

coupling, generated via a nano-magnet anchored on the membrane, entangles the membrane to the spin state of the BEC. We may then make an indirect observation of the center-of-mass position of the membrane through a measurement of the spins of the condensed atoms. This can be achieved generally speaking in two ways: through a strong, or projective, measurement of the spin state, or through a weak, or dispersive, measurement of the spins. An example of the former would be through a Stern-Gerlach-type measurement. Here, the atoms are subjected to a spatially inhomogenous field seperating out the different spin components. The different spin populations can then be measured via a standard absorptive imaging technique. A likely candidate for the latter type of measurement would be observation of the Larmor frequency through a phase contrast imaging technique, as described in Ref. (74). Since the Larmor frequency is proportional to the local magnetic field – which is modulated by the motion of the magnetic domain attached to the oscillating membrane – it provides a measure of the membrane motion. Either type of measurement

of the BEC spin can induce a back-action on the membrane, modifying its position and/or momentum in proportion to the strength of the measurement. The main goal of this section is thus to quantify the effect of using the BEC as a position sensor on the membrane and to evaluate the feasibility of measuring the back-action of such a measurement. In the case where the back-action is small we can indeed use the BEC to make ultraprecise measurements of the membrane, and when it is large, it may provide a means to observe the effects of a quantum measurement on a macroscopic object. So far such a quantum effect has only been observed in dilute and isolated systems like ultra-cold gases (100).

3.2.1 Model

We assume for simplicity that the magnetic domain is a point dipole located at the origin and polarized along the z-axis, $\mu_{\mathbf{m}} = \mu_m \hat{\mathbf{z}}$. The magnetic field due to that dipole is

$$\mathbf{B}(\mathbf{r}) = \frac{\mu_0}{4\pi}\frac{1}{r^3}\left(3(\mu_{\mathbf{m}} \cdot \hat{\mathbf{r}})\hat{\mathbf{r}} - \mu_{\mathbf{m}}\right). \tag{3.29}$$

The small spatial variation of the resulting magnetic field along the long axis of the condensate results in a variation of its Larmor precession frequency. As we show in the following, this dependence permits us to characterize the expectation value of center-of-mass mode of oscillation of the membrane.

The Zeeman interaction between the atoms in the condensate and the total magnetic field $\mathbf{B}_0 + \mathbf{B}(\mathbf{r})$ is described by the Hamiltonian

$$\begin{aligned} H &= -\mu_{\mathbf{a}} \cdot (\mathbf{B}_0 + \mathbf{B}(\mathbf{r})) \\ &= \mu_B g_F \left(F_x B_x + F_y B_y + F_z(B_0 + B_z)\right), \end{aligned} \tag{3.30}$$

where F_i is the i^{th} component of the spin-1 operator. As a result of the spatial dependence of the magnetic field, atoms at different positions along the long axis of the condensate precess at different frequencies and dephase over a period of time. It is this z-dependent phase difference that is picked up in spin population measurement.

We note that the transverse dependence of the magnetic field also results in an inhomogeneous broadening of the Larmor frequency. The effects of this broadening can be minimized, the more elongated along z and tightly confined in the transverse directions the condensate. In the following we consider for simplicity a condensate that is almost one-dimensional and confined to a region close to $y = 0$, so that $B_y \approx 0$ and $F_y B_y \simeq 0$. Furthermore, close to $z = 0$, i.e. for the fraction of the BEC directly above the dipole, the magnetic field $\mathbf{B}(\mathbf{r})$ is predominantly in the z- direction provided that x_0, the equilibrium distance between the BEC and the membrane, is much greater than the relevant coordinates y and z. In that case we can ignore the effects of B_x and B_y altogether.

As shown in detail in Appendix B, for small displacements x_m of the membrane compared to x_0 the magnetic coupling Hamiltonian (3.30) reduces to

$$V = \mu_B g_F F_z \left[B_0 + \frac{\mu_0 \mu_m}{4\pi x_0^4} \left(-x_0 + 3x_m \right) \right]. \tag{3.31}$$

The first and the second term of this expression are independent of time, while the third term, proportional to x_m, varies sinusoidally in time. We exploit this property by rewriting the magnetic Hamiltonian as

$$V = \mu_B g_F F_z \left(B_c + B_v' x_m \right), \tag{3.32}$$

where

$$B_v' = \frac{3\mu_o \mu_m}{4\pi x_0^4}, \tag{3.33}$$

see Appendix B. From here on we drop the subscript in membrane displacement, $x_m \rightarrow x$ for compactness. The total system Hamiltonian of the hybrid BEC-membrane system is then

$$H = H_m + H'_{\mathrm{BEC}} + V. \tag{3.34}$$

Here

$$H_m = p^2/2m + m\omega_m^2 x^2/2$$

is the membrane Hamiltonian and

$$H'_{\mathrm{BEC}} = H_{0,\mathrm{BEC}} + \mu_B g_F F_z B_c,$$

where $H_{0,\mathrm{BEC}}$ is the spin-independent part of the atomic Hamiltonian. Describing the condensate as a collection of N non-interacting spin-1 atoms at zero temperature, and assuming that the atoms are experiencing a constant magnetic field over the detector area of interest, we can then express the interaction Hamiltonian as

$$V = N\mu_B g_F F_z (B_c + B'_v x). \tag{3.35}$$

This simplifies the total Hamiltonian to

$$H = \frac{p^2}{2m} + \frac{1}{2} m\omega_m^2 \left(x + AF_z\right)^2 + \left\{\hbar\Omega_{L0} F_z - \hbar\delta\Omega F_z^2\right\} \tag{3.36}$$

where

$$A = \mu_B g_F N B'_v / m\omega^2, \tag{3.37}$$

which we call the *back-action parameter* in anticipation of the following sections, and

$$\delta\Omega = m\omega_m^2 A^2 / 2\hbar. \tag{3.38}$$

3.2.2 Spin Measurement

We now evaluate the backaction on the membrane of an arbitrary measurement operator that acts on the spin degree of freedom of the BEC. We consider the cases of a single and multiple spin measurements for a membrane initially perpared in a thermal and coherent state. The analytical expressions provided for the post measurement density matrix (and subsequently the Wigner function) are for a general measurement operator. However, to illustrate the backaction effects in an intuitive manner, we consider a particular case of simple projective measurements of F_y, corresponding to all atoms being in the $F_y = 0, +1$ or -1 state. While this is not

the most likely outcome of a typical Stern-Gerlach measurement, it does serve as a simple demonstration of backaction induced dynamics.

The measurement proceeds in the following way: at time $t = 0$ a $\pi/2$ pulse is applied to the condensate, preparing all atoms in $|F_x = 1\rangle$ state. Following that preparation stage, the atomic spins precess about the z-axis until a later time t when the spin population measurement is made.

Equation (3.36) already gives a clear indication of the back-action of the measuring apparatus – the condensate – on the membrane. As a result of their coupling the membrane Hamiltonian is modified from being a harmonic oscillator centered at the origin to one that is shifted by the quantity AF_z, indicating that the back-action depends on the outcome of a specific spin measurement. Here, we give an explicit description of the measurement process by evaluating the pre– and post-measurement density operator of the membrane, and the corresponding Wigner function.

We assume that the membrane and the condensate are initially uncorrelated,

$$\rho = \rho_m(0) \otimes \rho_{\rm BEC}(0)$$

and denote the initial density matrix elements of the BEC as $\rho^0_{\alpha,\beta}$, where $\rho_{\alpha,\beta} = \langle\alpha|\rho_{\rm BEC}|\beta\rangle$, and α, β are the various spin states, $\alpha, \beta = \{0, \pm 1\}$. We also assume for now that the membrane center-of-mass is initially in thermal equilibrium with temperature T. Defining

$$\eta = \hbar\omega_m/2k_BT,$$

its density matrix elements in position space are then

$$\begin{aligned} \rho_m(x_f, x_i, t = 0) &= \langle x_f|\rho_m|x_i\rangle = \sqrt{\frac{m\omega_m}{\pi\hbar}\tanh\eta}\times \\ &\quad \exp\left[-\frac{m\omega_m}{4\hbar}\left((x_f + x_i)^2\tanh\eta + (x_f - x_i)^2\coth\eta\right)\right]. \end{aligned} \tag{3.39}$$

For $t > 0$ the spin components of the condensate undergo a Larmor precession about the z-axis. Since $[H_{\rm BEC}, H_m + V] = 0$, we can use the Baker-Hausdorff relation

to re-express the propagator $U(t) = \exp(-iHt/\hbar)$ as

$$U(t) = e^{-itH_{\rm BEC}/\hbar} e^{-it(H_m+V)/\hbar}.$$

This allows to find the evolution of the system density matrix in a straightforward way. After an interaction time t, this evolution results in the matrix elements of the density operator of the membrane + condensate system to become

$$\begin{aligned}
&\langle \alpha, x_f|\rho(t)|\beta, x_i\rangle = \rho^0_{\alpha\beta} \exp[-i\Omega_{L0}(\alpha-\beta)t + i\delta\Omega_L(\alpha^2-\beta^2)t] \times \\
&\sqrt{\frac{m\omega_m}{\pi\hbar}\tanh\eta} \exp\Big[-\frac{m\omega_m}{4\hbar}\left\{(x_f + x_i + (\alpha+\beta)A(1-\cos\omega_m t))^2 \tanh\eta + \right. \\
&(x_f - x_i + (\alpha-\beta)A(1-\cos\omega_m t))^2 \coth\eta \\
&\left. +4iA\sin\omega_m t(\alpha x_f - \beta x_i) + 2iA^2(\alpha^2-\beta^2)\sin\omega_m t(2-\cos\omega_m t)\right\}\Big].
\end{aligned} \tag{3.40}$$

That is, the interaction of the membrane with the BEC displaces its center-of-mass motion in both position and momentum by amounts that depend explicitly on the spin components α and β, as well as on the back-action parameter A.

As already discussed, a measurement of arbitrary type but here taken to depend on F_y is carried out on the BEC at time t. The post-measurement density matrix of the membrane depends on the measurement outcome, and is given by

$$\langle x_f|\rho_m|x_i\rangle_\phi = \frac{1}{P(\phi)} {\rm tr}_{\rm BEC}(W^\phi \rho_{\rm sys}). \tag{3.41}$$

Here ϕ is the outcome of the F_y measurement, $P(\phi)$ is the probability of that outcome, W^ϕ is the Kraus operator corresponding to the effects of the measurement on the BEC's quantum state, and $\rho_{\rm sys}$ is the complete system density matrix given in (3.40).

The effect of the measurement on the state of the membrane can be visualized particularly clearly in terms of its Wigner distribution function

$$W(x,p) = \frac{1}{2\pi\hbar}\int d\xi e^{-ip\xi/\hbar}\langle x+\xi/2|\rho|x-\xi/2\rangle \tag{3.42}$$

For a harmonic oscillator in a thermal state, we have

$$W(x,p,t=0)=\frac{1}{\pi\hbar}\tanh\eta\exp\left[-\frac{m\omega_m}{\hbar}\left(x^2+\left(\frac{p}{m\omega_m}\right)^2\right)\tanh\eta\right] \tag{3.43}$$

an expression that should be contrasted to the post-measurement Wigner function, which is found to be

$$\begin{aligned}
&W(x,p,t)=\frac{1}{\pi\hbar}\tanh\eta\frac{1}{P(\phi)} \\
&\sum_{\alpha,\beta}W^{\phi}_{\beta\alpha}\rho^{0}_{\alpha\beta}\exp\left[-i\Omega_{L0}(\alpha-\beta)t+i\delta\Omega_L(\alpha^2-\beta^2)t\right]\times \\
&\exp\left[-\frac{m\omega_m}{\hbar}\left\{\left(\left(x+\frac{A_+}{2}(1-\cos(\omega_m t))\right)^2+\left(\frac{p}{m\omega_m}+\frac{A_+}{2}\sin(\omega_m t)\right)^2\right)\tanh\eta\right. \\
&\left.+iA_-\left(x\sin(\omega_m t)-\frac{p}{m\omega_m}\Big(1-\cos(\omega_m t)\Big)+\frac{A_+}{2}\sin(\omega_m t)\right)\right\}\Bigg].
\end{aligned} \tag{3.44}$$

Here, we have introduced $A_+ = A(\alpha+\beta)$ and $A_- = A(\alpha-\beta)$ for brevity. At time t the first line of Eq. (3.44) simply describes the imposition of a global phase in $W(x,p)$, with a value depending on the measurement outcome. More interesting are the last two lines in that expression: The second line describes a shift and stretch of the initial gaussian distribution, with a value dependent on the temperature and back-action parameter A. When this is the dominant term, the measurement results in an oblate gaussian Wigner function moving around the phase space at the membrane frequency. The measurement dependent position shift is derived in the next subsection.

The third line in $W(x,p,t)$ results in oscillations of the Wigner function. These are due to the fact that the initial state of the BEC, $|F_x=1\rangle$, is not an eigenstate of the interaction Hamiltonian (proportional to F_z). So, one can think of the condensate as experiencing three interaction Hamiltonians simultaneously, one for each of its spin components, and it is the interference between them that leads to the oscillations. We remark that the oscillations in the Wigner function can be seen as

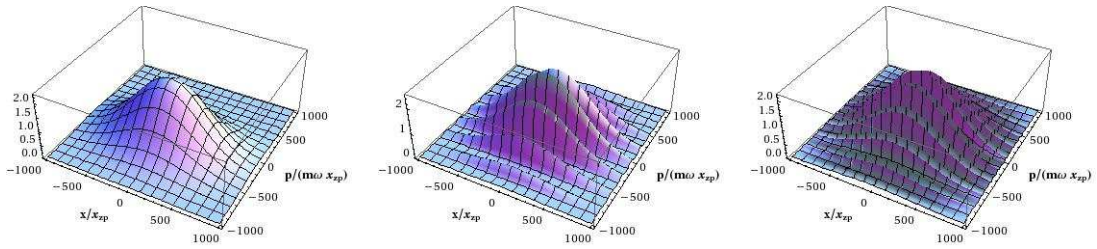

a. $A = 0.01A_0$ **b.** $A = 0.1A_0$ **c.** $A = A_0$

Figure 3.5: (Color online) Wigner distribution function of the membrane after one measurement giving the result $F_y = 1$, for several values of the back-action parameter: (a) $A = 0.01A_0$: (b) $A = 0.1A_0$ and (c) $A = A_0$, with $A_0 = 0.246\sqrt{\hbar/2m\omega_m}$. The evolution time is $t = \pi/\omega_m$ in all three cases. The Wigner function has been multiplied by 10^6 to make the axes legible.

long as

$$\frac{A}{x_{zp}} \gtrsim \sqrt{\tanh \eta} \tag{3.45}$$

where $x_{zp} = \sqrt{\hbar/2m\omega_m}$.

3.2.3 Back-action

To illustrate the effect of backaction, we assume the membrane parameters: $\omega_m = 2\pi 10^6$ rad/s, $m = 10^{-17}$ kg, $\mu_m = 10^{-12}\mathrm{A}\cdot\mathrm{m}^2$, and an initial temperature of 4K. The static external magnetic field is $B_0 = 0.1$ Gauss, and the condensate is $x_0 = 5\times 10^{-6}$ m away from the membrane, resulting in a single-atom back-action parameter $A_{\mathrm{sa}} = 2.25 \times 10^{-18}$ m. We assume that $N = 10^4$ atoms experience the same magnetic field in the detection region, yielding then an effective back-action parameter of $A_0 = NA_{\mathrm{sa}} = 2.25 \times 10^{-14}$m (for comparison, $A_0 = 0.246x_{zp}$). Fig. 3.5 shows the resulting post-measurement Wigner Function for this A_0 (figure c), and for the backaction parameter being $0.1A_0$ (figure b), and $0.01A_0$ (figure a)., assuming that a measurement of F_y with result 1 was made after an interaction time of $t_1 = \pi/\omega_m$.

As alluded to by Eq. (3.45), in order to observe the oscillations in the post-

measurement Wigner function, we can either increase the temperature or increase A. However, increasing the temperature leads to dissipation and decoherence losses that are ignored in the present analysis, but result of course in a fast thermalization and associated smoothing of $W(x,p)$. These effects will be discussed later in this section. A more promising approach to observe quantum intereference effects will be to increase A (Eq. (3.37)), either by increasing the number of atoms in the effective detection zone, or by increasing B_v' via a decrease of x_0. Since B_v' scales as $1/x_0^4$, this may be the easiest way to reach the regime of observable Wigner function oscillations. Note however that for decreasing x_0 the simplified interaction Hamiltonian (3.35) becomes less accurate as the components of the magnetic field along x and y become more important, so the approximations made in Eq. (3.36) will not be as valid.

An additional point of concern is that the BEC does not act as a good position sensor for high A, as can be seen in Fig 3.5. The act of measurement on the BEC creates a significant change in the phase-space distribution of the membrane that would invalidate any information gained about the position. However, as we show in Section V, a high value of A is beneficial for preparing the membrane in highly non-classical states via repeated measurements. As with all schemes for state preparation involving repeated measurements, its not very efficient for highly excited initial states like the one considered in Fig. 3.5 considering – at 4 K, and for the membrane parameters of this example, the mean phonon occupation number is 5.2×10^5.

The expectation value of the center-of-mass position $\langle x \rangle$ of a membrane in thermal equilibrium is zero, and its variance is

$$\sigma^2(x) = \langle x^2 \rangle - \langle x \rangle^2 = \langle x^2 \rangle = \frac{\hbar}{2m\omega_m} \coth \eta. \tag{3.46}$$

Immediately following the measurement, the membrane is no longer in thermal equilibrium, and $\langle x \rangle \neq 0$ in general. For large back-action parameters the oscillations

on $W(x,p)$ become quite significant, but on the other hand, these oscillations also indicate that in that regime the BEC is a poor position sensor, since its coupling to the membrane significantly perturbs the outcome of subsequent measurements. To investigate the efficiency of our setup as a position sensor, it is therefore appropriate to consider the limit of small A_0. Consider for concreteness the specific example where the outcome of the spin measurement is $F_y = 1$. Ignoring then terms of order A^2, and for $t = \pi/\Omega_{L0}$, we find

$$\langle x \rangle = -\frac{A}{2} \sin(\omega_m \pi/\Omega_{L0}) \coth \eta, \tag{3.47}$$

with $\langle x^2 \rangle$ remaining constant to lowest order in A. We then have

$$\sigma^2(x)_{\rm pm} = \frac{\hbar}{2m\omega_m} \coth \eta - \frac{A^2}{4} \sin^2 (\omega_m \pi/\Omega_{L0}) \coth^2 \eta \tag{3.48}$$

where the subscript "pm" indicates post-measurement. The minimum back-action occurs for $\eta \to \infty$, or $T \to 0$. It also vanishes when the membrane frequency is an integer multiple of Larmor precession frequency,

$$\omega_m = n\Omega_{L0}, \tag{3.49}$$

where n in an integer, in which case it is possible to carry out stroboscopic QND measurements of the membrane position.

3.2.4 Coherent state

We now turn to the situation where the center-of-mass state of the membrane is in a coherent state. an initial condition that can be prepared by driving the membrane with a classical force. The main result of this section is to demonstrate that each measurement splits the center-of-mass of membrane is split into a superposition of up to 9 discrete coherent states, hinting at the possibility to generate a macrsocopic Schrödinger cat.

The assumption that the membrane is initially in a coherent state allows us to eschew the density matrix formalism for the moment, and the initial state of the composite system is given by

$$|\Psi(0)\rangle \quad = \quad D(a_0 + ib_0)|0_{\rm mem}\rangle \otimes \sum_\alpha c_\alpha |\alpha\rangle \tag{3.50}$$

where $\sum_\alpha |c_\alpha|^2 = 1$ and

$$D(u) = \exp(u\hat{a}^\dagger - u^*\hat{a})$$

is the displacement operator for the center-of-mass state of the membrane.

Following a procedure similar to that for the initially thermal membrane, we arrive at the final Wigner function for the hybrid membrane-BEC system after a single, and successive measurements. These analytical results are given in ref. (85), and also in Appendix B. Figure 3.6(a) considers the particular case when the membrane was initially in state $|\alpha\rangle = 1/(2x_{\rm zp})(1 + i(1/(m\omega_m)))$. A measurement of F_y at time $t = \pi/\omega_m$ yielded a value 0. The interesting feature of this measurement is that the Wigner function becomes negative due to the measurement induced interferences between the displaced coherent states. Thus, only after a single spin measurement, we can get some non-classical features in the membrane motion. We now develop a theory for the evolution of such states in the presence of a thermal bath.

3.2.5 Effect of the thermal bath

We now introduce the coupling of membrane to a thermal reservoir in order to study how these non-classical states decay. We choose to solve the equation of motion for the Wigner quasi-probability density in the presence of a thermal reservoir. This formalism captures the classical and quantum features of the process in an intuitive manner. Furthermore, it can be solved analytically, at least for this simple case, and therefore gives us a better understanding of the underlying processes. Details

of the derivation of this equation of motion is given in Appendix B. Here, we just state the equation and its solution.

The equation of motion for the Wigner function of a membrane coupled to a BEC and a thermal reservoir after a single measurement is

$$\frac{\partial}{\partial t}W(x,p) = \sum_{\alpha_s,\beta_s}\langle F_y=\delta_s|\alpha_s\rangle\langle\alpha_s|\rho_{BEC}|\beta_s\rangle\langle\beta_s|F_y=\delta_s\rangle \tag{3.51}$$
$$\left\{-\frac{\partial}{\partial x}\left(\frac{p}{m}\right)+\frac{\partial}{\partial p}\left(m\omega_m^2 x+\gamma p+(\alpha_s+\beta_s)\frac{Am\omega_m^2}{2}\right)+\hbar m\omega_m\gamma_m\left(\bar{n}_{th}+\frac{1}{2}\right)\frac{\partial^2}{\partial p^2}\right.$$
$$\left.-i\Omega_{L0}(\alpha_s-\beta_s)-i(\alpha_s-\beta_s)\frac{Am\omega_m^2}{\hbar}x\right\}W(x,p)$$

Here, subscript "s" denotes the spin degrees of freedom. $F_y=\delta_s$ is the result of the spin measurement. Line 2 of equation (3.51) has the form of a Fokker-Planck equation for the Wigner quasi-probability distribution for a harmonic oscillator coupled to a thermal bath. The third line describes the coupling of the membrane to the spinor condensate. It is this coupling that is responsible for the generation of non-classical states. We shall solve this equation and these non-classical features decay due to the reservoir for case of a single measurement.

The Fokker-Planck equation, Eq.3.51 corresponds to Langevin equations given by

$$\dot{x} = \frac{p}{m} \tag{3.52}$$
$$\dot{p} = -m\omega_m^2 x-\gamma_m p-(\alpha_s+\beta_s)\frac{Am\omega_m^2}{2}+F_p(t), \tag{3.53}$$

where $F_p(t)$ denotes a Gaussian random process with zero mean and

$$\langle F_p(t_1)F_p(t_2)\rangle = 2m\omega_m\gamma_m\left(\bar{n}_{th}+\frac{1}{2}\right). \tag{3.54}$$

$F_p(t)$ denotes the random momentum kicks that lead to Brownian motion. These Langevin equations give us some physical insight into the processes of dissipation and measurement backaction. The equation of motion for momentum has two extra

terms than the normal harmonic oscillator. The first one is due to measurement backaction. A measurement of spin does indeed give the membrane momentum kicks proportional to the back-action parameter, A. The second term is the random momentum kick due to the thermal bath, as is the standard for any viscous damping process.

In order to simplify things a bit, we move to a set of dimensionless units: $x \rightarrow x/x_{zp}, A \rightarrow A/x_{zp}$ and $p \rightarrow p/m\omega_m x_{zp}$, where $x_{zp} = \sqrt{\hbar/2m\omega_m}$ is the zero point displacement.

The solution to Fokker-Planck equations of type

$$\begin{aligned} \frac{\partial}{\partial t}W_1(x,p) &= \left\{-\frac{\partial}{\partial x}\left(\omega_m p\right) + \frac{\partial}{\partial p}\left(\omega_m x + \gamma_m p + (\alpha_s+\beta_s)\frac{A\omega_m}{2}\right)\right. \\ &\left. +2\gamma_m\left(\bar{n}_{th}+\frac{1}{2}\right)\frac{\partial^2}{\partial p^2}\right\} W_1(x,p) \end{aligned} \tag{3.55}$$

are discussed in detail in ref. (101). Ignoring terms of order (γ/ω_m) and higher, we obtain the propagator:

$$\begin{aligned} K(x,p,t|x_0,p_0,0) &= \frac{1}{4\pi\left(\bar{n}_{th}+\frac{1}{2}\right)\left(1-e^{-\gamma_m t}\right)} \times \\ &\exp\left[-\frac{1}{4\left(\bar{n}_{th}+\frac{1}{2}\right)\left(1-e^{-\gamma_m t}\right)}\left\{(x-\langle x_0\rangle)^2+(p-\langle p_0\rangle)^2\right\}\right], \end{aligned} \tag{3.56}$$

where

$$\begin{aligned} \langle x_0\rangle &= \left[\left(x_0+\frac{A_+}{2}\right)\cos\omega_m t + p_0\sin\omega_m t\right]e^{-\gamma_m t/2} - \frac{A_+}{2} \\ \langle p_0\rangle &= \left[p_0\cos\omega_m t - \left(x_0+\frac{A_+}{2}\right)\sin\omega_m t\right]e^{-\gamma_m t/2}. \end{aligned} \tag{3.57}$$

Here, we have introduced $A_+ = (\alpha_s+\beta_s)$ for brevity. The Wigner function at time t is thus given by:

$$W_1(x,p,t) = \int_{-\infty}^{\infty}\int_{-\infty}^{\infty} K(x,p,t|x_0,p_0,0)W(x_0,p_0,0)\,dx_0 dp_0 \tag{3.58}$$

If we assume that the measurement process takes an infinitely small time to perform, we can keep evaluating the Wigner Function after successive measurements using this method. All we need to do is to input the results of the previous measurement to evaluate the Wigner function subject to dissipation and measurements.

Going back to the case of a single measurement, the equation of motion for the Wigner function (equation (3.51)) can be cast as

$$\frac{\partial}{\partial t}W(x,p) = \{\Xi\}W(x,p) + i\xi(t)W(x,p). \tag{3.59}$$

Given $W_1(x,p)$ satisfies $\partial W_1(x,p)/\partial t = i\{\Xi\}W_1(x,p)$, the solution to the complete equation of motion is

$$W(x,p,t) = W_1(x,p,t)\exp i\int_0^t \xi(t')dt'. \tag{3.60}$$

For our problem, $\xi(t) = -i\Omega_{L0}(\alpha_s - \beta_s) - i(\alpha_s - \beta_s)\frac{A\omega_m}{2}x(t)$, with
$x(t) = \left[\left(x + \frac{A}{2}(\alpha_s + \beta_s)\right)\cos\omega_m t + p\sin\omega_m t\right]e^{-\gamma_m t/2} - \frac{A}{2}(\alpha_s + \beta_s)$.

We now consider a specific example of the post single-measurement Wigner function for the initial coherent state $|\alpha\rangle = 1/2(1+i1)$ in these dimensionless units. The coherent state evolves under the interaction of the BEC and a thermal bath. A measurement of F_y is made after time $t = \pi/\omega_m$ giving the result 0. This measurement generates a non-classical state of the membrane as depicted in Figure 3.6. Figure 3.6(a) shows the Wigner function in the absence of a thermal bath. As demonstrated in the figure 3.6(b,c,d), as the coupling to the reservoir is increased, i.e. as γ_m is increased, we notice that the negative features of the Wigner Function disappear. For much higher values of γ_m, we also notice the blurring of coherent state as they become more like the steady state value of a thermal state. This is in agreement with our intuition that quantum states are very fragile, and very little coupling to the outside world can wash out all the quantum features much before the state is in equilibrium with the environment.

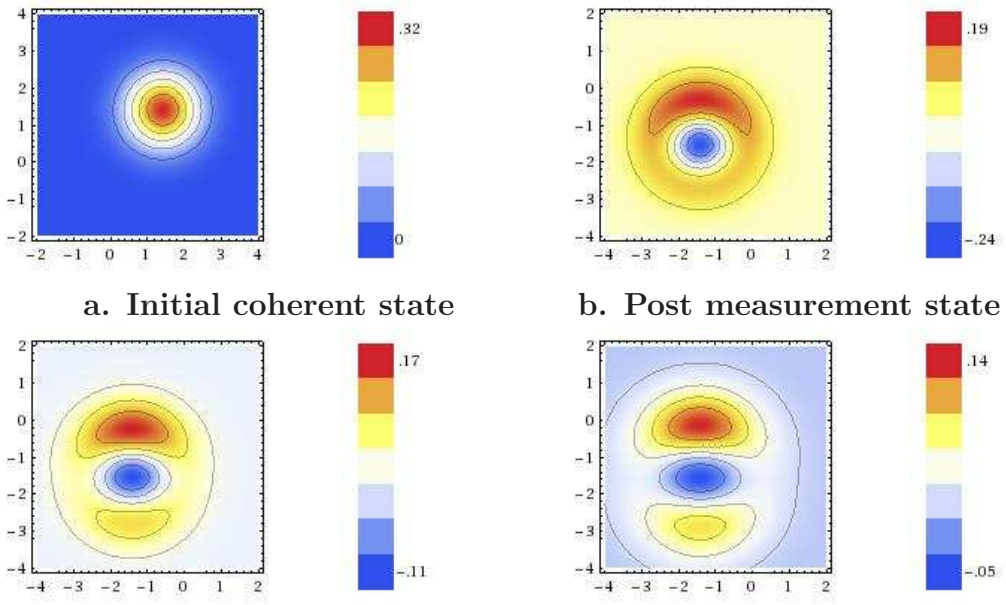

a. Initial coherent state **b. Post measurement state** $\gamma_m = 1$

c. Post measurement state $\gamma_m = 5$ **d. Post measurement state** $\gamma_m = 10$

Figure 3.6: Wigner distribution function of the membrane after the first spin measurement after time $t = \pi/\omega_m$ giving the result $F_y = 0$ for different values of γ_m. Stronger coupling to thermal bath leads to faster decay of non-classical features.

3.2.6 Conclusion

In conclusion, we have demonstrated that by coupling a magnetic membrane to a spinor BEC, we can monitor and manipulate the position of the membrane. A projective measurement procedure induces significant back-action that can be measured for reasonable experimental parameters. We investigated the effect of this interaction for different initial membrane states, namely thermal and coherent states. We discussed the possibility to measure back-action of a quantum measurement on the membrane via repeated measurements and the potential to generate cat states of the oscillator via such repeated measurements in the case of an initial coherent state. This would be a major accomplishment as such a state has not yet been prepared for a solid, macroscopic object.

Future work could investigate the effects of using a more dispersive (and more experimentally plausible) measurement scheme based on observation of the Larmor precession. Additionally, one could also study of the effects of including dissipation on the system's dynamics in more detail. Other possibilities for extending the model even further include inclusion of a general coupling to other spin components i.e. an interaction Hamiltonian of the form $\vec{F} \cdot \vec{r}$, because at short distances the other components of the magnetic field should not be neglected. Also, the BEC is a spatially finite system, so we may wish to exploit the ability to measure multiple "pixels" of the condensate in order to gain better information about the membrane's position or alternately better control of the membrane's state.

CHAPTER 4

DETECTION OF NON-CLASSICAL STATES

As a consequence of developments in cavity optomechanics, we can look forward to the development of a variety of quantum sensors and new applications in coherent control. Clearly, these rely on our ability not just to operate these systems in the quantum regime, but also to measure and control their state. However, to our knowledge there are currently very few practical schemes to fully characterize the state of a phonon field (102).

This chapter addresses two methods to get around the problems that arise due to the absence of phonon detectors. The first proposed solution involves coupling the phonon field to a classical optical field and a qubit simultaneously. By measuring the state of the qubit one can, in principle, get information about the entire density matrix (or equivalently the Wigner quasi-probability function) of the mechanical oscillator. The work presented here is published in ref. (103).

The second part of the this chapter discusses an example of quantum state transfer. There are several proposals about transferring quantum correlations from mechanical to optical fields, where state characterization techniques via homodyne spectroscopy are well established (104; 105; 106). Instead, we investigate a state transfer scheme between a Bose-condensate and mechanical oscillator that is mediated by the light field. Both atomic and mechanical systems have much lower dissipation than optical systems, and as such this approach opens up possibilities of studying quantum-classical transition in coupled atomic-mechanical systems. The work presented here is under review and is available in ref. (107).

4.1 Wigner Tomography in atomic-mechanical hybrid systems

This section discusses a scheme to measure the Wigner function of a mechanical oscillator by coupling it to optical fields and a qubit. Typical frequencies of the nanomechanical structures under consideration are in the MHz range, and the challenge is to characterize a phononic state in that frequency range, where there are no detectors. A related difficulty arises in microwave cavity QED, where, in contrast to the situation in the visible regime, the absence of photon counters results in the need to develop alternative methods such as nonlinear atomic homodyning (108) and Wigner tomography (109; 110; 3; 111; 4) to characterize the state of the intracavity field. A common feature of these methods is that they consist of a sequence of measurements that result in the reconstruction of the Wigner function of the field. In particular, Ref. (108) showed that the time-dependence of the upper state population of a two-state atom coupled to both the field to be characterized and a (classical) external field yields a direct measurement of the Wigner function of that field.

We show in the following that it is possible to extend this concept to the characterization of phononic fields, thereby providing a detection method to measure the quantum state of a nanomechanical oscillator. Our scheme relies on the fact that it is considerably easier to measure the state of excitation of an atom than it is to directly measure the state of a field. It proceeds by transferring the state of the mechanical oscillator to the atomic population of a "detector atom." This population can then easily be probed via a standard destructive measurement, like state-selective ionization. One difficulty in achieving this goal is the poor frequency match between nanomechanical and optical frequencies. One way to circumvent this mismatch is through the use of a Raman process.

Recent progress in the nanofabrication of high frequency, high-Q resonators and their successful cooling to extremely low thermal occupation numbers make them a

viable candidate to demonstrate our scheme. The specific system that we have in mind is a doubly clamped nanomechanical resonator. The resonator is coupled to a two-level atom through a magnetic domain deposited on its surface. Good atomic candidates include alkali with hyperfine splitting close to the resonator's vibration frequency, such as ^{6}Li or ^{23}Na.

4.1.1 Model

The mode of vibration of the resonator to be measured is described as a simple harmonic oscillator of effective mass m_c and frequency ω_c, with Hamiltonian $H_c = \hbar\omega_c \left(c^\dagger c + \frac{1}{2}\right)$, where c and $c^\dagger$ are bosonic annihilation and creation operators. The two-state system is described by the Hamiltonian $H_a = \hbar\omega_0\sigma_z/2$, ω_0 being the hyperfine splitting between the two atomic states in the presence of an external magnetic field B_z. The quantization axis z is chosen orthogonal to the direction of vibration, x, of the resonator, so that the Zeeman coupling of the atom to the oscillator is given in the rotating wave approximation by (79)

$$H_{ac} = \mu_B g_F m_{Fx} G_B x_c, \tag{4.1}$$

with $\mu_B g_F m_{Fx}$ being the atomic dipole operator. Here μ_B is the Bohr magneton, g_F is the Landé factor of the F quantum number of the atom, m_{Fx} is the projection of F in the x-direction. G_B is the gradient of the magnetic field experienced by the atom, and x_c is the position operator of the resonator's vibrational mode of interest, $x_c = \sqrt{\frac{\hbar}{2\omega_c m_c}}(c + c^\dagger)$. Such a coupling between a mechanical resonator and alkali atoms has been demonstrated experimentally in Ref. (77).

At resonance, $\omega_c = \omega_0$, and in the rotating wave approximation, the interaction between the resonator and the atom is described by the Jaynes-Cummings Hamiltonian

$$H_{ac} = \hbar g_{ac}(c^\dagger\sigma_- + c\sigma_+) \tag{4.2}$$

where $g_{ac} = \mu_B g_F m_{Fx} G_B \sqrt{\frac{\hbar}{2\omega_c m_c}}$.

Approximating the ferromagnetic domain as a magnetic dipole results in the magnetic field gradient $|G_B| = 3\mu_0|\mu_c|/4\pi r^4$, where μ_c is the dipole moment of the resonator magnet. The strong dependence of G_B on r, the distance between the atom and the resonator, enables us to achieve very strong gradients close to the resonator. It also provides us with a wide range of tunability of the interaction strength which, when combined with the tunable splitting of various m_F levels via a static magnetic field applied in the z-direction ($B_z \gg B_x$), can result in a strong resonant coupling for an experimentally reasonable range of parameters. In the case of optically trapped atoms, possible hyperfine transitions include the use of collisionally stable stretched states. Alternatively, one can consider magnetically trappable hyperfine states in an atom chip trap, which would provide greater tunability in terms of distance between the atom and the oscillator. Combining ultra-cold atoms with cryogenics has already been demonstrated in the context of atom chips with superconducting wires (112; 113).

The coupling of the oscillator to a two-state system is not sufficient to determine its state, since in the Jaynes-Cummings interaction the state of the system depends only on correlation functions of the phononic field of the form $\langle (c^\dagger c)^n \rangle$, $\langle (c^\dagger c)^n c \rangle$ or $\langle (c^\dagger c)^n c^\dagger \rangle$, where n is an integer. To fully characterize it, we need instead access to a full set of correlation functions of the generic form $\langle c^\dagger c^\dagger \dots c^\dagger c c \dots c \rangle$. As discussed in Ref. (108) this can be achieved by coupling the atom to an additional external field. To account for the frequency mismatch between optical and hyperfine transition frequencies, in the present case that additional coupling is provided by a Raman transition involving a virtual transition to an additional excited state $|i\rangle$. That state is coupled via electric dipole interaction to the lower state $|g\rangle$ by a far detuned classical field of Rabi frequency $\Omega_L = dE_L/\hbar$, where d is the electric dipole moment of the transition, and E_L is the electric field amplitude. The state $|i\rangle$ is also coupled to the other ground state $|e\rangle$ by a quantized field described by the bosonic annihilation and creation operators a_k and $a_k^\dagger$. The vacuum Rabi frequency of that transition is

$\Omega_k = d\sqrt{\omega_k/2\epsilon_0\hbar V}$.

Adiabatically eliminating the upper state $|i\rangle$, this Raman process is described by the effective Hamiltonian (114; 115)

$$H_{\text{Raman}} = -\hbar\frac{\Omega_L\Omega_k}{\delta_L}(a_k\sigma_+ + a_k^\dagger\sigma_-), \tag{4.3}$$

where $\delta_L \gg \omega_0$ is the detuning of the two optical transitions involved in the process.

The situation is particularly simple if the coupling strength of the atom to the resonator and the Raman fields are equal, $g_{ac} = -\Omega_L\Omega_k/\delta_L \equiv g$, a condition that can be realized either by adjusting the strength of the classical Raman field, or the Raman detuning, or the distance between the atom and the resonator. In that case the interaction Hamiltonian reduces to

$$H = \hbar\sqrt{2}g(\sigma_- A^\dagger + \sigma_+ A) \tag{4.4}$$

where we have introduced the bosonic operator $A = \frac{1}{\sqrt{2}}(a_k + c)$ with $[A, A^\dagger] = 1$.

As a realistic example leading to this simplified description, a doubly clamped beam of Si of length l =2.2 μm, width w =250 nm, and thickness t =200 nm with a permanent magnet of magnetization 5×10^6 A/m and dimensions (700,250,100) nm deposited on it has a fundamental mechanical mode at 228 MHz (116), which corresponds to the hyperfine splitting of ^{6}Li. This setup produces a coupling of g=15.5 kHz at a distance of 200 nm from the beam. That same coupling strength can be obtained for a Raman transition driven by a laser field intensity of 0.336 mW/cm^2 and a detuning of 5 GHz. We use these parameters for the numerical estimates presented in this paper.

The Hamiltonian (4.4) is again a Jaynes-Cummings Hamiltonian, but in terms of the phononic-photonic composite mode $a_k + c$. The key point here is that the correlation functions involved in the atomic evolution are now of the form $\langle(A^\dagger A)^n\rangle$, $\langle(A^\dagger A)^n A\rangle$ or $\langle(A^\dagger A)^n A^\dagger\rangle$, and it is the appearance of composite modes in these correlation functions that permit access to all correlation functions of the resonator.

At first sight, this might appear to raise the question of conservation of energy, since the photon energy $\hbar\omega_k$ is vastly higher than the phonon energy $\hbar\omega_c$. But while this is not explicitly apparent when one of the optical fields is treated classically, at the microscopic level the emission (absorption) of a photon in mode k is always accompanied by the absorption (emission) of energy by the other Raman field, and it is the energy difference $\hbar\omega_0$ between these two processes that is relevant.

For an atom in the initial mixture $\rho_{\rm atom} = \rho_e|e\rangle\langle e| + \rho_g|g\rangle\langle g|$ and initially uncorrelated atom, resonator, and optical fields, $\rho(0) = \rho_a(0) \otimes \rho_c(0) \otimes \rho_o(0)$, the probability P_g to find the atom in the ground state at time τ is

$$\begin{aligned} P_g &= \frac{1}{2}\rho_g\langle\cos\left(2\sqrt{2}g\tau\sqrt{A^\dagger A+1}\right)\rangle \\ &\quad -\frac{1}{2}\rho_e\langle\cos\left(2\sqrt{2}g\tau\sqrt{A^\dagger A+1}\right)\rangle - \frac{1}{2} \end{aligned} \tag{4.5}$$

where $\langle X\rangle \equiv Tr\left(\rho_c(0)\rho_o(0)X\right)$.

Considerable insight can be gained by investigating the situation where the resonator state is close to the ground state, with $\langle n_c\rangle \equiv \langle c^\dagger c\rangle \simeq 1$, a situation of much experimental interest, and the Raman field is in a coherent state $|\beta_k\rangle$ with $\langle\beta_k\rangle = \sqrt{I}\exp(i\phi)$ and $|\beta_k|^2 \equiv I \gg \langle n_c\rangle$. We then have

$$\begin{aligned} \sqrt{A^\dagger A+1} &\approx \sqrt{A^\dagger A} \\ &= \sqrt{\frac{1}{2}\left[\langle n_c\rangle + I + I^{1/2}(c^\dagger e^{i\phi} + ce^{-i\phi})\right]} \\ &\approx \sqrt{\frac{I}{2}} + \frac{1}{2\sqrt{2}}\left(c^\dagger e^{i\phi} + ce^{-i\phi}\right) \end{aligned} \tag{4.6}$$

and the ground state probability simplifies to

$$P_g = \frac{1}{4}\left(\rho_g - \rho_e\right)\left(e^{2ig\tau\sqrt{I}}C_W(\mu) + h.c.\right) - \frac{1}{2} \tag{4.7}$$

where $\mu = ig\tau\exp(i\phi)$ and C_W is the Wigner characteristic function of the resonator phonon mode,

$$C_W(\mu) = Tr(\rho_c(0)e^{\mu c^\dagger - \mu^* c}). \tag{4.8}$$

As is the case in Wigner tomography, the full Wigner characteristic function, and hence the Wigner function of the phonon mode, can be reconstructed by varying the interaction time τ and/or the phase ϕ of the Raman field. We emphasize that this is a destructive measurement scheme, and that in general a large sequence of measurements that scan μ in the complex plane starting from identical initial conditions is necessary to reconstruct the state of the resonator. This is similar to the situation in cavity QED and in circuit QED (3; 4).

4.1.2 Measurement Backaction

The back-action of a sequence of repeated measurements of the kind proposed here on the state of the resonator is normally very significant. To illustrate this point we assume that a series of measurements on the resonator are performed by a sequence of detector atoms initially in their ground state. Their ground-state population is measured after an interaction time τ. It is easy to show that for classical Raman fields and in the absence of dissipation, a resonator initially in a pure state remains then in a pure state. We concentrate on this simple case for clarity, noting that the extension to mixed states is straightforward.

Immediately following the i-th measurement, the state of the oscillator is given by (117)

$$|\psi_{c,i}\rangle = \frac{\langle g|U(\tau)|\psi_{c,i-1}; g\rangle}{\sqrt{P_g(\tau)}} \tag{4.9}$$

where $U(\tau)$ is the evolution operator associated with the Jaynes-Cummings Hamiltonian (4.4) and $|\psi_{c,i}; g\rangle$ is the state of the full system (resonator+atom) just as the i-th detector atom is switched on. In the limiting case $I \gg \langle n_c\rangle$ this yields

$$\begin{aligned}|\psi_{c,i}\rangle = &\frac{1}{2\sqrt{P_g}}\left(\cos(g\tau\sqrt{I})\,[D(\mu/2) + D(\mu/2)]\right) + \\ &\frac{1}{2\sqrt{P_e}}\left(i\sin(g\tau\sqrt{I})\,[D(\mu/2) - D(-\mu/2)]\right)|\psi_{c,i-1}\rangle,\end{aligned} \tag{4.10}$$

where $D(\mu) = \exp(\mu c^\dagger - \mu^* c)$ is the displacement operator. At the beginning of

the $(i+1)$-th measurement, the initial state of the full system is therefore $|\psi_{c,i}; g\rangle$ (neglecting dissipation and the free evolution between atoms), from which the next iteration is started. The successive measurements therefore displace the state of the resonator into different regions of phase space, and the distance between these regions keeps increasing as a function of time. This is illustrated in Fig. 4.1 that shows the Wigner Function of the resonator (with the paramaters mentioned earlier) after successive measurements done at equal time intervals of $\tau = 0.5$ ms, for a resonator intially in vacuum state.

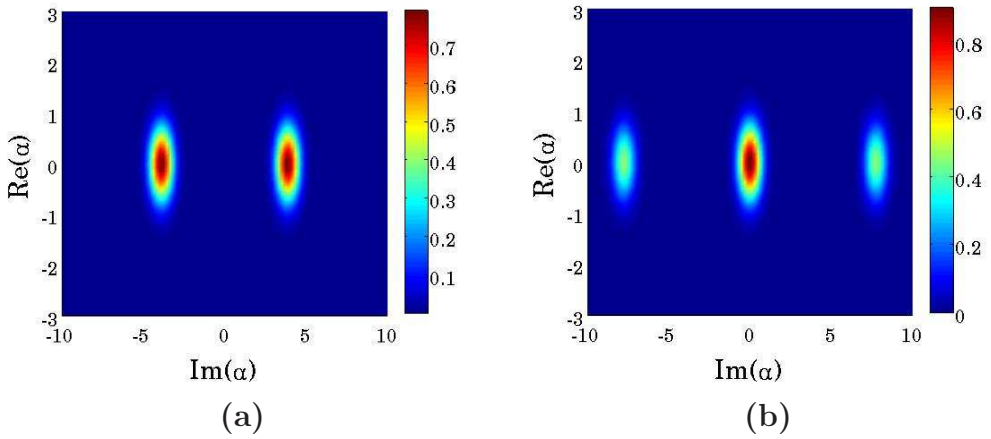

Figure 4.1: Wigner distribution function of the resonator after (a) a first measurement after time τ=.5ms of evolution, and (b) subsequent measurement after equal duration τ. Here the resonator was taken to be initially in the ground state (hence, Wigner Function already determined), and μ is purely imaginary μ=7.75i.

It is interesting to compare this measurement scheme to the Quantum Non-Demolition (QND) measurements used to reconstruct the Wigner function of microwave cavity fields (3). QND measurements of the diagonal elements of the field density operator are realized by an interaction that is sensitive only to the photon number. The determination of its off-diagonal elements require then displacing the cavity field by external coherent pulses $|\alpha\rangle$, and carrying QND measurements for that particular α. However, due to the current absence of experimental techniques

to displace phonon fields, we resort to the proposed non QND homodyne measurement scheme. Provided the dissipation is kept under control, that scheme has no significant disadvantage compared to a QND approach. The only difference is that the resonator needs to be re-prepared in the same initial state after each atomic detection, instead of just for each different α. The actual number of measurements required to completely determine the Wigner Function depends on the state of the mechanical oscillator (determination of fock state would require more points in phase space), and the accuracy desired.

4.1.3 Concluding remarks

We conclude by commenting on the role of dissipation in the proposed scheme. In order to measure the Wigner function of the oscillator, the measurement process takes place in a time short compared to the dissipation time of both the cantilever and the detector atom. In our specific example of ^{6}Li atoms coupled to a Si resonator, the time scale of the coherent cantilever-detector coupling is given by $1/g \approx$65 μs, a time that must be significantly shorter than the characteristic times of the various decoherence and dissipation mechanisms. Typical lifetimes of atoms trapped in optical or magnetic traps range from 100 ms to a few seconds, and hence much longer than $1/g$ and not a serious concern. The spontaneous decay rates associated with allowed optical dipole transitions are in the tens of MHz to GHz range. For Raman transitions, these rates must be weighted by the probability $\approx \Omega_L\Omega_k/\delta_L^2$ of occupation of the virtual intermediate state. For our parameters, this yields a Raman decay time of the order of a few milliseconds.

The second major source of dissipation is the coupling of the nanomechanical resonator to its mechanical support, which acts as a thermal reservoir. The associated thermal dissipation rate is proportional to $\Gamma\bar{n}_{th}$, where $\Gamma = \omega_c/Q$, Q is the quality factor of the relevant mode of vibration of the mechanical oscillator, and $\bar{n}_{th}$ is the mean thermal occupation number for the reservoir, $\bar{n}_{th} \approx k_B T_{bath}/\hbar\omega_c$.

For a Q-factor of 5×10^6 and a cryogenic environment with $T_{bath} = 10$mK, this yields a characteristic dissipation time of the order of 4×10^{-3} s. We would like to note that while such high Q-factors are yet to be experimentally demonstrated in similar nanomechanical systems, a Q-factor of 10^5 at room temperature has already been attained for a 10 MHz beam resonator made of SiN (118). Such strides in improved fabrication methods for these structures make us optimistic, and we believe that while these parameters look challenging for current experimental setups, they should be within the reach of next generation experiments in the field.

These values indicate that while certainly challenging, conditions under which dissipation and decoherence can largely be ignored in the analysis of the proposed detection scheme are within experimental reach. Future work will include the effects of weak decoherence due to the coupling of the nanoscale oscillator to a thermal bath, considering in particular the situation of non-classical states and entanglement between several oscillators(119) or between an oscillator and an optical field (120).

In summary, we have proposed a destructive measurement scheme to determine the Wigner function of a mechanical resonator cooled near its ground state of vibration. Our proposed setup involves a detector atom coupled to the phonon mode of relevance, and to a pair of optical fields that induce a Raman transition between the ground and excited state of the detector atom. We remark that the same coupling scheme can also be used to prepare an arbitrary quantum state of the resonator, as can be seen by a straightforward extension of the results of Ref. (121), which demonstrated that a two-level system coupled to a classical and a quantum field can be used to generate an arbitrary state of that field, provided the two couplings can be tuned independently. An experimental realization of such quantum states was recently demonstrated in a circuit-QED system by Hofheinz et al. (4). By independently controlling the Raman and magnetic coupling, the present system can likewise provide the ability to generate arbitrary quantum states of the resonator.

4.2 State Transfer

This section investigates the possibility of quantum state transfer between momentum excitations of a Bose-condensate and a micro-mechanical oscillator. An impressive recent breakthrough in the study of quantum degenerate atomic gases is the ability to manipulate atoms trapped in optical lattices. This opens up a number of new possibilities in several frontier topics, including the control and quantum simulation of strongly correlated quantum systems (122; 123; 124; 125) and quantum information. Alternatively, one could think of generating macroscopic cat states in mechanical systems (34). As such it would be of considerable interest to transfer quantum states between ultra-cold atomic systems and mechanical oscillators, as this would offer an intriguing route to study the quantum dynamics of truly macroscopic systems and the quantum to classical transition. One particularly attractive aspect of quantum state transfer between micromechanical structures and atomic Schrödinger fields is that both subsystems can have extremely low dissipation and decoherence rates compared to optical fields in resonators.

While there are now well understood optomechanical quantum state transfer protocols between optical and phonon fields and between electromagnetic fields of different frequencies (104; 105; 106), this is not yet the case for state transfer between Schrödinger fields and phonon fields. This section describes a scheme that achieves that goal for the case of single-mode fields in a hybrid system consisting of an atomic BEC trapped inside a Fabry-Pérot cavity with a suspended end-mirror or equivalent micromechanical analog. While most manybody states of interest in condensed matter physics involve multimode fields, achieving single-mode state transfer is an essential first step. A key result of our analysis is the demonstration that under appropriate conditions our hybrid system can be described by an effective beamsplitter Hamiltonian with a quantum noise source due to the eliminated optical field. The beam splitter Hamiltonian is well known as a paradigm for state

transfer between subsystems and its appearance for our hybrid system opens the door to state transfer between a BEC and a micromechanical element.

4.2.1 Model

The interaction between the oscillating end-mirror, the (non-interacting) BEC and the single-mode intracavity field is described by the Hamiltonian

$$\begin{aligned} H &= \hbar\omega_c \hat{A}^\dagger \hat{A} + i\hbar\eta(\hat{A}^\dagger e^{-i\omega_l t} - \hat{A}e^{i\omega_l t}) \\ &+ \int dx \hat{\psi}^\dagger(x) \left[-\frac{\hbar^2}{2m_a}\frac{d^2}{dx^2} + \frac{\hbar g^2 \hat{A}^\dagger \hat{A}}{\Delta_a}\cos^2(kx) \right] \hat{\psi}(x) \\ &+ \frac{\hat{p}^2}{2m_m} + \frac{1}{2}m_m \Omega_m^2 \hat{q}^2 - \hbar\xi \hat{A}^\dagger \hat{A}\hat{q} + H_{\rm d}. \end{aligned} \tag{4.11}$$

Here $\hat{A}$ and $\hat{A}^\dagger$ are the bosonic annihilation and creation operators of the intracavity light field, $\hat{p}$ and $\hat{q}$ are the momentum and position operators of the mirror of effective mass m_m and frequency Ω_m, $\eta = \sqrt{P\kappa/\hbar\omega_l}$ describes the external driving of the optical cavity, where P and ω_l are the laser power and frequency, ω_c is the cavity frequency, L its length and κ its decay rate, $\xi = \omega_c/L$ is the optomechanical coupling constant. The second term in the square brackets describes the off-resonant dipole coupling between the condensate atoms and the intracavity light field of wavelength $\lambda = 2\pi/k$, in the form of an optical potential of period $\lambda/2$. Here, g is the resonant Rabi frequency and $\Delta_a = \omega_l - \omega_a$ is the detuning between the light field and the atomic transition, assumed large enough that the upper electronic state can be adiabatically eliminated. Finally $\hat{\psi}(x)$ is the Schrödinger field operator for the condensate of atoms of mass m_a, and H_d describes the coupling of the optical field, the condensate and the optomechanical mirror to thermal reservoirs. In what follows we neglect the dissipation of the matter-wave and mechanical modes, as they are orders of magnitude slower than the optical decay rate.

The cavity field propagating along the x-axis can predominantly impart a photon recoil $2\hbar k$ to the initial zero-momentum cold atoms via Bragg scattering, and

we assume that phase-matching limits the production of higher scattering orders. Restricting our analysis to one-dimension (x) for simplicity we may expand the Schrödinger field as

$$\hat{\psi}(t) \approx \hat{c}_0\psi_0(x) + \hat{c}_2\psi_2(x), \tag{4.12}$$

where $\psi_0 = \sqrt{1/L}$ and $\psi_2 = \sqrt{2/L}\cos 2kx$, with $\hat{c}_0^\dagger\hat{c}_0 + \hat{c}_2^\dagger\hat{c}_2 = N_a$, the total number of atoms. Substituting this form into the atom-light part of the Hamiltonian (4.11) gives

$$\begin{aligned} H_{\mathrm{a-l}} &= \frac{\hbar(2k)^2}{2m_a}\hat{c}_2^\dagger\hat{c}_2 + \frac{\hbar g^2}{2\Delta_a}\hat{A}^\dagger\hat{A}\left(\hat{c}_0^\dagger\hat{c}_0 + \hat{c}_2^\dagger\hat{c}_2\right) \\ &\quad + \frac{\hbar g^2}{\Delta_a\sqrt{8}}\hat{A}^\dagger\hat{A}\left(\hat{c}_0^\dagger\hat{c}_2 + \hat{c}_2^\dagger\hat{c}_0\right). \end{aligned} \tag{4.13}$$

Assuming that the depletion of the zero-momentum component of the condensate is small, we treat it classically via the replacement $\hat{c}_0, \hat{c}_0^\dagger \to \sqrt{N_a}$. Then neglecting unimportant constant terms, the total Hamiltonian becomes

$$\begin{aligned} H &= \hbar\tilde{\omega}_c\hat{A}^\dagger\hat{A} + i\hbar\eta(\hat{A}^\dagger e^{-i\omega_l t} - \hat{A}e^{i\omega_l t}) \\ &+ \hbar\Omega_m\hat{c}_m^\dagger\hat{c}_m + \hbar\Omega_2\hat{c}_2^\dagger\hat{c}_2 \\ &+ \hbar\hat{A}^\dagger\hat{A}\left[-\xi_m(\hat{c}_m^\dagger + \hat{c}_m) + \xi_2(\hat{c}_2^\dagger + \hat{c}_2)\right] + H_{\mathrm{d}}, \end{aligned} \tag{4.14}$$

where $\tilde{\omega}_c = \omega_c + g^2N_a/2\Delta_a$ is the cavity frequency shifted by the presence of the atomic medium, $\hat{q} = \sqrt{\hbar/2m\Omega_m}(\hat{c}_m + \hat{c}_m^\dagger)$, $\Omega_2 = 2\hbar k^2/m_a$ is four times the recoil frequency of the atoms, $\xi_m = \sqrt{\hbar/2m\Omega_m}\xi$, and $\xi_2 = \hbar g^2\sqrt{2N_a}/(4\Delta_a)$.

The operator $(\hat{c}_2 + \hat{c}_2^\dagger)$ can be interpreted as the dimensionless "position" of the recoiled condensate side mode in Eq. (4.12). Hence, the last non-dissipative term in Eq. (4.14) is an optomechanical term where the position of the recoiled condensate component is subjected to the radiation pressure of the intracavity light field. The Hamiltonian (4.14) therefore describes the interaction of the light field with two oscillating mirrors, one real and one effective. The sign difference between the optomechanical coupling of the suspended mirror and the condensate results

from the fact that while the mirror is pushed by radiation pressure, the atoms in the condensate can be either attracted to regions of high field intensity or of low field intensity, depending on the laser's detuning from the atomic transition, as apparent from the definition of ξ_2.

4.2.2 Elimination of cavity field

In a frame rotating at laser frequency ω_l and with $\hat{a}(t) = \hat{A}(t)e^{i\omega_L t}$, the Heisenberg-Langevin equations of motion are

$$\frac{d\hat{a}}{dt} = \left(i\tilde{\Delta}_c + i\hat{\Phi} - \kappa/2\right)\hat{a} + \eta + \sqrt{\kappa}\hat{a}_{\rm in}e^{i\omega_l t}, \tag{4.15}$$

$$\frac{d\hat{c}_m}{dt} = -i\Omega_m\hat{c}_m + i\xi_m\hat{a}^\dagger\hat{a}, \tag{4.16}$$

$$\frac{d\hat{c}_2}{dt} = -i\Omega_2\hat{c}_2 - i\xi_2\hat{a}^\dagger\hat{a}, \tag{4.17}$$

where $\tilde{\Delta}_c = \omega_l - \tilde{\omega}_c$ is the cavity detuning and

$$\hat{\Phi} \equiv [\xi_m(\hat{c}_m^\dagger + \hat{c}_m) - \xi_2(\hat{c}_2^\dagger + \hat{c}_2)] \tag{4.18}$$

is the combined optomechanical phase shift of the recoiled condensate and the moving mirror.

We now introduce the dimensionless position and momentum variables $\hat{x}_j = (\hat{c}_j + \hat{c}_j^\dagger)/2$ and $\hat{p}_j = i(\hat{c}_j^\dagger - \hat{c}_j)/2$, where $j = \{m, 2\}$. In order to adiabatically eliminate the dynamics of the optical field we proceed by first linearizing the system of operator equations around the classical steady state, with

$$\begin{aligned} \hat{x}_j &\rightarrow \langle\hat{x}_j\rangle + \delta\hat{x}_j, \\ \hat{p}_j &\rightarrow \langle\hat{p}_j\rangle + \delta\hat{p}_j, \\ \hat{a} &\rightarrow \langle\hat{a}\rangle + \delta\hat{a}, \end{aligned} \tag{4.19}$$

and $\hat{a}^\dagger\hat{a} \approx \langle a^\dagger a\rangle + \langle\hat{a}^\dagger\rangle\delta\hat{a} + \langle\hat{a}\rangle\delta\hat{a}^\dagger$. The equation of motion for the expectation value $\langle\hat{a}\rangle$ of the intracavity field is then

$$\frac{d\langle\hat{a}\rangle}{dt} = i\Delta'\langle\hat{a}\rangle + \eta, \tag{4.20}$$

with steady-state value $\langle\hat{a}\rangle_s = -\eta/i\Delta'$, where we have introduced the complex detuning $\Delta' = \tilde{\Delta}_c + \langle\Phi\rangle + i\kappa/2$, which accounts for the optomechanical frequency shift. The fluctuations about the steady state are given in the usual input-output formalism by (126)

$$\frac{d\delta\hat{a}}{dt} = i\Delta'\delta\hat{a} + i\delta\hat{\Phi}\langle\hat{a}\rangle_s + \sqrt{\kappa}\hat{a}_{\rm in}. \tag{4.21}$$

This equation can be formally integrated to give

$$\begin{aligned}\delta\hat{a}(t) &= \delta\hat{a}(0)e^{i\Delta' t} + i\langle\hat{a}\rangle_s \int_0^t dt'\delta\hat{\Phi}(t')e^{i\Delta'(t-t')} \\ &\quad +\sqrt{\kappa}\int_0^t dt'\hat{a}_{\rm in}(t')e^{i\Delta'(t-t')}.\end{aligned} \tag{4.22}$$

For times long compared to κ^{-1}, and a cavity decay rate much faster that the inverse response time of both the effective and mechanical mirror (characterized by their oscillation frequencies), the first term on the RHS of this equation decays to zero, and the operator $\delta\hat{\Phi}(t')$ can be evaluated at t to give

$$\delta\hat{a}(t) = \delta\hat{a}(0)e^{i\Delta' t} - \frac{i\eta(1-e^{i\Delta' t})}{\Delta'^2}\delta\hat{\Phi}(t) + \hat{f}(t), \tag{4.23}$$

with $\hat{f}(t)$ being the last term in Eq. (4.22). Since $\hat{a}_{\rm in}$ is a noise operator with $[\hat{a}_{\rm in}(t), \hat{a}^\dagger_{\rm in}(t')] = \delta(t-t')$ (we take the thermal photon number $n_{\rm th} = 0$ for optical frequencies) we have for $t_1 < t_2$

$$[\hat{f}(t_1), \hat{f}^\dagger(t_2)] = e^{-i\Delta'(t_2-t_1)}\left(e^{-\kappa(t_2-t_1)} - e^{-\kappa t_2}\right), \tag{4.24}$$

with a similar form for $t_1 > t_2$. This commutator vanishes rapidly over the characteristic time scale of the mirror dynamics ($1/\Omega_m$) for large κ, except for $t_1 = t_2$. Over that time scale, $\hat{f}(t)$ can therefore be thought of as a delta-correlated noise operator as far as the mirror motion is concerned, with

$$[\hat{f}(t_1), \hat{f}^\dagger(t_2)] \approx \frac{\kappa}{[(\tilde{\Delta}_c + \langle\hat{\Phi}\rangle)^2 + \kappa^2/4]}\delta(t_1 - t_2). \tag{4.25}$$

A more detailed analysis that includes resonator memory effects results in the familiar optical spring effect and cold damping description. In the Doppler regime

$\Omega_m \ll \kappa$ considered here, cold damping is however negligible (of the order of 30 Hz for the examples discussed below) , and likewise the optical spring effect does not significantly modify the rate of quantum state transfer.

From now on we consider the situation where the steady-state value of the phase shift is $\langle\Phi\rangle$=0. With $e^{-\kappa t/2} \to 0$, the linearization ansatz (4.19) then results in the equations of motion

$$\begin{aligned} \delta\dot{\hat{c}}_m &= -i\Omega_m \delta\hat{c}_m + i\xi_m \left(\langle\hat{a}\rangle_s \delta\hat{a}^\dagger + \langle\hat{a}^\dagger\rangle_s \delta\hat{a}\right) \\ \delta\dot{\hat{c}}_2 &= -i\Omega_2 \delta\hat{c}_2 - i\xi_2 \left(\langle\hat{a}\rangle_s \delta\hat{a}^\dagger + \langle\hat{a}^\dagger\rangle_s \delta\hat{a}\right), \end{aligned} \tag{4.26}$$

with

$$\langle\hat{a}\rangle_s \delta\hat{a}^\dagger + \text{h.c.} = -\frac{2|\langle\hat{a}\rangle_s|^2 \tilde{\Delta}_c}{\tilde{\Delta}_c^2 + \kappa^2/4} \delta\hat{\Phi}(t) + \left(\langle\hat{a}^\dagger\rangle_s \hat{f}(t) + \text{h.c.}\right).$$

Specifically, consider a system prepared such that the shifted frequencies of the two oscillators Ω'_m and Ω'_2 are equal, where $\Omega'_j = \Omega_j + \xi_j^2(2|\langle\hat{a}\rangle_s|^2\tilde{\Delta}_c)/(\tilde{\Delta}_c^2 + \kappa^2/4)$, $j = \{m, 2\}$. In an interaction picture with the time variation due to the shifted frequencies of the two oscillator operators removed, under the rotating wave approximation, and neglecting constant terms, we can then describe the coupling between the mechanical oscillator and the BEC by the effective Hamiltonian

$$H_{\text{eff}} = -\hbar \left[\Omega_{\text{ST}} \delta c_m^\dagger \delta c_2 - \langle\hat{a}^\dagger\rangle_s \hat{f}(t) \delta\hat{\Phi} + \text{h.c.}\right] + H_d, \tag{4.27}$$

resulting in the equations of motion

$$\frac{d}{dt}\begin{bmatrix} \delta\hat{x}_2 \\ \delta\hat{p}_2 \\ \delta\hat{x}_m \\ \delta\hat{p}_m \end{bmatrix} = \Omega_{\text{ST}} \begin{bmatrix} 0 & 0 & 0 & -1 \\ 0 & 0 & 1 & 0 \\ 0 & -1 & 0 & 0 \\ 1 & 0 & 0 & 0 \end{bmatrix} \begin{bmatrix} \delta\hat{x}_2 \\ \delta\hat{p}_2 \\ \delta\hat{x}_m \\ \delta\hat{p}_m \end{bmatrix} + \hat{\chi}' \begin{bmatrix} 0 \\ -\xi_2 \\ 0 \\ \xi_m \end{bmatrix}$$

where $\Omega_{\text{ST}} = 2|\langle\hat{a}\rangle_s|^2 \tilde{\Delta}_c \xi_2 \xi_m / (\tilde{\Delta_c}^2 + \kappa^2/4)$, and

$$\hat{\chi}' = 2\left[\langle\hat{a}^\dagger\rangle_s \hat{f}(t) + \langle\hat{a}\rangle_s \hat{f}^\dagger(t)\right]. \tag{4.28}$$

The coherent part of the Hamiltonian (4.27) has a beamsplitter form, resulting in the periodic exchange of correlations between the real and effective mirrors. The appearance of the beamsplitter Hamiltonian is the key result of this paper and follows from the quantum fluctuations of the cavity field. The coupling between the real and effective mirrors is reminiscent of the Casimir force between two mirrors that arises from vacuum field fluctuations. In our case, however, there is no average net force between the mirrors but rather the cavity field fluctuations serve to dynamically exchange fluctuations in the quadratures of the two mirrors at the state transfer frequency $\Omega_{\rm ST}$. The term proportional to χ' is a noise term due to random momentum kicks arising from cavity field fluctuations. (Note that if the optical field is treated classically the quantum states of the two "mirrors" are uncoupled, although their oscillation frequencies depend on a common classical intracavity intensity, which in turn depends on the expectation value $\langle\hat{\Phi}\rangle$ of the optomechanical phase shift.)

Since both $\Omega_{\rm ST}$ and the noise term depend on the same system parameters, these must be chosen carefully to optimize the fidelity of state transfer. For resonant frequencies $\Omega_2' = \Omega_{\rm m}'$, and equal optomechanical couplings $\xi_2 = \xi_m$, we find that $\langle\hat{\chi}'\hat{\chi}'^{\dagger}\rangle/\Omega_{\rm ST} \approx \kappa/\tilde{\Delta}_c$.

4.2.3 Examples of quantum state transfer

As an example we consider an oscillating mirror of mass $m_m = 5$ ng and frequency $\Omega_m = 2\pi \times 100$ kHz forming the end mirror of a Fabry-Pérot cavity of length 190 μm and cavity decay rate $\kappa = 6 \times 10^6$ rad/sec^{-1}. The cavity is filled with a small ^{23}Na condensate with $N_a = 5 \times 10^4$ atoms. The incident laser light, with $\tilde{\Delta}_c = 6\kappa$ and $\eta = 20\kappa$, is detuned by $\Delta_a = -2\pi \times 461$ GHz from the D2 transition line (whose recoil frequency is 25 KHz). These parameters result in $\xi_2 = \xi_m = 6.90 \times 10^4$ Hz and a state transfer frequency of $\Omega_{\rm ST} = 2.90$ KHz.

We first consider a gaussian state described by the Wigner function

$$W(x,p) = \frac{1}{2\pi\sigma_x\sigma_p}\exp\left[-\frac{(x-x_0)^2}{2\sigma_x^2} - \frac{(p-p_0)^2}{2\sigma_p^2}\right] \tag{4.29}$$

and evaluate specifically the state transfer fidelity of a coherent state of the BEC ($\sigma_x = \sigma_p = 0.5$) with $x_0 = 1, p_0 = 0$ as a function of $\tilde{\Delta}_c/\kappa$ by evaluating the overlap between this and the membrane state after time $t = \pi/(2\Omega_{\rm ST})$, see Fig. 4.2. While the fidelity increases for larger detunings, we note that eventually the state transfer frequency becomes very low (e.g. $\Omega_{\rm ST} = 865$ Hz for $\tilde{\Delta}_c/\kappa = 9$). Also, care must be taken to avoid reaching a regime where the behavior of the mechanical system may become bistable. The example of Fig. 4.3 shows the state transfer

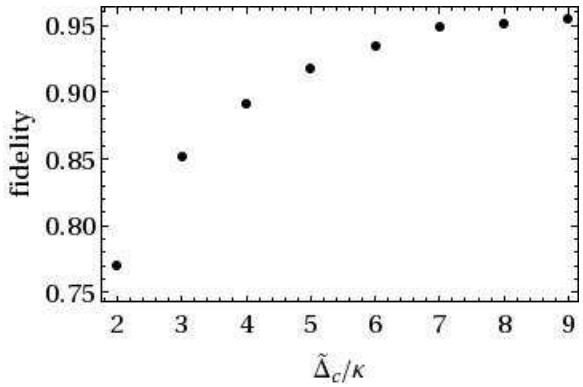

Figure 4.2: State transfer fidelity of a condensate coherent state to an oscillating end mirror initially in its ground state of center-of-mass motion as a function of detuning $\tilde{\Delta}_c$ in units of κ. The system parameters are given in the text.

from the mechanical membrane to the BEC side mode of the Schrödinger cat state $\frac{1}{\sqrt{\mathcal{N}}}(|\alpha\rangle + |-\alpha\rangle)$, with $\alpha = 2/x_{\rm zp}$, $x_{\rm zp} = \sqrt{\hbar/2m_m\Omega_m}$ being the width of the mirror ground state, and $\mathcal{N}$ a normalization constant. The upper plot is the initial Wigner distribution $W(x_m, p_m, t = 0)$ for the mirror, and the lower plot is the corresponding Wigner distribution $W(x_2, p_2, t)$ of the BEC at time $t = \pi/(2\Omega_{\rm ST})$. The similarity of the initial and transferred states indicates that the cat state nature of the initial state has been mostly preserved. The fidelity of the state transfer (the magnitude of the

overlap between the two Wigner functions), is 0.835. Everything else being equal, the reduction in state transfer fidelity for a cat state, as compared to a coherent state, is a result of its faster decoherence from the quantum noise of the optical field. This suggests that in that case the fidelity could be improved by driving the resonator with a field with squeezed quantum fluctuations in the appropriate quadrature. In general, though, it is a nontrivial task to predict the dependence of state transfer fidelity on the specific quantum state under consideration. As would be intuitively

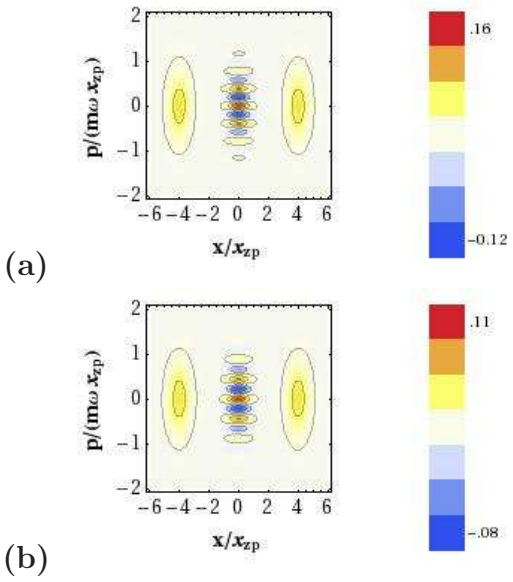

Figure 4.3: Transfer of cat states: Wigner distribution functions of (a) initial state of membrane $1/\sqrt{\mathcal{N}}(|\alpha\rangle + |-\alpha\rangle)$, where $\alpha = 2$ in our dimensionless units, and (b) BEC after an interaction time of $t = \pi/(2\Omega_{\rm ST})$.

expected, we also confirmed numerically that next to controlling quantum noise the most important condition to achieve a high state transfer fidelity is that $\Omega_2' = \Omega_m'$. While in the specific example of ^{23}Na BEC considered here we have $\Omega_2 = \Omega_m$ and $\xi_2 = \xi_m$, this dual equality does not have to be satisfied in general. The resonance condition $\Omega_2' = \Omega_m'$ can be realized by independently adjusting ξ_2 and ξ_m, e.g. by changing the atomic detuning, the length of the cavity, and/or the number of atoms

(at the cost of unequal noise in the two mirrors).

We finally remark that our analysis ignored the dissipation and decoherence of both the BEC and the mechanical oscillators, as well as the additional damping term resulting from the adiabatic elimination of the optical field. This is an appropriate approximation for high enough Ω_{ST} and low bath temperatures, and in the Doppler regime $\kappa \gg \tilde{\Delta}_c$. A more detailed discussion of these noise mechanisms, including an extension of this work to the resolved sideband regime where they may become more important, as well as the analysis of the use of squeezed light to improve state transfer fidelity is currently under investigation, but beyond the scope of this dissertation.

In summary, we have introduced a novel mechanism for state transfer between a trapped atomic gas and an optomechanical end-mirror that is mediated by the quantum fluctuations of a cavity field. We also presented the example of coherent and cat state transfer to illustrate the promise and pitfalls for high fidelity state transfer. In future work we plan to extend of these ideas to multi-mode state transfer as appropriate to condensed matter systems, to add many-body effects, and to use quantum control and dark state approaches for improving the fidelity of state transfer.

CHAPTER 5

SUMMARY AND OUTLOOK

This thesis explored problems at the boundary between two emerging fields of physics: ultra-cold atomic physics and cavity optomechanics. Much of the research was guided by the many parallels between these two fields and quantum optics. In quantum optics, the goal is to exploit the quantum features of electromagnetic fields to gain both a more profound understanding of fundamental physics questions such as entanglement, decoherence, and the quantum measurement process, as well as to develop novel applications and technologies, e.g. quantum information science and quantum metrology. Quantum degenerate gases provide an ideal, tunable system for testing and extending these ideas to many-body systems. Likewise, progress in cavity optomechanics is helping drive acoustics to a new regime where quantum effects become dominant and can be controlled. Here, the idea is to prepare, manipulate, detect and exploit phonon fields in the quantum regime in order to explore fundamental physics such as the classical-quantum transition, along with investigating possibilities to make sensors that operate near the fundamental limits set by quantum measurement theory. Thus, it is fitting to explore ideas that involve a merger of precision measurement and control capability of atomic systems with the robust infrastructure provided by mechanical systems.

As mentioned in the beginning, this thesis was primarily concentrated on generating and measuring non-classical states of mechanical oscillators by coupling them to atomic and molecular quantum systems. Here we summarize the main ideas discussed.

We started with a discussion of what novel physics can be explored by mechanical systems operating in the quantum regime. We then discussed one exciting approach

that is making it a possibility- cavity optomechanics, particularly optomechanical cooling. We investigated the limits of optomechanical cooling and reviewed how the coupling of mechanical oscillators to external heat baths via structural supports limits the minimum attainable phonon occupation number. As a possible alternative that circumvents this problem we considered an all-optical approach where the mechanical element (in this case, a Bragg mirror) is suspended via optical forces, and discussed some limitations of this all-optical approach.

We then explored several schemes aimed at the generation and detection of quantum states in mechanical oscillators. We considered specifically two examples: one in which the mechanical oscillator is coupled to another oscillator via nonlinear forces, and another where is coupled to a spin ensemble. The first example emphasized the generation of squeezed and entangled states of motion of polar molecules. Here, we showed that the nonlinearity produced by dipole-dipole interaction can generate parametric squeezing and entanglement. The second project dealt with a BEC that is magnetically coupled to a membrane mechanical oscillator. This coupling was used to illustrate the generation of measurement back-action induced quantum states of motion. We commented on the conditional nature of these states, and the effect of thermal dissipation of the mechanical system on the degree of "quantumness" of the generated states.

We then turned to the discussion of possible methods to fully characterize the state of a mechanical oscillator operating deep in the quantum regime. The first method involved the tomographic reconstruction of the mechanical Wigner function by simultaneously coupling the oscillator to a classical optical oscillator and to an atomic hyperfine transition qubit and monitoring the state of that qubit. The second approach relied on a state transfer scheme between momentum excitations of a Bose-Einstein condensate trapped in a high-Q optical cavity with the mechanical element serving as an oscillating end-mirror.

Now that ground-state cooling of the center-of-mass motion of nanomechanical

cantilevers has been successfully demonstrated (34; 16; 52), an important next goal is to move to "beyond ground state" physics. The systems investigated in this thesis, which were concerned both with the preparation and control and with the detection of the state of single-mode phonon fields, can be understood as initial steps in that direction, and they open the way to a number of possible further directions of research. One particular example is the BEC-membrane hybrid system discussed in chapter 3, where the quantum backaction of the BEC spin measurement creates superposition states of mechanical motion. By adding a feedback scheme (perhaps a dynamic change in magnetic field), one can change these non-classical states from being conditional to probabilistic. Furthermore, one could use such measurement feedback techniques to preserve a Schrödinger cat like state from decoherence, as theoretically discussed in ref.(127).

Another interesting direction involves the use of *artificial atoms* such as Josephson junction qubits, nitrogen vacancy (NV) centers in diamond or quantum dots. The availability of several types of artificial atoms as processor and memory qubits coupled to optomechanical elements, are emerging as technologically viable alternatives for the quantum state preparation and control of massive objects. For example, the coherent manipulation of a NV centers in diamond was recently used to sense minute changes in the position of a magnetized cantilever (128), demonstrating coherent coupling between a mechanical system and a qubit. Coupled with an optical field, such systems may become an experimentally viable candidate to demonstrate the Wigner tomography scheme talked about in Chapter 4.

Another potentially important extension of this work would be to broaden it to include multimode systems. All the systems considered in this thesis were concerned with single modes of mechanical motion. However, a rich spectrum of problems and situations requires the inclusion of other modes of motion. For example, the optical driving of a mechanical membrane could result in the entanglement of several vibrational modes. In another example, most exotic, strongly correlated states now

being generated in quantum degenerate gases, for example Mott insulator states, comprise of a discrete superposition of momentum components. Any scheme to transfer such states to a mechanical systems would inevitably involve more modes than the single mode case discussed in Chapter 4.

APPENDIX A

CLASSICAL THEORY OF OPTOMECHANICAL COOLING

In Chapter 1 we briefly reviewed a number of cavity optomechanical configurations currently being developed in the laboratory. A generic model that accounts for the main physical effects underlying these systems is a Fabry-Perot cavity with one fixed end mirror and the other end mirror undergoing harmonic motion, as described in Fig.1.1(a). For a high finesse resonator with a large spectral range compared to all relevant dissipation rates, it is sufficient to consider a single-mode description of the Fabry-Pérot. In this appendix we derive a simple theory for the dynamics of coupled electric field and the mirror motion in such a Febry-Pérot. We show that the field dynamics already allows us to explore a wide range of non-linear effects including the optical spring effect, cold damping, optical bistability, dynamical instabilities and parametric amplification, and more. The model presented here borrows heavily from similar derivations for the case of microtoroidal cavities presented in ref.(129; 130).

In order to draw parallels between the classical equations of motion, and the quantum Heisenberg Langevin equations of motion, we proceed by defining new variables a and a_{in} such that the intra-cavity energy U_c and input power $P_{\rm in}$ are:

$$U_c = \frac{1}{2}\epsilon_0 |E|^2 V = \hbar\omega_c a^* a, \tag{A.1}$$

$$P_{\rm in} = \hbar\omega_c a_{\rm in}^* a_{\rm in}. \tag{A.2}$$

Here, E is the intra-cavity electric field, ϵ_0 is the permittivity of free space and V is the mode volume of the light field in the cavity. Thus, $a = \sqrt{\epsilon_0 V/2\hbar\omega_c}E$, is simply the re-scaled electric field, and $a_{\rm in}$ has dimensions of electric field$\times$time$^{-1/2}$, and is chosen to draw parallels between classical and quantum formulations.

The equation of motion for the intra-cavity field is given by

$$\frac{da}{dt} = i\Omega a - \frac{\kappa}{2}a + \sqrt{\kappa}a_{\rm in}. \tag{A.3}$$

Here, Ω is the cavity mode frequency. For the simple case with fixed boundary conditions, $\Omega = \omega_c$. However, since the mechanics modifies the cavity frequency we consider it to be a function $\Omega(t)$ to be determined by a linear response theory calculation. For simplicity, we assume that the intracavity intensity decay rate κ is limited solely by the mirror reflectivities, with no internal material and diffraction losses, $\kappa = t_1 t_2 c/2L$, where t_1,t_2 are the amplitude transmission of the two mirrors and L is the equilibrium length of the cavity. The electric field decays exponentially at rate $\kappa/2$ and the driving field $a_{\rm in}$ couples into the cavity at that same rate.

Integrating both sides from -∞ to time t, we get the field at time t to be

$$a(t) = \sqrt{\kappa}e^{i\phi(t)-\kappa t/2}\int_{-\infty}^{t} dt' a_{\rm in}(t')e^{-i\phi(t')+\kappa t'/2}. \tag{A.4}$$

Here, $\phi(t) = \int_0^t \Omega(t')dt'$. In all derivations that follow the input field is assumed to be a single mode monochromatic field, i.e. $a_{\rm in}(t) = a_{\rm in}e^{i\omega_L t}$, where ω_L is the frequency of the laser. For optomechanical effects, $\Omega(t) = \omega_c + gx(t)$. Here, ω_c is the frequency of the optical resonator, and $g = \partial\omega_c/\partial x$ accounts for its linear dependence on small changes x in the position of the oscillating end-mirror. For a Fabry-Perot cavity,we have simply $g = -\omega_c/L$.

A.1 Static effects

To set the stage we consider first the simple case where the mirror does not move significantly over the time interval of interest $(t - t')$, i.e. $x = x_0$, a constant. In this case, the phase acquired by the intracavity field is simply $\phi(t) = (\omega_c + gx_0)t$. Inserting this value into Eq. (A.4,) and defining

$$\Delta_c = \omega_L - \omega_c,$$

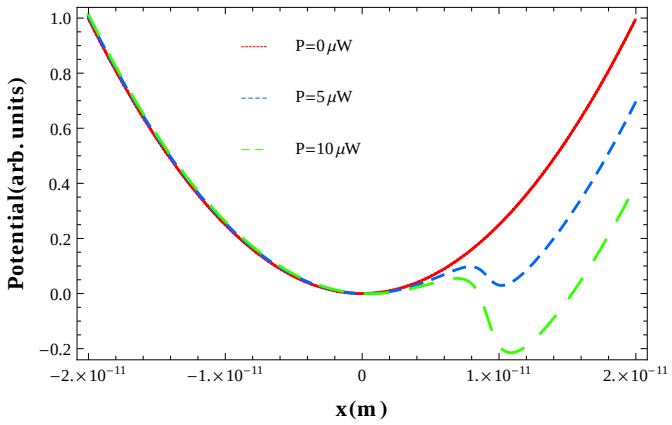

Figure A.1: Potential vs. position for optomechanical parameters given in ref. (1) for different input powers. When the laser intensity is sufficiently high, there are two stable local minimas in the effective mechanical potential, and this leads to bistable behavior.

we obtain

$$a(t) = \frac{\sqrt{\kappa} a_{\rm in} e^{i\omega_L t}}{i(\Delta_c - g x_0) + \kappa/2}. \tag{A.5}$$

Given the electric field, we now evaluate the radiation pressure force, $F_{\rm RP,s} = 2P_c/c$, where P_c is the intracavity power, the factor of 2 comes from the fact that the light gets retro-reflected from the moving mirror, and the subscript "s" reminds us that this is a static value. In our units, the intra-cavity power is simply $\hbar\omega_c |a|^2/t_{\rm rt}$, where the round-trip time $t_{\rm rt} = 2L/c$. Therefore, the radiation pressure force on the small mirror is

$$F_{\rm RP,s} = \frac{1}{L} \frac{\kappa P_{\rm in}}{(\Delta_c - g x_0)^2 + (\kappa/2)^2}. \tag{A.6}$$

In typical experiments, the damping rate of the mechanical oscillator is order of magnitude smaller than κ. Neglecting its effects for now, the equation of motion for the moving mirror is

$$m\ddot{x} = -kx + F_{\rm RPs} = -\frac{\partial V}{\partial x}, \tag{A.7}$$

where V is the effective potential

$$\begin{aligned} V(x) &= \frac{1}{2}kx^2 - \int_0^x dx' F_{\mathrm{RPs}}(x') \\ &= \frac{1}{2}kx^2 - \frac{2P_{\mathrm{in}}}{\omega_c}\left[\arctan\left(\frac{2(\Delta_c - \omega_c x_0/L)}{\kappa}\right)\right]. \end{aligned} \tag{A.8}$$

Here, we have ignored the constant shift. This effective potential the mechanics can be significantly modified by the light field. In fact, if the laser intensity is sufficiently high, two stable local minimas appear in the effective mechanical potential, and this leads to bistable behavior in the mechanics. Fig. A.1 plots the effective potential for a Fabry-Perot cavity with micro-mirrors considered in ref. (1). We notice the deviation from harmonic potential, and the appearance of another local minima as the laser power input to the cavity is increased. This radiation pressure induced bistability was first theoretically studied in ref. (44), and has been observed in optical (48) and microwave systems (131).

A.2 Dynamical effects

Consider now the situation when the mechanical element undergoes harmonic motion of the form $x(t) = x_0 \sin(\omega_m t)$. In that case, the phase $\phi(t')$ takes the form

$$\phi(t') = \omega_c t' + g\frac{x_0}{\omega_m}\left(1 - \cos(\omega_m t')\right). \tag{A.9}$$

Inserting this expression into Eq. (A.4) we find

$$a(t) = \sqrt{\kappa}a_{\mathrm{in}}e^{(i\omega_c - \kappa/2)t - igx_0\cos(\omega_m t)/\omega_m}\int_{-\infty}^{t} dt' e^{i(\omega_L - \omega_c)t' + \kappa/2t' + igx_0/\omega_m\cos(\omega_m t')}. \tag{A.10}$$

Using the Jacobi-Anger identity $e^{i\beta\cos y} = \sum_{n=-\infty}^{\infty} i^n J_n(\beta)e^{iny}$ and $e^{-i\beta\cos y} = \sum_{n=-\infty}^{\infty} i^{-n}J_n(\beta)e^{iny}$, the intracavity field becomes

$$\begin{aligned} a(t) &= \sum_{n=-\infty}^{\infty}\frac{i^{-n}J_n(\beta)}{i(\Delta_c + n\omega_m) + \kappa/2}\sqrt{\kappa}a_{\mathrm{in}}e^{i\omega_L t}e^{i(n\omega_m t + \beta\cos\omega_m t)} \\ &= \sum_{n,m=-\infty}^{\infty}\frac{i^{m-n}J_n(\beta)J_m(\beta)}{i(\Delta_c + n\omega_m) + \kappa/2}\sqrt{\kappa}a_{\mathrm{in}}e^{i\omega_L t}e^{i(n+m)\omega_m t}, \end{aligned} \tag{A.11}$$

where $\beta = \omega_c x_0/(L\omega_m)$. For small mirror oscillation amplitudes we can truncate the series to lowest order in β. This gives $a(t) = a_0(t) + a_1(t)$, where

$$a_0(t) = \sqrt{\kappa} a_{\rm in} e^{i\omega_L t} \frac{J_0(\beta)^2}{i\Delta_c + \kappa/2}, \tag{A.12}$$

and

$$a_1(t) \simeq \sqrt{\kappa} a_{\rm in} \frac{\omega_m J_0(\beta) J_1(\beta)}{i\Delta_c + \kappa/2} \left[-\frac{e^{i(\omega_L+\omega_m)t}}{i(\Delta_c+\omega_m)+\kappa/2} + \frac{e^{i(\omega_L-\omega_m)t}}{i(\Delta_c-\omega_m)+\kappa/2} \right]. \tag{A.13}$$

For $\beta \ll 1$, $J_0(\beta) \approx 1$ and $J_1(\beta) \approx \beta/2$. Substituting these values in the expression for the electric field we obtain

$$a(t) \approx \frac{\sqrt{\kappa} a_{\rm in} e^{i\omega_L t}}{i\Delta_c + \kappa/2} \left[1 - \frac{\omega_c x_0}{2L} \left(\frac{e^{i\omega_m t}}{i(\Delta_c+\omega_m)+\kappa/2} - \frac{e^{-i\omega_m t}}{i(\Delta_c-\omega_m)+\kappa/2} \right) \right]. \tag{A.14}$$

This expression for the electric field has the three frequency components mentioned in section 1.2. It shows that for small oscillation amplitudes the mechanical motion generates two sidemodes in the electric field at frequencies $\omega_L \pm \omega_m$. These two side modes are weighted differently by the cavity response – note the different resonance denominators. The $(\omega_L+\omega_m)$ component can be thought of as an anti-Stokes Raman sidemode, and the side mode at $(\omega_L - \omega_m)$ is the Stokes component.

The intracavity intensity is now

$$\begin{aligned} |a(t)|^2 \;\approx\; & \frac{\kappa |a_{\rm in}|^2}{\Delta_c^2 + (\kappa/2)^2} \,(1+ \\ & -\frac{\omega_c x_0}{L} \left[\frac{\Delta_c+\omega_m}{(\Delta_c+\omega_m)^2+(\kappa/2)^2} + \frac{\Delta_c-\omega_m}{(\Delta_c-\omega_m)^2+(\kappa/2)^2} \right] \sin(\omega_m t) \\ & -\frac{\omega_c x_0}{L} \left[\frac{\kappa/2}{(\Delta_c+\omega_m)^2+(\kappa/2)^2} - \frac{\kappa/2}{(\Delta_c-\omega_m)^2+(\kappa/2)^2} \right] \cos(\omega_m t) \Big), \end{aligned}$$

resulting in the dynamic radiation pressure force

$$\begin{aligned} F_{\rm RP,d} \;=\; & \frac{\kappa P_{\rm in}}{L[\Delta_c^2 + (\kappa/2)^2]} \,\{1 \\ & -\frac{\omega_c x_0}{L} \left[\frac{\Delta_c+\omega_m}{(\Delta_c+\omega_m)^2+(\kappa/2)^2} + \frac{\Delta_c-\omega_m}{(\Delta_c-\omega_m)^2+(\kappa/2)^2} \right] \sin(\omega_m t) \\ - \;& \frac{\omega_c x_0}{L} \left[\frac{\kappa/2}{(\Delta_c+\omega_m)^2+(\kappa/2)^2} - \frac{\kappa/2}{(\Delta_c-\omega_m)^2+(\kappa/2)^2} \right] \cos(\omega_m t) \Big\}. \end{aligned} \tag{A.15}$$

The first term in this expression can be thought of as a modified spring constant, since we have $F_{\mathrm{RPd}} = -k_{\mathrm{opto}}x$, where

$$k_{\mathrm{opto}} = \frac{-\omega_c \kappa P_{\mathrm{in}}}{L^2(\Delta_c^2 + (\kappa/2)^2)} \left[\frac{\Delta_c + \omega_m}{(\Delta_c + \omega_m)^2 + (\kappa/2)^2} + \frac{\Delta_c - \omega_m}{(\Delta_c - \omega_m)^2 + (\kappa/2)^2} \right]. \quad \text{(A.16)}$$

This modification of the mechanical spring constant is known as the dynamical optical spring effect. We point out that this effect is different from the modification of spring constant by static effects, as in the case of optical tweezers. By changing the detuning of the input laser with respect to the cavity resonance, one can in principle produce either a tighter or a shallower trap for the mechanics. Increasing the effective mechanical frequency, we reduce the average number of thermal phonons in each energy level. While not stricly speaking a cooling method, this approach has been used successfully to approach the quantum regime of operation of mechanical oscillators, as demonstrated e.g. in a gram-scale mirror by the LIGO team (73).

In addition to comprising of the terms originating in the Stokes and anti-Stokes side modes, $F_{\mathrm{RP,d}}$ can be divided into two terms, one of them in phase with the motion of the oscillator ($\propto x_0 \sin \omega_m t$) the other in quadrature with it, or proportional to the velocity ($\propto x_0 \cos \omega_m t$). The component of the force proportional to the velocity of the mechanical oscillator, call it $F_Q \propto v$, leads to viscous damping or amplification of motion, depending on the sign of the proportionality constant.

Given the force, the average power transferred from mechanics is $\langle P_m \rangle = \langle F_Q v \rangle$, which gives

$$\langle P_m \rangle = \frac{-\omega_c \omega_m x_0^2 \kappa P_{\mathrm{in}}}{2L^2(\Delta_c^2 + (\kappa/2)^2)} \left[\frac{\kappa/2}{(\Delta_c + \omega_m)^2 + (\kappa/2)^2} - \frac{\kappa/2}{(\Delta_c - \omega_m)^2 + (\kappa/2)^2} \right]. \quad \text{(A.17)}$$

where we have used $\langle \cos \omega_m t^2 \rangle = 1/2$. From this we can evaluate an energy transfer/cooling rate since $\langle P_m \rangle = -\Gamma_{\mathrm{opto}} \langle E_m \rangle$, $\langle E_m \rangle$ is the average mechanical energy, $\langle E_m \rangle = m\omega_m^2 x_0^2/2$. This cooling rate is

$$\Gamma_{\mathrm{opto}} = \frac{\omega_c \kappa P_{\mathrm{in}}}{m\omega_m L^2(\Delta_c^2 + (\kappa/2)^2)} \left[\frac{\kappa/2}{(\Delta_c + \omega_m)^2 + (\kappa/2)^2} - \frac{\kappa/2}{(\Delta_c - \omega_m)^2 + (\kappa/2)^2} \right]. \quad \text{(A.18)}$$

If Δ_c is negative, i.e. the laser is red detuned from the cavity frequency, the anti-Stokes sideband contribution is stronger than the Stokes contribution, and hence Γ_{opto} is positive. As a result, we have a damping force and the mechanical oscillator loses energy. In a quantum picture, this implies that the rate of phonon loss the mechanics is higher than the phonon gain. However, if Δ_c is positive, we instead have a stronger Stokes contribution, and hence Γ_{opto} is negative. In this case, we have an anti-damping force, and we instead have parametric amplification of the motion, which leads to heating of the mechanical element.

The first theoretical and experimental study of dynamical backaction of radiation pressure was done as early as 1967 in microwave cavities (132; 47). Later, it was observed in kg-scale mechanical resonators for gravitational wave detection (133). However, clear demonstration of the suppression of brownian motion of mechanical oscillators by intrinsic damping due to radiation pressure came much later, with the miniaturization of the optical and mechanical resonators (134; 21; 50).

To conclude the discussion of classical optomechanical effects, we shall discuss the limitations of this approach. The primary assumptions are that the moving mirror amplitude of motion is much less than a wavelength of light in the cavity and that the decay rate of the cavity κ must be larger than the intrinsic decay rate of the mechanics γ_m, since light takes energy out of the mechanics, and then the cavity in the case of cooling. If this condition is not satisfied, the field will build up in the cavity, and we would have heating of the mechanics. As long as these conditions are satisfied, we can use this theory for dynamic backaction effects in optomechanics.

APPENDIX B

DETAILED CALCULATIONS FOR BEC- MEMBRANE HYBRID SYSTEM

In this appendix, we give details of the calculations behind some of the results stated in Chapter 3, section 3.2– where we discuss the hybrid system consisting of micro-mechanical membrane magnetically coupled to a spinor BEC.

B.1 Derivation of interaction Hamiltonian

Our starting assumption is that the magnetic domain on the membrane is a point dipole located at the origin. The magnetic field due to that dipole is

$$\mathbf{B}(\mathbf{r}) = \frac{\mu_0}{4\pi}\frac{1}{r^3}\left(3(\mu_{\mathbf{m}}.\hat{\mathbf{r}})\hat{\mathbf{r}} - \mu_{\mathbf{m}}\right) \tag{B.1}$$

It is the small inhomogeneity of the resulting magnetic field along the long axis z of the condensate, and the resulting variation in Larmor precession frequency, that permits to characterize the center-of-mass mode of oscillation of the membrane.

For a dipole polarized along the z-axis ($\mu_{\mathbf{m}} = \mu_m\hat{\mathbf{z}}$), and distance $r = (x^2 + y^2 + z^2)^{1/2}$, the components of the magnetic field (B.1) are

$$B_x(x,y,z) = \frac{\mu_0}{4\pi}\frac{\mu_m}{r^3}\left[\frac{3xz}{r^2}\right] \tag{B.2}$$

$$B_y(x,y,z) = \frac{\mu_0}{4\pi}\frac{\mu_m}{r^3}\left[\frac{3yz}{r^2}\right] \tag{B.3}$$

$$B_z(x,y,z) = \frac{\mu_0}{4\pi}\frac{\mu_m}{r^3}\left[\frac{3z^2}{r^2} - 1\right] \tag{B.4}$$

With $x = x_0 + x_m$, where x_0 is the equilibrium value of x for a condensate atom, $x = 0$ is the equilibrium position of the membrane, and x_m its small sinusoidal

displacement of the membrane around the origin. Expanding the expression for magnetic fields for small x_m (up to first order) we get

$$B_x \approx \frac{\mu_0\mu_m}{4\pi r_0^5}\left[3x_0 z - \frac{3z(4x_0^2 - y^2 - z^2)}{r_0^2}x_m\right] \tag{B.5}$$

$$B_y \approx \frac{\mu_0\mu_m}{4\pi r_0^5}\left[3yz - \frac{15x_0 yz}{r_0^2}x_m\right] \tag{B.6}$$

$$B_z \approx \frac{\mu_0\mu_m}{4\pi r_0^5}\left[(2z^2 - x_0^2 - y^2) + \frac{3x_0(x_0^2 + y^2 - 4z^2)}{r_0^2}x_m\right] \tag{B.7}$$

here, $r_0 = (x_0^2 + y^2 + z^2)^{1/2}$. Assuming a two-dimensional condensate (i.e. $y \approx 0$), we can set $B_y \to 0$. For theoretical simplicity, we assume that the measurements are made on the part of the condensate directly above the magnet, i.e. close to $z = 0$. Under these approximations, the magnetic field simplifies to just being in the z-direction,

$$B_z \approx \frac{\mu_0\mu_m}{4\pi x_0^4}\left[-x_0 + 3x_m\right]. \tag{B.8}$$

Combining this with the quantization field B_0, we end up with the interaction Hamiltonian of the form

$$V = \mu_B g_F F_z\left[B_0 - \frac{\mu_0\mu_m}{4\pi x_0^3} + \frac{3\mu_0\mu_m}{4\pi x_0^4}x_m\right]. \tag{B.9}$$

We can break this total magnetic field into a constant part, B_c (sum of the first two terms), and a component that varies at the membrane frequency, $B_v' x_m$. Here, the gradient of the magnetic field,

$$B_v' = \frac{3\mu_0\mu_m}{4\pi x_0^4}. \tag{B.10}$$

This is the form used in Equation (3.32).

B.2 Derivation of Fokker-Planck equation

The system can be described by the total Hamiltonian given by

$$H = H_{mem} + H_{BEC} + V + H_{bath} + H_{mem-bath} \tag{B.11}$$

where the different components are given by

$$\begin{aligned} H_{mem} &= \hbar\omega_m \hat{a}^\dagger \hat{a}, \\ H_{BEC} &= H_{0BEC} + \hbar\Omega_{L0}\hat{F}_z \\ V &= N\mu_B g_f B'_v \hat{F}_z \hat{x} = Am\omega_m^2 \hat{F}_z \hat{x} \\ H_{bath} &= \hbar \sum_k \omega_k \hat{b}_k^\dagger \hat{b}_k \\ H_{mem-bath} &= \hbar \sum_k g_k \left\{ \left(\hat{a} + \hat{a}^\dagger\right) \hat{b}_k + \left(\hat{a} + \hat{a}^\dagger\right) \hat{b}_k^\dagger \right\}. \end{aligned} \tag{B.12}$$

We will drop the hats on a, b, F to denote that they are operators at this point. The Master equation for the membrane is given by:

$$\begin{aligned} \dot{\rho} &= -\frac{i}{\hbar}[H, \rho] \\ &\quad -\frac{\gamma}{2}\left(\bar{n}_{th} + \frac{1}{2}\right)\left(a^\dagger a\rho + \rho a^\dagger a - 2a\rho a^\dagger\right) - \frac{\gamma}{2}\bar{n}_{th}\left(aa^\dagger\rho + \rho aa^\dagger - 2a^\dagger\rho a\right) \\ &\quad -\frac{\gamma}{2}\left(\bar{n}_{th} + \frac{1}{2}\right)\left(aa^\dagger\rho + \rho aa^\dagger - 2a\rho a^\dagger\right) - \frac{\gamma}{2}\bar{n}_{th}\left(a^\dagger a\rho + \rho aa^\dagger - 2a^\dagger\rho a\right), \end{aligned} \tag{B.13}$$

where ρ is the membrane density matrix. In typical textbook expressions for the Master equation, we do not have the terms on the second line. However, these terms (that are due to the counter-rotating terms of the membrane-bath hamiltonian) are required to get the Fokker-Planck equation that corresponds to a physical random process. In our case, it gives us random momentum kicks.

Solving through, we get

$$\begin{aligned} \dot{\rho} &= -\frac{i}{\hbar}\sum_{\alpha_s,\beta_s} \langle F_y = \gamma_s|\alpha_s\rangle\langle\alpha_s|\rho_{BEC}|\beta_s\rangle\langle\beta_s|F_y = \gamma_s\rangle \\ &\quad \left\{\hbar\omega_m(a^\dagger a\rho - \rho a^\dagger a) + Am\omega_m^2 x_{zp}\left(\alpha_s(a + a^\dagger)\rho - \beta_s\rho(a + a^\dagger)\right)\right\} \\ &\quad +(\text{bath} + \text{membrane}) \text{ terms} \end{aligned} \tag{B.14}$$

We now proceed to derive the Fokker-Planck equation for the quasi-probability distribution from the master equation. But before we do this, let us first justify this

approach instead of just numerically integrating the density matrix, or the classic approach involving Heisenberg-Langevin equations. This approach is chosen because both the other formalisms for dealing with open quantum systems work efficiently when the average number of phonons in the system is considerably small. For a 1 MHz membrane simply coupled to a thermal bath, the average thermal phonon occupation is around 10^5, which makes any computational approach impossible. This is why a Fokker-Planck approach was chosen, as it captures both the quantum and classical features of the coupled system.

From the Master equation, we can get the equation of motion for the Characteristic Wigner Function. The Characteristic Wigner Function is defined as

$$C_W(\lambda, \lambda^*) = Tr\left[\rho e^{\lambda a^\dagger - \lambda^* a}\right] \tag{B.15}$$

We make use of relations

$$\begin{aligned} C_W[\rho a^\dagger] &= \left(\frac{\partial}{\partial\lambda} + \frac{\lambda^*}{2}\right) C_W[\rho] \\ C_W[\rho a] &= \left(\frac{\partial}{\partial\lambda^*} - \frac{\lambda}{2}\right) C_W[\rho] \\ C_W[a^\dagger \rho] &= \left(\frac{\partial}{\partial\lambda} - \frac{\lambda^*}{2}\right) C_W[\rho] \\ C_W[a\rho] &= \left(\frac{\partial}{\partial\lambda^*} + \frac{\lambda}{2}\right) C_W[\rho] \end{aligned} \tag{B.16}$$

After some algebraic manipulation, we get the equation of motion for the Characteristic Wigner function, and it is

$$\begin{aligned} \frac{\partial}{\partial t} C_W[\rho] \;=\; & \sum_{\alpha_s,\beta_s} \langle F_y = \gamma_s|\alpha_s\rangle\langle\alpha_s|\rho_{BEC}|\beta_s\rangle\langle\beta_s|F_y = \gamma_s\rangle \\ & \left[-i\omega_m\left(\frac{\partial}{\partial\lambda}\lambda - \frac{\partial}{\partial\lambda^*}\lambda^*\right)\right. \\ & -i\frac{Am\omega_m^2 x_{zp}}{\hbar}\left\{(\alpha_s - \beta_s)\left(\frac{\partial}{\partial\lambda^*} + \frac{\partial}{\partial\lambda}\right) + (\alpha_s + \beta_s)\left(\frac{\lambda}{2} - \frac{\lambda^*}{2}\right)\right\} \\ & \left.+(\text{bath} + \text{membrane})\text{ terms}\right] C_W[\rho]. \end{aligned} \tag{B.17}$$

The Wigner quasi-probability distribution function is defined as

$$W(\alpha,\alpha^*)=\frac{1}{\pi^2}\int C_W(\lambda,\lambda^*)e^{\lambda*\alpha-\lambda\alpha^*}d^2\lambda. \tag{B.18}$$

Since the characteristic Wigner function is relation to the Wigner distribution function via a Fourier transform, the relations mentioned in equation B.16 become

$$\begin{aligned}
\lambda C_W &\rightarrow \frac{\partial}{\partial\alpha^*}W \\
\lambda^* C_W &\rightarrow \frac{\partial}{\partial\alpha}W \\
\frac{\partial}{\partial\lambda}C_W &\rightarrow \alpha^* W \\
\frac{\partial}{\partial\lambda^*}C_W &\rightarrow \alpha W
\end{aligned} \tag{B.19}$$

Furthermore, using the relation

$$\alpha=\sqrt{\frac{m\omega_m}{2\hbar}}\left(x+i\frac{p}{m\omega_m}\right), \tag{B.20}$$

and its complex conjugate for α^*, we can write the equation of motion for the Wigner function in the more familiar position and momentum basis. It is

$$\begin{aligned}
\frac{\partial}{\partial t}W(x,p)=\sum_{\alpha_s,\beta_s} \quad & \langle F_y=\gamma_s|\alpha_s\rangle\langle\alpha_s|\rho_{BEC}|\beta_s\rangle\langle\beta_s|F_y=\gamma_s\rangle \\
& \left\{-\frac{\partial}{\partial x}\left(\frac{p}{m}\right)+\frac{\partial}{\partial p}\left(m\omega_m^2 x+\gamma p+(\alpha_s+\beta_s)\frac{Am\omega_m^2}{2}\right)\right. \\
& +\hbar m\omega_m\gamma\left(\bar{n}_{th}+\frac{1}{2}\right)\frac{\partial^2}{\partial p^2} \\
& \left.-i\Omega_{L0}(\alpha_s-\beta_s)-i(\alpha_s-\beta_s)\frac{Am\omega_m^2}{\hbar}x\right\}W(x,p)
\end{aligned} \tag{B.21}$$

Line 2 of equation (3.51) has the form of a Fokker-Planck equation for the Wigner quasi-probability distribution for a harmonic oscillator coupled to a thermal bath. The third line describes the coupling of the membrane to the spinor condensate. It is this coupling that is responsible for the generation of non-classical states. We solve this differential equation in Chapter 3.

REFERENCES

[1] S. Gröblacher, K. Hammerer, M. R. Vanner, and M. Aspelmeyer, "Observation of strong coupling between a micromechanical resonator and an optical cavity field," *Nature*, vol. 460, pp. 724–727, Aug. 2009.

[2] P. Meystre and M. S. III, *Elements of Quantum Optics*. Springer Verlag, 1998.

[3] S. Deléglise, I. Dotsenko, C. Sayrin, J. Bernu, M. Brune, J.-M. Raimond, and S. Haroche, "Reconstruction of non-classical cavity field states with snapshots of their decoherence," *Nature*, vol. 455, pp. 510–514, Sept. 2008.

[4] M. Hofheinz, H. Wang, M. Ansmann, R. C. Bialczak, E. Lucero, M. Neeley, A. D. O'Connell, D. Sank, J. Wenner, J. M. Martinis, and A. N. Cleland, "Synthesizing arbitrary quantum states in a superconducting resonator," *Nature*, vol. 459, pp. 546–549, May 2009.

[5] D. M. Meekhof, C. Monroe, B. E. King, W. M. Itano, and D. J. Wineland, "Generation of nonclassical motional states of a trapped atom," *Phys. Rev. Lett.*, vol. 76, pp. 1796–1799, Mar 1996.

[6] S. Chu, "Cold atoms and quantum control," *Nature*, vol. 416, pp. 206–210, Mar. 2002.

[7] M. Shapiro and P. Brumer, *Principles of the Quantum Control of Molecular Processes*. Wiley-VCH, Feb. 2003.

[8] D. Press, T. D. Ladd, B. Zhang, and Y. Yamamoto, "Complete quantum control of a single quantum dot spin using ultrafast optical pulses," *Nature*, vol. 456, pp. 218–221, Nov. 2008.

[9] B. B. Buckley, G. D. Fuchs, L. C. Bassett, and D. D. Awschalom, "Spin-Light Coherence for Single-Spin Measurement and Control in Diamond," *Science*, vol. 330, pp. 1212–, Nov. 2010.

[10] A. Aspect, P. Grangier, and G. Roger, "Experimental realization of einstein-podolsky-rosen-bohm *Gedankenexperiment* : A new violation of bell's inequalities," *Phys. Rev. Lett.*, vol. 49, pp. 91–94, Jul 1982.

[11] M. Brune, E. Hagley, J. Dreyer, X. Maître, A. Maali, C. Wunderlich, J. M. Raimond, and S. Haroche, "Observing the progressive decoherence of the "meter" in a quantum measurement," *Phys. Rev. Lett.*, vol. 77, pp. 4887–4890, Dec 1996.

[12] W. H. Zurek, "Pointer basis of quantum apparatus: Into what mixture does the wave packet collapse?," *Phys. Rev. D*, vol. 24, pp. 1516–1525, Sep 1981.

[13] A. O. Caldeira and A. J. Leggett, "Influence of damping on quantum interference: An exactly soluble model," *Phys. Rev. A*, vol. 31, pp. 1059–1066, Feb 1985.

[14] E. Joos and H. D. Zeh, "The emergence of classical properties through interaction with the environment," *Zeitschrift fr Physik B Condensed Matter*, vol. 59, pp. 223–243, 1985.

[15] P. A. M. Dirac, "The quantum theory of the emission and absorption of radiation," *Proc. Roy. Soc. A*, vol. 114, pp. 243–265, Mar. 1927.

[16] J. D. Teufel, T. Donner, D. Li, J. W. Harlow, M. S. Allman, K. Cicak, A. J. Sirois, J. D. Whittaker, K. W. Lehnert, and R. W. Simmonds, "Sideband cooling of micromechanical motion to the quantum ground state," *Nature*, vol. 475, pp. 359–363, July 2011.

[17] B. Abbott, R. Abbott, R. Adhikari, P. Ajith, B. Allen, G. Allen, R. Amin, S. B. Anderson, W. G. Anderson, M. A. Arain, and et al., "Observation of a kilogram-scale oscillator near its quantum ground state," *New Journal of Physics*, vol. 11, p. 073032, July 2009.

[18] J. A. Sidles, "Spin microscopy's heritage, achievements, and prospects," *Proceedings of the National Academy of Science*, vol. 106, pp. 2477–2478, Feb. 2009.

[19] H. J. Mamin and D. Rugar, "Sub-attonewton force detection at millikelvin temperatures," *Applied Physics Letters*, vol. 79, p. 3358, Nov. 2001.

[20] M. Li, H. X. Tang, and M. L. Roukes, "Ultra-sensitive NEMS-based cantilevers for sensing, scanned probe and very high-frequency applications," *Nature Nanotechnology*, vol. 2, pp. 114–120, Feb. 2007.

[21] O. Arcizet, P.-F. Cohadon, T. Briant, M. Pinard, and A. Heidmann, "Radiation-pressure cooling and optomechanical instability of a micromirror," *Nature*, vol. 444, pp. 71–74, Nov. 2006.

[22] D. Rugar, R. Budakian, H. J. Mamin, and B. W. Chui, "Single spin detection by magnetic resonance force microscopy," *Nature*, vol. 430, pp. 329–332, July 2004.

[23] K. Jensen, K. Kim, and A. Zettl, "An atomic-resolution nanomechanical mass sensor," *Nature Nanotechnology*, vol. 3, pp. 533–537, Sept. 2008.

[24] C. M. Caves, K. S. Thorne, R. W. P. Drever, V. D. Sandberg, and M. Zimmermann, "On the measurement of a weak classical force coupled to a quantum-mechanical oscillator. i. issues of principle," *Rev. Mod. Phys.*, vol. 52, pp. 341–392, Apr 1980.

[25] V. B. Braginsky, F. Y. Khalili, and K. S. Thorne, *Quantum Measurement*. Cambridge University Press, 1992.

[26] V. B. Braginsky, Y. I. Vorontsov, and K. S. Thorne, "Quantum nondemolition measurements," *Science*, vol. 209, p. 547, 1980.

[27] A. A. Clerk, F. Marquardt, and K. Jacobs, "Back-action evasion and squeezing of a mechanical resonator using a cavity detector," *New Journal of Physics*, vol. 10, p. 095010, Sept. 2008.

[28] M. Aspelmeyer, S. Gröblacher, K. Hammerer, and N. Kiesel, "Quantum optomechanics-throwing a glance," *J. Opt. Soc. Am. B*, vol. 27, pp. A189–A197, Jun 2010.

[29] O. Romero-Isart, "Quantum superposition of massive objects and collapse models," *Phys. Rev. A*, vol. 84, p. 052121, Nov 2011.

[30] R. Kaltenbaek, G. Hechenblaikner, N. Kiesel, O. Romero-Isart, K. Schwab, U. Johann, and M. Aspelmeyer, "Macroscopic quantum resonators (MAQRO) Testing quantum and gravitational physics with massive mechanical resonators," *Experimental Astronomy*, 2012.

[31] S. Gerlich, S. Eibenberger, M. Tomandl, S. Nimmrichter, K. Hornberger, P. J. Fagan, J. Tüxen, M. Mayor, and M. Arndt, "Quantum interference of large organic molecules," *Nature Communications*, vol. 2, Apr. 2011.

[32] I. Pikovski, M. R. V. M. Aspelmeyer, M. S. Kim, and C. Brukner, "Probing Planck-scale physics with quantum optics," *Nature Physics*, 2012.

[33] L. F. Buchmann, L. Zhang, A. Chiruvelli, and P. Meystre, "Macroscopic tunneling of a membrane in an optomechanical double-well potential," *arXiv*, 2012.

[34] A. O'Connell, M. Hofheinz, M. Ansmann, R. C. Bialczak, M. Lenander, E. Lucero, M. Neeley, D. Sank, H. Wang, M. Weides, J. Wenner, J. M. Martinis, and A. N. Cleland, "Quantum ground state and single-phonon control of a mechanical resonator," *Nature*, vol. 464, pp. 697–703, Apr. 2010.

[35] C. Monroe, D. M. Meekhof, B. E. King, S. R. Jefferts, W. M. Itano, D. J. Wineland, and P. Gould, "Resolved-sideband raman cooling of a bound atom to the 3d zero-point energy," *Phys. Rev. Lett.*, vol. 75, pp. 4011–4014, Nov 1995.

[36] T. W. Hansch and A. L. Schawlow, "Cooling of gases by laser radiation," *Optics Communications*, vol. 13, p. 68, Jan. 1975.

[37] D. Wineland and H. Dehmelt *Bull. Am. Phys. Soc.*, vol. 20, p. 637, 1975.

[38] F. Marquardt, J. P. Chen, A. A. Clerk, and S. M. Girvin, "Quantum theory of cavity-assisted sideband cooling of mechanical motion," *Phys. Rev. Lett.*, vol. 99, p. 093902, Aug 2007.

[39] I. Wilson-Rae, N. Nooshi, W. Zwerger, and T. J. Kippenberg, "Theory of ground state cooling of a mechanical oscillator using dynamical backaction," *Phys. Rev. Lett.*, vol. 99, p. 093901, Aug 2007.

[40] M. Aspelmeyer, T. J. Kippenberg, and F. Marquardt, "Cavity Optomechanics," *Reviews of Modern Physics*, p. TBP, 2012.

[41] M. Fleischhauer, A. Imamoglu, and J. P. Marangos, "Electromagnetically induced transparency: Optics in coherent media," *Rev. Mod. Phys.*, vol. 77, pp. 633–673, Jul 2005.

[42] S. Weis, R. Rivière, S. Deléglise, E. Gavartin, O. Arcizet, A. Schliesser, and T. J. Kippenberg, "Optomechanically Induced Transparency," *Science*, vol. 330, pp. 1520–, Dec. 2010.

[43] A. H. Safavi-Naeini, T. P. M. Alegre, J. Chan, M. Eichenfield, M. Winger, Q. Lin, J. T. Hill, D. E. Chang, and O. Painter, "Electromagnetically induced transparency and slow light with optomechanics," *Nature*, vol. 472, pp. 69–73, Apr. 2011.

[44] P. Meystre, E. M. Wright, J. D. McCullen, and E. Vignes, "Theory of radiation-pressure-driven interferometers," *Journal of the Optical Society of America B Optical Physics*, vol. 2, pp. 1830–1840, Nov. 1985.

[45] J. D. Thompson, B. M. Zwickl, A. M. Jayich, F. Marquardt, S. M. Girvin, and J. G. E. Harris, "Strong dispersive coupling of a high-finesse cavity to a micromechanical membrane," *Nature*, vol. 452, pp. 72–75, Mar. 2008.

[46] J. C. Sankey, C. Yang, B. M. Zwickl, A. M. Jayich, and J. G. E. Harris, "Strong and tunable nonlinear optomechanical coupling in a low-loss system," *Nature Physics*, vol. 6, pp. 707–712, Sept. 2010.

[47] V. B. Braginsky and M. Y. T. A. B. Manukin *Sov. Phys. JETP*, vol. 31, p. 829, 1970.

[48] A. Dorsel, J. D. McCullen, P. Meystre, E. Vignes, and H. Walther, "Optical bistability and mirror confinement induced by radiation pressure," *Phys. Rev. Lett.*, vol. 51, pp. 1550–1553, Oct 1983.

[49] P. F. Cohadon, A. Heidmann, and M. Pinard, "Cooling of a mirror by radiation pressure," *Phys. Rev. Lett.*, vol. 83, pp. 3174–3177, Oct 1999.

[50] A. Schliesser, P. Del'Haye, N. Nooshi, K. J. Vahala, and T. J. Kippenberg, "Radiation pressure cooling of a micromechanical oscillator using dynamical backaction," *Phys. Rev. Lett.*, vol. 97, p. 243905, Dec 2006.

[51] A. Schliesser, O. Arcizet, R. Rivière, G. Anetsberger, and T. J. Kippenberg, "Resolved-sideband cooling and position measurement of a micromechanical oscillator close to the Heisenberg uncertainty limit," *Nature Physics*, vol. 5, pp. 509–514, July 2009.

[52] J. Chan, T. P. M. Alegre, A. H. Safavi-Naeini, J. T. Hill, A. Krause, S. Gröblacher, M. Aspelmeyer, and O. Painter, "Laser cooling of a nanomechanical oscillator into its quantum ground state," *Nature*, vol. 478, pp. 89–92, Oct. 2011.

[53] J. D. Teufel, D. Li, M. S. Allman, K. Cicak, A. J. Sirois, J. D. Whittaker, and R. W. Simmonds, "Circuit cavity electromechanics in the strong-coupling regime," *Nature*, vol. 471, pp. 204–208, Mar. 2011.

[54] M. D. Lahaye, J. Suh, P. M. Echternach, K. C. Schwab, and M. L. Roukes, "Nanomechanical measurements of a superconducting qubit," *Nature*, vol. 459, pp. 960–964, June 2009.

[55] T. Li, S. Kheifets, D. Medellin, and M. G. Raizen, "Measurement of the Instantaneous Velocity of a Brownian Particle," *Science*, vol. 328, pp. 1673–, June 2010.

[56] A. Ashkin, "Optical Trapping and Manipulation of Neutral Particles Using Lasers," *Proceedings of the National Academy of Science*, vol. 94, pp. 4853–4860, May 1997.

[57] F. Brennecke, S. Ritter, T. Donner, and T. Esslinger, "Cavity Optomechanics with a Bose-Einstein Condensate," *Science*, vol. 322, pp. 235–, Oct. 2008.

[58] T. P. Purdy, D. W. C. Brooks, T. Botter, N. Brahms, Z.-Y. Ma, and D. M. Stamper-Kurn, "Tunable cavity optomechanics with ultracold atoms," *Phys. Rev. Lett.*, vol. 105, p. 133602, Sep 2010.

[59] A. A. Clerk, M. H. Devoret, S. M. Girvin, F. Marquardt, and R. J. Schoelkopf, "Introduction to quantum noise, measurement, and amplification," *Rev. Mod. Phys.*, vol. 82, pp. 1155–1208, Apr 2010.

[60] S. Singh, G. A. Phelps, D. S. Goldbaum, E. M. Wright, and P. Meystre, "All-optical optomechanics: An optical spring mirror," *Phys. Rev. Lett.*, vol. 105, p. 213602, Nov 2010.

[61] O. Romero-Isart, M. L. Juan, R. Quidant, and J. I. Cirac, "Toward quantum superposition of living organisms," *New Journal of Physics*, vol. 12, p. 033015, Mar. 2010.

[62] D. E. Chang, C. A. Regal, S. B. Papp, D. J. Wilson, J. Ye, O. Painter, H. J. Kimble, and P. Zoller, "Cavity opto-mechanics using an optically levitated nanosphere," *Proceedings of the National Academy of Science*, vol. 107, pp. 1005–1010, Jan. 2010.

[63] P. F. Barker and M. N. Shneider, "Cavity cooling of an optically trapped nanoparticle," *Phys. Rev. A*, vol. 81, p. 023826, Feb 2010.

[64] A. Ashkin and J. M. Dziedzic, "Optical levitation in high vacuum," *Applied Physics Letters*, vol. 28, p. 333, Mar. 1976.

[65] J. Venermo and A. Sihvola, "Dielectric polarizability of circular cylinder," *Journal of Electrostatics*, vol. 63, p. 101, 2005.

[66] L. Landau and E. Lifshitz, *Electrodynamics of Continuous Media*. Addison Wesley, 1968.

[67] K. Bonin, B. Kourmanov, and T. G. Walker, "Light torque nanocontrol, nanomotors and nanorockers," *Optics Express*, vol. 10, p. 984, Sept. 2002.

[68] G. Rempe, R. J. Thompson, H. J. Kimble, and R. Lalezari, "Measurement of ultralow losses in an optical interferometer," *Optics Letters*, vol. 17, pp. 363–366, Mar. 1992.

[69] M. E. Gehm, K. M. O'Hara, T. A. Savard, and J. E. Thomas, "Dynamics of noise-induced heating in atom traps," *Phys. Rev. A*, vol. 58, pp. 3914–3921, Nov 1998.

[70] R. W. Boyd, *Non-linear Optics*. Academic Press, 2003.

[71] G. A. Phelps and P. Meystre, "Laser phase noise effects on the dynamics of optomechanical resonators," *Phys. Rev. A*, vol. 83, p. 063838, Jun 2011.

[72] P. Rabl, C. Genes, K. Hammerer, and M. Aspelmeyer, "Phase-noise induced limitations on cooling and coherent evolution in optomechanical systems," *Phys. Rev. A*, vol. 80, p. 063819, Dec 2009.

[73] T. Corbitt, Y. Chen, E. Innerhofer, H. Müller-Ebhardt, D. Ottaway, H. Rehbein, D. Sigg, S. Whitcomb, C. Wipf, and N. Mavalvala, "An All-Optical Trap for a Gram-Scale Mirror," *Physical Review Letters*, vol. 98, p. 150802, Apr. 2007.

[74] M. Vengalattore, J. M. Higbie, S. R. Leslie, J. Guzman, L. E. Sadler, and D. M. Stamper-Kurn, "High-resolution magnetometry with a spinor bose-einstein condensate," *Phys. Rev. Lett.*, vol. 98, p. 200801, May 2007.

[75] J. M. Obrecht, R. J. Wild, M. Antezza, L. P. Pitaevskii, S. Stringari, and E. A. Cornell, "Measurement of the temperature dependence of the casimir-polder force," *Phys. Rev. Lett.*, vol. 98, p. 063201, Feb 2007.

[76] T. van Zoest et. al, "Bose-Einstein Condensation in Microgravity," *Science*, vol. 328, pp. 1540–, June 2010.

[77] Y.-J. Wang, M. Eardley, S. Knappe, J. Moreland, L. Hollberg, and J. Kitching, "Magnetic resonance in an atomic vapor excited by a mechanical resonator," *Phys. Rev. Lett.*, vol. 97, p. 227602, Dec 2006.

[78] D. Hunger, S. Camerer, T. W. Hänsch, D. König, J. P. Kotthaus, J. Reichel, and P. Treutlein, "Resonant coupling of a bose-einstein condensate to a micromechanical oscillator," *Phys. Rev. Lett.*, vol. 104, p. 143002, Apr 2010.

[79] P. Treutlein, D. Hunger, S. Camerer, T. W. Hänsch, and J. Reichel, "Bose-einstein condensate coupled to a nanomechanical resonator on an atom chip," *Phys. Rev. Lett.*, vol. 99, p. 140403, Oct 2007.

[80] C. Genes, D. Vitali, and P. Tombesi, "Emergence of atom-light-mirror entanglement inside an optical cavity," *Phys. Rev. A*, vol. 77, p. 050307, May 2008.

[81] K. Hammerer, M. Wallquist, C. Genes, M. Ludwig, F. Marquardt, P. Treutlein, P. Zoller, J. Ye, and H. J. Kimble, "Strong coupling of a mechanical oscillator and a single atom," *Phys. Rev. Lett.*, vol. 103, p. 063005, Aug 2009.

[82] S. Singh and P. Meystre, "Atomic probe wigner tomography of a nanomechanical system," *Phys. Rev. A*, vol. 81, p. 041804, Apr 2010.

[83] K. Hammerer, K. Stannigel, C. Genes, P. Zoller, P. Treutlein, S. Camerer, D. Hunger, and T. W. Hänsch, "Optical lattices with micromechanical mirrors," *Phys. Rev. A*, vol. 82, p. 021803, Aug 2010.

[84] S. Singh, M. Bhattacharya, O. Dutta, and P. Meystre, "Coupling nanomechanical cantilevers to dipolar molecules," *Phys. Rev. Lett.*, vol. 101, p. 263603, Dec 2008.

[85] S. K. Steinke, S. Singh, M. E. Tasgin, P. Meystre, K. C. Schwab, and M. Vengalattore, "Quantum-measurement backaction from a bose-einstein condensate coupled to a mechanical oscillator," *Phys. Rev. A*, vol. 84, p. 023841, Aug 2011.

[86] J. Doyle, B. Friedrich, R. V. Krems, and F. Masnou-Seeuws, "Editorial: Quo vadis, cold molecules?," *European Physical Journal D*, vol. 31, pp. 149–164, Nov. 2004.

[87] R. González-Férez, M. Mayle, P. Sánchez-Moreno, and P. Schmelcher, "Comparative study of the rovibrational properties of heteronuclear alkali dimers in electric fields," *EPL (Europhysics Letters)*, vol. 83, p. 43001, Aug. 2008.

[88] P. Rabl and P. Zoller, "Molecular dipolar crystals as high-fidelity quantum memory for hybrid quantum computing," *Phys. Rev. A*, vol. 76, p. 042308, Oct 2007.

[89] A. K. S. J. F. W. G. A . Garrett, A. G. Rojo and R. Merlin, "Vacuum squeezing of solids: Macroscopic quantum states driven by light pulses," *Science*, vol. 275, p. 1638, 1997.

[90] X. Hu and F. Nori, "Phonon squeezed states generated by second-order raman scattering," *Phys. Rev. Lett.*, vol. 79, pp. 4605–4608, Dec 1997.

[91] K. Wódkiewicz and M. S. Zubairy, "Effect of laser fluctuations on squeezed states in a degenerate parametric amplifier," *Phys. Rev. A*, vol. 27, pp. 2003–2007, Apr 1983.

[92] G. Raithel, G. Birkl, W. D. Phillips, and S. L. Rolston, "Compression and parametric driving of atoms in optical lattices," *Phys. Rev. Lett.*, vol. 78, pp. 2928–2931, Apr 1997.

[93] N. W. Ashcroft and N. D. Mermin, *Solid State Physics*. Brooks Cole, 1976.

[94] K. N. Pathak, "Theory of anharmonic crystals," *Phys. Rev.*, vol. 139, pp. A1569–A1580, Aug 1965.

[95] H. X. K. Ahmed and M. Zubairy, "The influence of laser fluctuations on entanglement generation in a non-degenerate parametric amplifier," *Optics Communications*, vol. 262, p. 129, 2006.

[96] L.-M. Duan, G. Giedke, J. I. Cirac, and P. Zoller, "Inseparability criterion for continuous variable systems," *Phys. Rev. Lett.*, vol. 84, pp. 2722–2725, Mar 2000.

[97] P. Kinsler, M. Fernée, and P. D. Drummond, "Limits to squeezing and phase information in the parametric amplifier," *Phys. Rev. A*, vol. 48, pp. 3310–3320, Oct 1993.

[98] D. D. Crouch and S. L. Braunstein, "Limitations to squeezing in a parametric amplifier due to pump quantum fluctuations," *Phys. Rev. A*, vol. 38, pp. 4696–4711, Nov 1988.

[99] H. Seok, L. F. Buchmann, S. Singh, S. K. Steinke, and P. Meystre, "Generation of mechanical squeezing via magnetic dipoles on cantilevers," *Phys. Rev. A*, vol. 85, p. 033822, Mar 2012.

[100] K. W. Murch, K. L. Moore, S. Gupta, and D. M. Stamper-Kurn, "Observation of quantum-measurement backaction with an ultracold atomic gas," *Nature Physics*, vol. 4, pp. 561–564, 2008.

[101] G. S. Agarwal, "Brownian motion of a quantum oscillator," *Phys. Rev. A*, vol. 4, pp. 739–747, Aug 1971.

[102] M. R. Vanner, I. Pikovski, G. D. Cole, M. S. Kim, C. Brukner, K. Hammerer, G. J. Milburn, and M. Aspelmeyer, "Pulsed quantum optomechanics," *Proceedings of the National Academy of Science*, vol. 108, pp. 16182–16187, Sept. 2011.

[103] S. Singh and P. Meystre, "Atomic probe wigner tomography of a nanomechanical system," *Phys. Rev. A*, vol. 81, p. 041804, Apr 2010.

[104] J. Zhang, K. Peng, and S. L. Braunstein, "Quantum-state transfer from light to macroscopic oscillators," *Phys. Rev. A*, vol. 68, p. 013808, Jul 2003.

[105] L. Tian and H. Wang, "Optical wavelength conversion of quantum states with optomechanics," *Phys. Rev. A*, vol. 82, p. 053806, Nov 2010.

[106] F. Khalili, S. Danilishin, H. Miao, H. Müller-Ebhardt, H. Yang, and Y. Chen, "Preparing a mechanical oscillator in non-gaussian quantum states," *Phys. Rev. Lett.*, vol. 105, p. 070403, Aug 2010.

[107] S. Singh, H. Jing, E. M. Wright, and P. Meystre, "Quantum state transfer between a Bose-Einstein condensate and an optomechanical mirror," *ArXiv e-prints*, Feb. 2012.

[108] M. Wilkens and P. Meystre, "Nonlinear atomic homodyne detection: A technique to detect macroscopic superpositions in a micromaser," *Phys. Rev. A*, vol. 43, pp. 3832–3835, Apr 1991.

[109] K. Banaszek and K. Wódkiewicz, "Direct probing of quantum phase space by photon counting," *Phys. Rev. Lett.*, vol. 76, pp. 4344–4347, Jun 1996.

[110] L. G. Lutterbach and L. Davidovich, "Method for direct measurement of the wigner function in cavity qed and ion traps," *Phys. Rev. Lett.*, vol. 78, pp. 2547–2550, Mar 1997.

[111] S. Haroche and J. M. Raimond, *Exploring the quantum – atoms, cavities and photons*. Oxford, 2006.

[112] D. Cano, B. Kasch, H. Hattermann, R. Kleiner, C. Zimmermann, D. Koelle, and J. Fortágh, "Meissner effect in superconducting microtraps," *Phys. Rev. Lett.*, vol. 101, p. 183006, Oct 2008.

[113] C. Hufnagel, T. Mukai, and F. Shimizu, "Stability of a superconductive atom chip with persistent current," *Phys. Rev. A*, vol. 79, p. 053641, May 2009.

[114] S. Barnett and P. Radmore, *Methods in Theoretical Quantum Optics*. Oxford, 1997.

[115] H. Uys and P. Meystre, "Superradiant raman scattering in an ultracold bose gas at finite temperature," *Phys. Rev. A*, vol. 77, p. 063614, Jun 2008.

[116] K. L. Ekinci, Y. T. Yang, and M. L. Roukes, "Ultimate limits to inertial mass sensing based upon nanoelectromechanical systems," *Journal of Applied Physics*.

[117] T. Zaugg, M. Wilkens, and P. Meystre, "Back-action in the measurement of "macroscopic quantum superpositions" in microwave cavities," *Foundations of Physics*, vol. 23, pp. 857–871, June 1993.

[118] Q. P. Unterreithmeier, E. M. Weig, and J. P. Kotthaus, "Universal transduction scheme for nanomechanical systems based on dielectric forces," *Nature*, vol. 458, pp. 1001–1004, Apr. 2009.

[119] M. J. Hartmann and M. B. Plenio, "Steady state entanglement in the mechanical vibrations of two dielectric membranes," *Phys. Rev. Lett.*, vol. 101, p. 200503, Nov 2008.

[120] D. Vitali, S. Gigan, A. Ferreira, H. R. Böhm, P. Tombesi, A. Guerreiro, V. Vedral, A. Zeilinger, and M. Aspelmeyer, "Optomechanical entanglement between a movable mirror and a cavity field," *Phys. Rev. Lett.*, vol. 98, p. 030405, Jan 2007.

[121] C. K. Law and J. H. Eberly, "Arbitrary control of a quantum electromagnetic field," *Phys. Rev. Lett.*, vol. 76, pp. 1055–1058, Feb 1996.

[122] W. S. Bakr, P. M. Preiss, M. E. Tai, R. Ma, J. Simon, and M. Greiner, "Orbital excitation blockade and algorithmic cooling in quantum gases," *Nature*, vol. 480, pp. 500–503, Dec. 2011.

[123] J. Simon, W. S. Bakr, R. Ma, M. E. Tai, P. M. Preiss, and M. Greiner, "Quantum simulation of antiferromagnetic spin chains in an optical lattice," *Nature*, vol. 472, pp. 307–312, Apr. 2011.

[124] M. Endres, M. Cheneau, T. Fukuhara, C. Weitenberg, P. Schauß, C. Gross, L. Mazza, M. C. Bañuls, L. Pollet, I. Bloch, and S. Kuhr, "Observation of Correlated Particle-Hole Pairs and String Order in Low-Dimensional Mott Insulators," *Science*, vol. 334, pp. 200–, Oct. 2011.

[125] M. Cheneau, P. Barmettler, D. Poletti, M. Endres, P. Schauß, T. Fukuhara, C. Gross, I. Bloch, C. Kollath, and S. Kuhr, "Light-cone-like spreading of correlations in a quantum many-body system," *Nature*, vol. 481, pp. 484–487, Jan. 2012.

[126] G. J. Milburn and D. F. Walls, *Quantum Optics*. Springer Verlag, Berlin, 1994.

[127] D. Vitali, P. Tombesi, and G. J. Milburn, "Quantum-state protection in cavities," *Phys. Rev. A*, vol. 57, pp. 4930–4944, Jun 1998.

[128] S. Kolkowitz, A. C. B. Jayich, Q. P. Unterreithmeier, S. D. Bennett, P. Rabl, J. G. E. Harris, and M. D. Lukin, "Coherent Sensing of a Mechanical Resonator with a Single-Spin Qubit," *Science*, vol. 335, no. 6076, p. 1603, 2012.

[129] T. J. Kippenberg and K. J. Vahala, "Cavity Opto-Mechanics," *Optics Express*, vol. 15, p. 17172, 2007.

[130] A. schliesser, *Cavity Optomechanics and Optical Frequency Comb Generation with silica Whispering-Gallery-Mode Microresonators*. PhD thesis, Ludwig Maximilians University, Munich, 2009.

[131] A. Gozzini, F. Maccarrone, F. Mango, I. Longo, and S. Barbarino, "Light-pressure bistability at microwave frequencies," *Journal of the Optical Society of America B Optical Physics*, vol. 2, pp. 1841–1845, Nov. 1985.

[132] V. B. braginsky and A. Manukin *Sov. Phys. JETP*, vol. 25, p. 653, 1967.

[133] B. D. Cuthbertson, M. E. Tobar, E. N. Ivanov, and D. G. Blair, "Parametric back-action effects in a high-Q cyrogenic sapphire transducer," *Review of Scientific Instruments*, vol. 67, pp. 2435–2442, July 1996.

[134] S. Gigan, H. R. Böhm, M. Paternostro, F. Blaser, G. Langer, J. B. Hertzberg, K. C. Schwab, D. Bäuerle, M. Aspelmeyer, and A. Zeilinger, "Self-cooling of a micromirror by radiation pressure," *Nature*, vol. 444, pp. 67–70, Nov. 2006.